SUBDUCTION BENEATH THE QUEEN CHARLOTTE ISLANDS?   THE RESULTS OF
A SEISMIC REFRACTION SURVEY

by

DAVID MACKIE

B.   Sc. (Honours), University of Toronto, 1982

A THESIS SUBMITTED IN PARTIAL FULFILMENT OF

THE REQUIREMENTS FOR THE DEGREE OF

MASTER OF SCIENCE

in

THE FACULTY OF GRADUATE STUDIES

Department of Geophysics and Astronomy

We accept this thesis as conforming

to the required standard

THE UNIVERSITY OF BRITISH COLUMBIA

October 1985

In presenting this thesis in partial fulfilment of the
requirements for an advanced degree at the University
of British Columbia, I agree that the Library shall make
it freely available for reference and study. I further
agree that permission for extensive copying of this thesis
for scholarly purposes may be granted by the head of my
department or by his or her representatives. It is
understood that copying or publication of this thesis
for financial gain shall not be allowed without my written
permission.

Department of _Geophysics and Astronomy_

The University of British Columbia
1956 Main Mall
Vancouver, Canada
V6T 1Y3

Date _July 2 1985_

Abstract

The Queen Charlotte transform fault zone, which lies immediately east of the Queen Charlotte Islands, marks the boundary between the oceanic Pacific and the continental North American plates. Relative plate motions suggest that oblique underthrusting of the Pacific plate beneath North America may be presently occurring along this transform fault. To investigate this plate boundary and the implications of oblique subduction on crustal structure beneath the region, an onshore-offshore seismic refraction survey was conducted in 1983. The survey was designed to sample the crust beneath the Queen Charlotte Islands and across Hecate Strait to the mainland of British Columbia. Six ocean bottom seismographs and 11 land based stations were deployed along a 200 km line extending from 20 km west of the the Queen Charlotte Islands to the mainland. Thirteen 540 kg and twenty 60 kg explosive charges were detonated along a 110 km long east-west line in the ocean to the west of the receivers. The multiple shots recorded on multiple receivers, all along the same line, effectively reverses the profile over some of its length.

The objective of this study is to provide a model of the deep crustal structure beneath the fault zone, the Queen Charlotte Islands, and Hecate Strait. An exemplary subset of the extensive data set was selected to meet this objective. Beneath the deep ocean the Moho dips at about 2° to the east. At the Queen Charlotte terrace, a 25 km wide zone immediately west of the active Queen Charlotte fault, the dip of the Moho

increases to about 5°. The crust is about 12 km thick at the terrace and 18 km thick at the eastern edge of the Queen Charlotte Islands, and in excess of 30 km thick at the mainland. The terrace unit itself is divided into two units - an upper unit with low velocity (4.1 km/s) and high gradient (0.3 km/s/km) and a lower unit with a high velocity (6.5 km/s) and a low gradient (0.05 km/s/km). This model, while not definitive, supports the interpretation of oblique shallow underthrusting of the Pacific plate beneath the Queen Charlotte Islands. The upper terrace unit could represent a sedimentary accretionary wedge and the lower terrace unit - the subducting slab. A model in which compression across the Queen Charlotte transform fault zone is taken up by deformation of the Queen Charlotte Islands in the form of crustal shortening and thickening is not compatible with the thin crust beneath the islands and Hecate Strait.

Table of Contents

List of Tables

List of Figures

Acknowledgement

captain and crew helped to make the marine part of the field program a success. The assistance of Chief Al Wood and M/S George Cox, who expertly detonated the explosives, is especially appreciated. The help of personnel from the Pacific Geoscience Centre is always appreciated. I would also like to thank Patrick Morel and crew from the Earth Physics Branch and Dr. J. Wright for their work in carrying out the land-based aspect of this experiment.

I. INTRODUCTION

1.1 The Tectonic History of the Queen Charlotte Islands

1.1.1 Accretionary History

The Queen Charlotte Islands are situated immediately east of the active plate boundary between the North American and Pacific plates (figure 1). To understand the tectonic history of the Queen Charlotte Islands it is necessary to understand the framework upon which the North American Cordillera was formed. Recent concensus is that throughout Mesozoic and early Cenozoic time the North American Cordillera grew by peripheral accretion of crustal fragments to the leading edge of the craton (Monger et al., 1972; Coney et al., 1980; Monger, 1984). The identification of these fragments or terranes is based primarily on stratigraphy and does not necessarily imply a tectonic origin or past (Coney et al., 1980). However, interdisciplinary studies using biostratigraphic, paleomagnetic, paleophysiographic, paleobiogeographic, and seismic techniques, combined with geologic cross-cutting relationships provide data that is helping to unravel the tectonic history of these 'suspect' terranes (Saleeby, 1983; Coney et al., 1980). A terrane is termed 'suspect' if its paleogeographical setting is uncertain with respect to the Cordillera. If a terrane has a paleogeographical setting that is known to be different from the craton, it is called 'allochthonous'.

The Queen Charlotte Islands are members of the
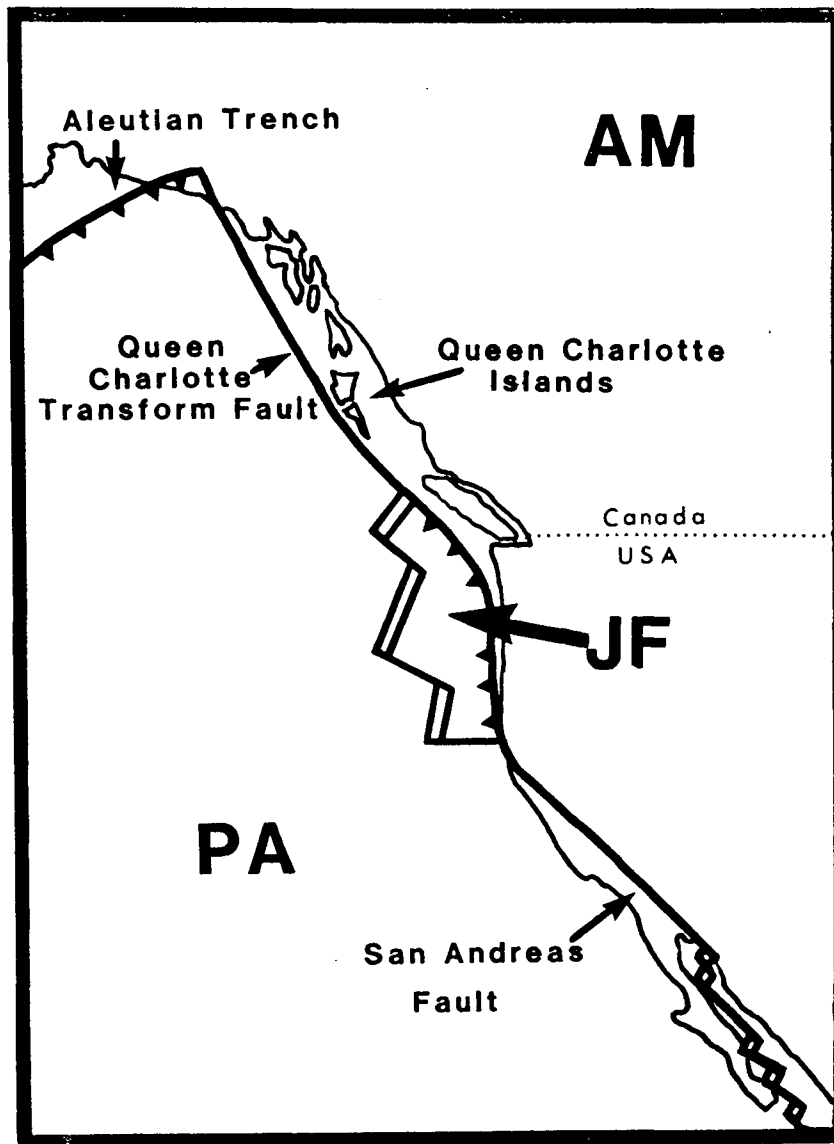
Figure 1 - Present day plate tectonic configuration
along the west coast of North America.

The Queen Charlotte transform fault marks the boundary between the Pacific and North American plates adjacent to the Queen Charlotte Islands. PA - Pacific plate, NA - North American plate, JF - Juan de Fuca plate system.

allochthonous terrane Wrangellia, which also includes Vancouver Island, parts of southeast Alaska, and the Hells Canyon area in eastern Oregon (Yorath and Chase, 1981; Jones et al., 1977). Figure 2 shows the geographical extent of Wrangellia and other major terranes in the Canadian Cordillera. The terranes important in the following discussion are Wrangellia, the Alexander terrane, Stikinia, and Quesnellia.

Wrangellia, first defined by Jones et al. (1977), is a Mesozoic terrane composed of Middle to Upper Triassic tholeiitic basalts and calcareous sedimentary rocks. Yorath and Chase (1981) also include volcanic and sedimentary Jurassic rocks (Maude and Yakoun Formations on the Queen Charlotte Islands; Bonanza Group on Vancouver Island) as part of Wrangellia. These two Jurassic Formations lie conformably on the Late Triassic to Lower Jurassic Karmutsen and Kunga Formtions on the Queen Charlotte Islands (Sutherland Brown, 1968). No pre-Triassic rocks are known to occur on the Queen Charlotte Islands; however, on Vancouver Island the Karmutsen Formation rests unconformably on the Paleozoic calcareous sediments of the Sicker Group. The exotic nature of Wrangellia was first demonstrated by paleomagnetic studies of the Nicolai Greenstone in the Wrangell Mountains (Hillhouse, 1977) indicating that Wrangellia lay within 15° of the paleoequator in the Triassic. This requires that Wrangellia has moved northward either 3000 km or 6300 km (depending upon whether a northern or southern hemisphere solution is favoured) since the Triassic to occupy its present position. Yole and Irving (1980) report paleopoles

AX   Alexander

BR   Bridge River

CA   Cassiar

CC   Cache Creek

CG   Chugach

CS   Cascade

KO   Kootenay

MO   Monashee

OC   Olympic

PR   Pacific Rim

QN   Quesnellia

SM   Slide Mountain

SS   Stikinia

WR   Wrangellia

YT   Yukon-Tanana

CP   Coast Plutonic
      Complex *

* may represent suture
  between Wrangellia
  and Stikinia.
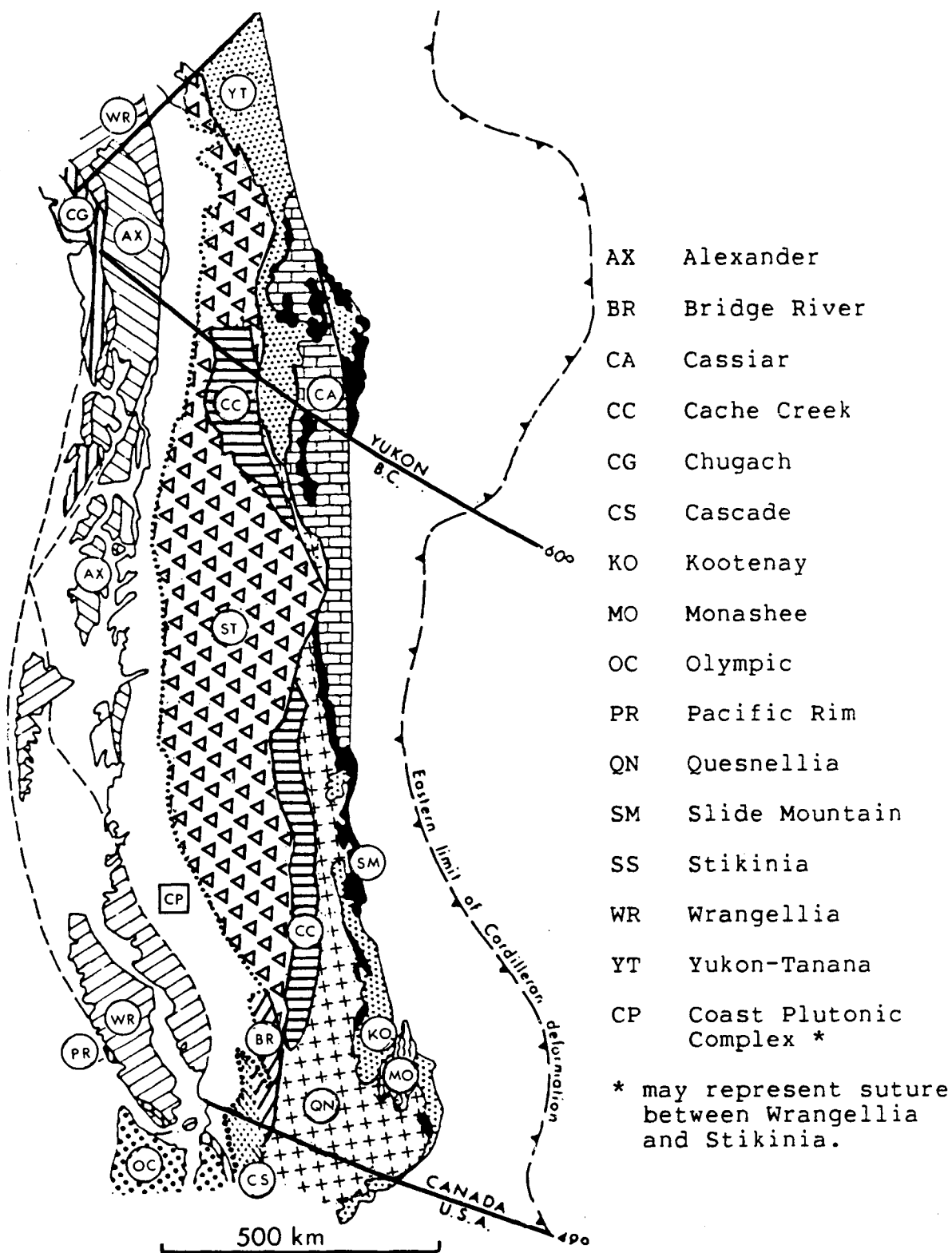
Figure 2 - Suspect terranes of the Canadian Cordillera
(from Monger, 1984).

from the Vancouver Island Karmutsen Formation that, together with Pacific plate reconstructions (Hilde et al., 1977), favour an 18° southern hemisphere origin for Wrangellia. Paleomagnetic results (Packer and Stone, 1974) from southern Alaska indicate that the Jurassic location of Wrangellia was parallel to the present day location of southern Oregon. Clearly, Wrangellia is an allochthonous terrane.

The Alexander terrane is an assemblage of Late Precambrian (~650 Ma) to Late Paleozoic (~250 Ma) sedimentary, igneous, and metamorphic rocks (figure 2). Tipper et al., (1981) include metasedimentary and metavolcanic rocks along the western margin of the Coast Mountains as part of the Alexander terrane. In the southern part of the terrane, Late Triassic rocks overlie Permian limestones (Berg et al., 1978). Paleomagnetic results from southeast Alaska indicate that the Alexander terrane has undergone about 1800 km of northward displacement relative to cratonic North America between Late Carboniferous (~280 Ma) and Triassic time (Van der Voo et al., 1980). The Upper Triassic Hound Island volcanics which overlie the Paleozoic rocks indicate no significant latitudinal displacement, suggesting that the Alexander terrane was in its present latitudinal position by the Late Triassic (~230 Ma) (Hillhouse and Gromme, 1980).

Although paleomagnetic studies indicate that each of these terranes originated far south of their present position little is known about their northward journeys. Several different hypotheses have been proposed in the literature. Yorath and

Chase (1981) reconstruct the history of the Alexander terrane and Wrangellia (figure 3). They suggest that both terranes were drifting northward separately until they collided with each other in the Late Jurassic to earliest Cretaceous (~140 Ma), close to their present latitudinal position, amalgamating into a larger terrane. Both the Alexander terrane and Wrangellia are intruded by a series of similar synorogenic plutons that date the collision (Yorath and Chase, 1981). Young (1981) gives the average age of these plutons as 144 Ma (Late Jurassic). The Lower Cretaceous Longarm Formation contains clasts of these plutons in its coarse sandstones and conglomerates. This lithology represents erosion due to rapid uplift - expected when two landmasses collide. The two terranes were most certainly amalgamated by at least the Late Jurassic as both are overlapped by the Lower Cretaceous to Upper Jurassic Gravina-Nutzotin assemblage (Berg et al., 1972). This superterrane then accreted to the North American craton sometime in the Late Cretaceous to mid-Tertiary (90 Ma to 40 Ma). As it approached North America, uplift which has been dated by Roddick and Hutchison (1974) at 50 to 80 Ma began in the Coast Plutonic Complex. Monger et al. (1972) and Monger (1984) also favour this hypothesis. Monger (1984) gives a very complete review of Cordilleran tectonics. Between 90 Ma and 40 Ma the west coast of Wrangellia, and thus the Queen Charlotte Islands, became the active edge of cratonic North America.

Irving et al. (1985) propose a somewhat different scenario. They report new paleomagnetic data from the Coast
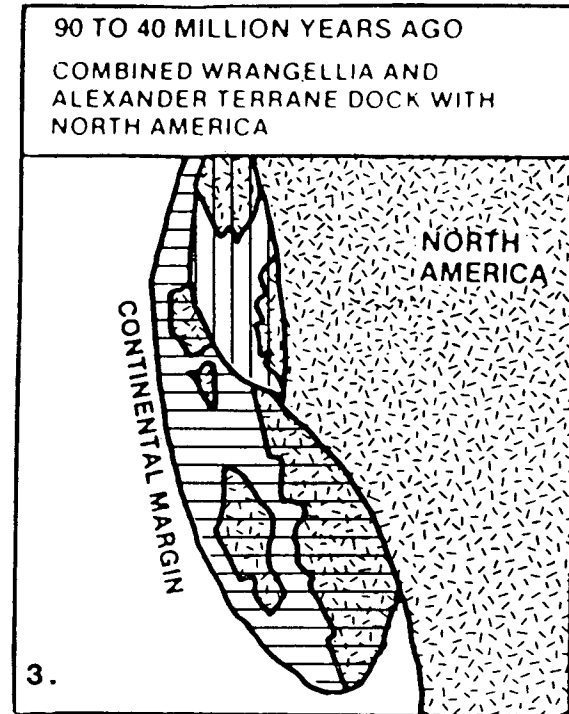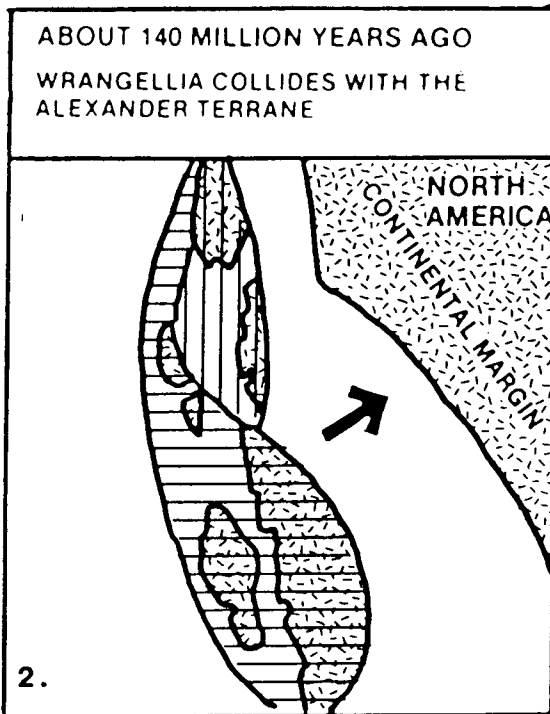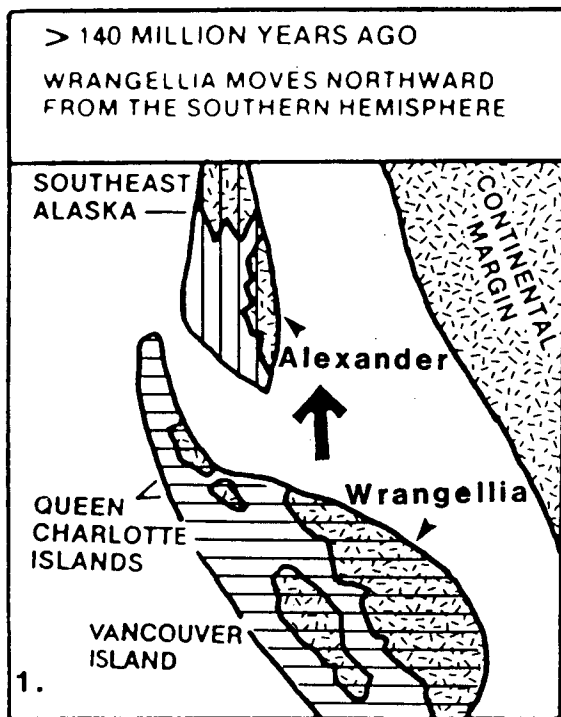
Figure 3 - The accretion of the Alexander and
Wrangellia terranes with North America.

See text for explanation. (from Yorath and Cameron, 1982).

Plutonic Complex indicating that it has moved 2400 km northward since the mid-Cretaceous. This paleomagnetic data is also consistent with a 30° tilt to the southwest of the southern Coast Plutonic Complex and the Cascades; however, they regard translation of the rocks, rather than such a consistent regional tilt, as a more probable explanation. They also note that paleopoles from overprints in the Triassic rock units of Wrangellia on Vancouver Island (Yole and Irving, 1980, Schwarz et al., 1980) and Quesnellia (Symons, 1973, 1976) agree with the mid-Cretaceous Coast Plutonic Complex results and thus argue that these paleopoles are of that age. This places the mid-Cretaceous position of Wrangellia, the southern Coast Plutonic Complex, the Cascades, Stikinia, and perhaps Quesnellia at the present day latitude of Mexico (Irving et al., 1985). It is suggested, therefore, that these terranes accreted south of their present location and then continued northward as one unit (figure 4). The Coast Plutonic Complex represents the suture joining Stikinia with Wrangellia. Concordance of mid-Tertiary paleomagnetic results from the Cascades and cratonic North America indicate that relative motion between the two had ceased by then.

Irving et al.'s model indicates that the Queen Charlotte Islands became the leading edge of the North American continent by at least the mid-Tertiary (~40 Ma). If this is correct then Stikinia must have slipped in behind the Alexander terrane which had been lying offshore from North America close to its present day latitude since the Late Triassic, as has been suggested by
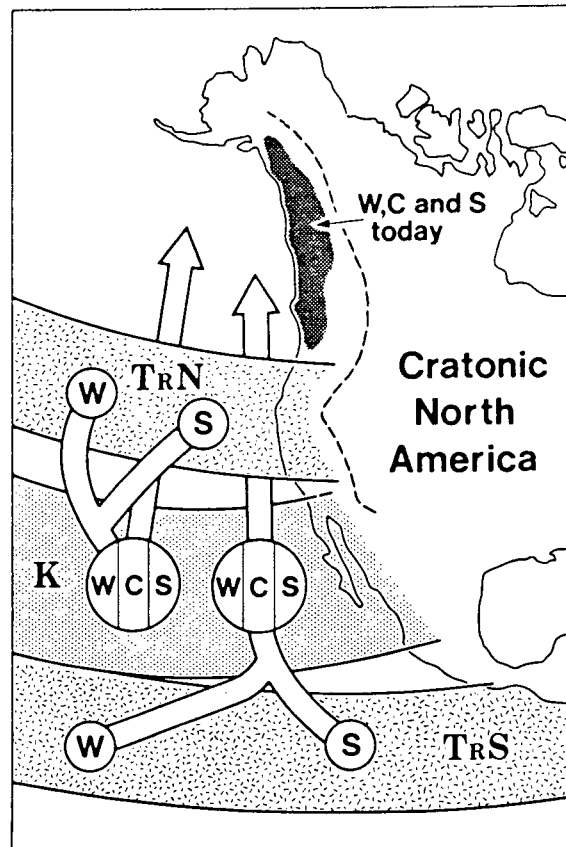
Figure 4 - The accretionary history of Wrangellia,
Stikinia and the Coast Plutonic Complex.

Compare this with the scenario in Figure 3. W - Wrangellia,
S - Stikinia and C - Coast Plutonic Complex. See the text
for explanation. The two stippled bands marked $T_R N$ and $T_R S$
indicate the two possible Triassic origins (northern
hemisphere and southern hemisphere respectively) for
Wrangellia and Stikinia before accreting together (from
Irving et al., 1985).

Monger and Irving (1980) and Yorath and Chase (1981).
Subsequent to this, Wrangellia must have been smeared along the
western edge of the Alexander terrane by a transcurrent movement
to attain the present situation with the Alexander terrane
sandwiched between Wrangellia and Stikinia (figure 2).

There have been several proposals as to what kind of plate
boundary separated North America and the oceanic plate that
carried these exotic terranes northward. Van der Voo et al.
(1980) have suggested that the Alexander terrane was displaced
along a major transcurrent fault running northward from
California. Yorath and Chase (1981) and Monger and Price (1979)
infer that both Wrangellia and the Alexander terrane accreted to
North America along a subduction zone. A combination of the two
previous ideas was proposed by Monger (1984) who suggests that a
zone of 'transpression' existed from the Late Cretaceous to
early Tertiary. The mobile terranes, being displaced northwards
by the various Pacific plates, collided with a westward moving
North American craton. Irving et al. (1985) note that the
present day latitudinal spread of Wrangellia is about three
times that of its paleolatitudinal spread in the Late Triassic.
Perhaps, Wrangellia and some of the other terranes were smeared
out along the Cordillera during this phase of 'transpression'.

1.1.2 <u>Post Accretionary History of the Queen Charlotte Islands</u>

After the mid-Cretaceous the Queen Charlotte Islands became the leading edge of the Canadian Cordillera. The details of the tectonic regime along the coast from 90 Ma to about 30 Ma is unclear. The complex patterns of magnetic stripes on the Pacific plate and the Juan de Fuca plate system, along with absolute plate motions determined from the Hawaiian-Emperor chain, provide evidence for the plate motions that occurred along the North American coast. Several different models have been published (eg. Atwater, 1970; Coney, 1976; Cooper et al., 1976; Stone, 1977; Riddihough, 1982a). All of these models require the existence of three oceanic plates west of North America: Pacific, Farallon, and Kula (figure 5a, top). The now wholly subducted Kula plate (Grow and Atwater, 1970) is necessary to explain the existence of the Alaskan Magnetic Bight anomaly pattern (Pitman and Hayes, 1968; Grow and Atwater, 1970). This anomaly pattern well defines trends of the Kula-Pacific and Pacific-Farallon ridges. The Kula-Farallon (KF) ridge trend is constrained only after 60 Ma because most of the ridge and the anomalies it produced have been consumed by convergence (Atwater, 1970). (Is it not somehow significant that all of the magnetic anomalies which would answer our questions have been subducted?) The position of this ridge with respect to North America is important in defining the plate regime at the Queen Charlotte Islands from about 90 Ma to 30 Ma.

Cooper et al. (1976) constructed two models: one based on paleomagnetic data and the other on absolute plate motions
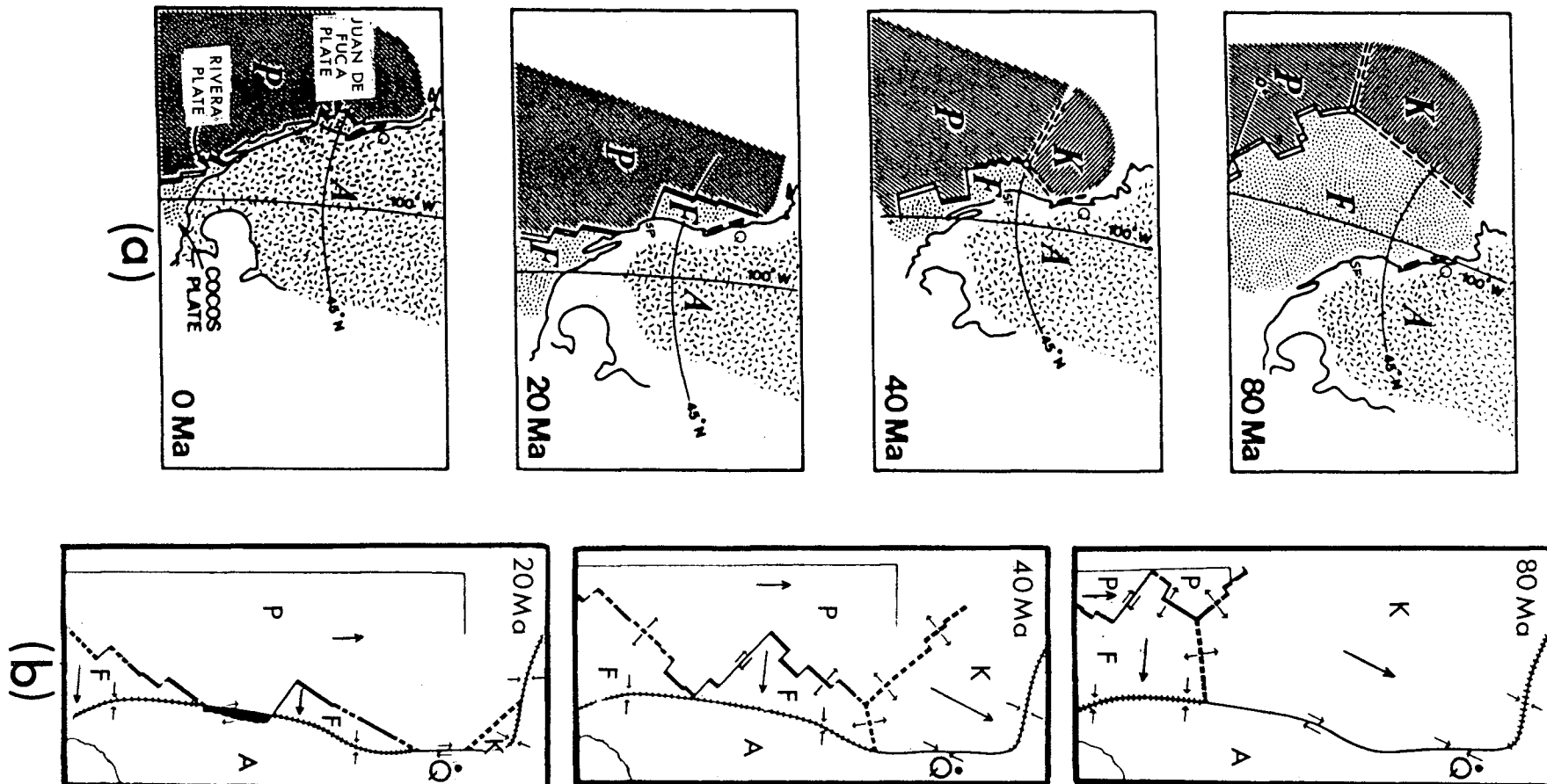
Figure 5 - Pacific plate tectonic reconstruction from
80 Ma

A - North American plate, K - Kula plate, F - Farallon
plate, P - Pacific plate. Q represents the latitude of the
Queen Charlotte Islands, and SF represents the latitude of
San Francisco.
(a) - the Kula-Farallon-North America triple junction
migrates from the Gulf of Alaska southwards along the coast
(after Riddihough, 1982a).
(b) - the Kula-Farallon-North America triple junction
migrates northwards from southern California (after Atwater,
1970).

determined from the Hawaiian-Emperor Seamount Chain. Both models show the Kula-Farallon (KF) ridge perpendicular to the Aleutian trench at 80 Ma (figure 5a). Assuming constant plate motion, the Kula-Farallon-North America (KFN) triple junction migrated southward to the Queen Charlotte Islands by 50 Ma to 30 Ma with oblique convergence or transcurrent motion of the Kula and North American plates replacing the subducting Farallon plate along the boundary. The Kula-North America motion vector is poorly constrained but it appears to have had a significant component of strike-slip motion (Atwater 1970). Harper et al. (1981) infer a relative velocity of 120 mm/yr at N8°E for the Queen Charlotte Islands region. The Farallon-North American relative motion vector was largely convergent (McKenzie and Morgan, 1969; Atwater, 1970) and has been estimated at 100 mm/y at N57°E near Vancouver Island (Harper et al., 1981).

Atwater (1970), Coney (1970), and Atwater and Molnar (1973) reconstructed models back to 80 Ma using relative plate motions (figure 5b). At 80 Ma, Atwater (1970) shows the Kula-Pacific-Farallon (KPF) triple junction off the coast of California with the KF ridge perpendicular to the coastline. Using extrapolated relative plate motions the KFN triple junction migrates northwards to Vancouver Island by 40 Ma with the Farallon-North America trench developing behind it. The models of Cooper et al. (1976), Atwater (1970), Riddihough (1982a), and Stone (1977) indicate that sometime between 50 Ma and 30 Ma the KFN triple junction lay just north of Vancouver Island (figure 5a and b). North of this triple junction, oblique

convergence or transcurrent motion between the Kula and North American plates occurred. South of it the Farallon plate was being subducted beneath North America. From 30 Ma to the present the plate movements are less uncertain and the gross characteristics of most models agree. At 29-30 Ma the Farallon-Pacific ridge began to be subducted beneath California and transcurrent motion began along the San Andreas Fault (figure 5b). As the Farallon Plate descended beneath North America it remained in one piece until the gap created by the absence of subduction at the San Andreas Fault reached melting temperature at about 20 Ma (Dickinson and Snyder, 1979). At this time the two portions of the Farallon began to move independently and the Juan de Fuca plate was born (Atwater, 1970; Riddihough, 1982a).

All of these models also predict the subduction of the KF ridge beneath North America near the Queen Charlotte Islands. Between 10 Ma and 20 Ma the KF ridge was totally subducted beneath North America. When the KPF triple junction was subducted, transcurrent motion between the Pacific and North American plates was initiated in the Queen Charlotte Islands region. As the Kula continued to subduct to the north the KPN triple junction migrated northwards along the coast and the transcurrent Pacific-North America boundary lengthened. By 20 Ma the Kula plate was totally subducted and the Pacific plate was in contact with North America from Vancouver Island north to the Aleutians (Riddihough, 1982a; Atwater, 1970); although, Byrne (1979) suggests that the Kula plate may have ceased to act

as an independent plate at about 55 Ma. At the same time the San Andreas transform fault grew in length as the Juan de Fuca plate continued to subduct. The southern Juan de Fuca-Pacific-North America (JPN) triple junction migrated northwards to its present position at Cape Mendocino (Riddihough, 1982a). The northern JPN triple junction has remained stable just north of Vancouver Island for the last 10 Ma (Riddihough, 1977). Table I provides a comparison of the gross characteristics of the foregoing models.

1.1.3 Present Tectonic Situation at the Queen Charlotte Islands

The Queen Charlotte transform fault marks the present day boundary between the Pacific and North American plates. The North America-Pacific relative motion is mainly strike-slip at 55 mm/yr (Minster and Jordan, 1978). Global plate motion analyses (Minster et al., 1974; Minster and Jordan, 1978) indicate that the Pacific-North America relative motion vector trends 10° to 20° east of the trace of the Queen Charlotte fault (figure 1). A component of oblique underthrusting at a rate of 10 to 20 mm/yr is necessary to be consistent with this discrepancy. Figure 6 illustrates the probable extent of the underthrust slab given a convergence rate of 20 mm/yr for the past 6 Ma.

There is an increasing amount of physiographic, geologic, and geophysical evidence that supports oblique subduction of the Pacific plate beneath North America along the Queen Charlotte transform fault. Figure 7 shows a schematic representation of

Table 1 - Cenozoic Plate Interaction at the Queen Charlotte Islands.

(after Young, 1982.)

DATA SOURCE	Atwater(1970) Atwater & Molnar(1973) Coney(1976)	Cooper et al.(1976)	Stone(1977)	Riddihough(1982a)
MODEL	Constant relative motion	Hot spot, seamount paleomagnetics, relative motion	Constant motion Pacific Hotspot	Relative motion
AGE (MA)				
0				
10			Transform (N. America -Pacific)	Pacific-N America Transform
20	Transform (N. America-Pacific)		Interaction Farallon -Pacific ridge- N. America	Farallon subduction
30	Transform or oblique convergence(N. America -Kula)	Transform or oblique convergence (N. America -Kula)	Subduction Farallon plate / Interaction Kula-Farallon ridge- N. America	
40		Interaction Kula-Farallon ridge-N. America	Transform or oblique convergence Kula-N. America	Interaction Kula Farallon ridge- N. America Subduction (Farallon)
50		Subduction (Farallon)		

Figure 6 - Possible subducted Pacific slab beneath
North America.

The shaded region represents the possible extent of a
subducted Pacific plate beneath North American given that
oblique subduction has occurred for the past 6 Ma at 20
mm/yr. The long arrow represents the relative motion of the
North American and Pacific plates for the last 6 Ma. Medium
length arrows perpendicular to the Queen Charlotte fault
indicate the direction of the component of subduction. The
smallest arrows indicate transcurrent motion taken up along
the transform faults in the region (after Yorath and
Hyndman, 1983).
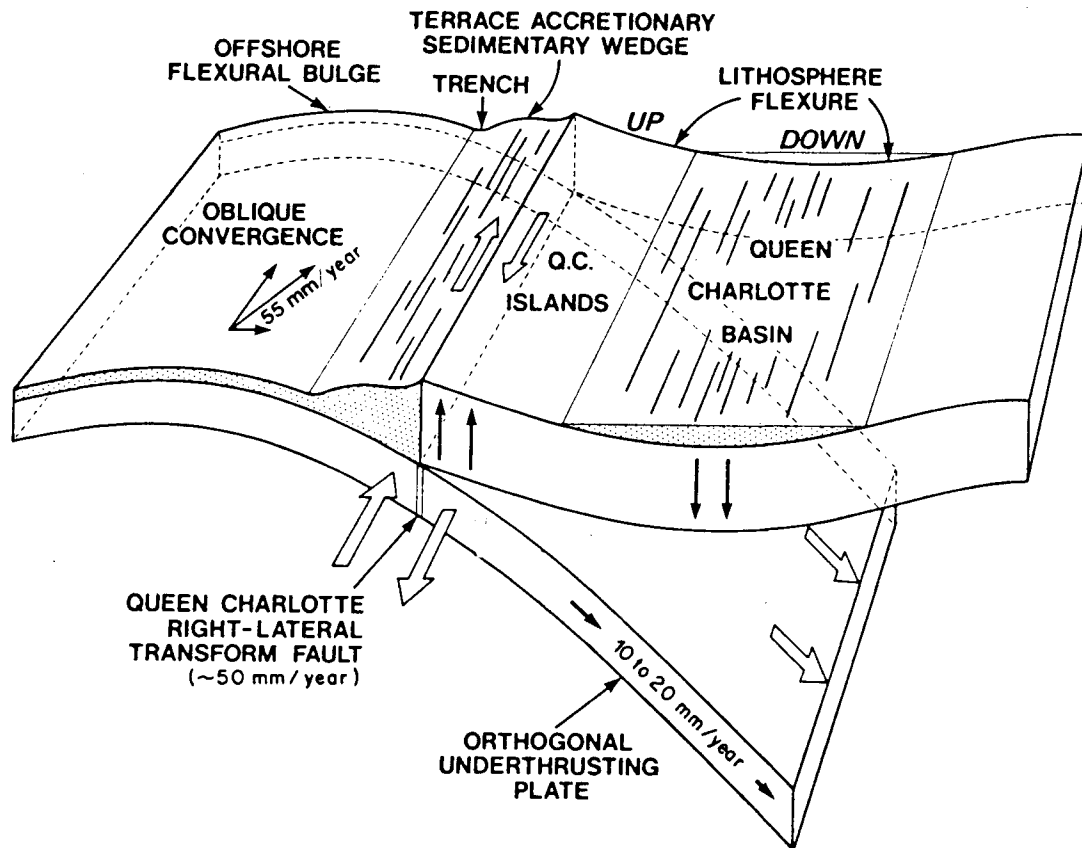
Figure 7 - Physiographic features of the Queen
Charlotte Islands Region.

This three dimensional drawing shows the observed
physiographic features that are consistent with subduction
beneath the Queen Charlotte Islands (from Yorath and
Hyndman, 1983).

the major physiographic features associated with the Queen Charlotte Islands region. Such features are consistent with other known subduction zones around the world.

A broad gentle bulge in the ocean floor is present about 100 km seaward of the shore (figure 7 and figure 8). Called the Oshawa Rise, it extends to the southern edge of the islands and is about 100 km wide. A positive free-air gravity anomaly is associated with the rise. The close correlation of such a gravity anomaly with the seaward topographic rise is a feature of many subduction zones (Uyeda and Kanamori, 1979; Watts and Talwani, 1974). Seismic profiles across this feature indicate that the acoustic basement rises with the bathymetric high, suggesting that this is a tectonic feature (Chase et al., 1975). The bulge is considered to be a flexural response to horizontal compressive stress in the oceanic plate caused by the convergence of the overriding continental plate (Watts and Talwani, 1974).

Flexure in the overriding continent (figure 7) has also been observed in various zones of convergence around the world. Uplift along the western margin on the Queen Charlotte Islands and subsidence in Hecate Strait has been documented by several studies. Parrish (1982) studied uplift rates in the Coast Mountains and the Queen Charlotte Islands using fission-track dating of apatites and zircons. Uplift along the coast of the Queen Charlotte Islands has been occurring for the last 10 Ma. Riddihough (1982b) also suggests a similar contemporary flexure pattern based on sea tidal levels, geodetic relevelling, and
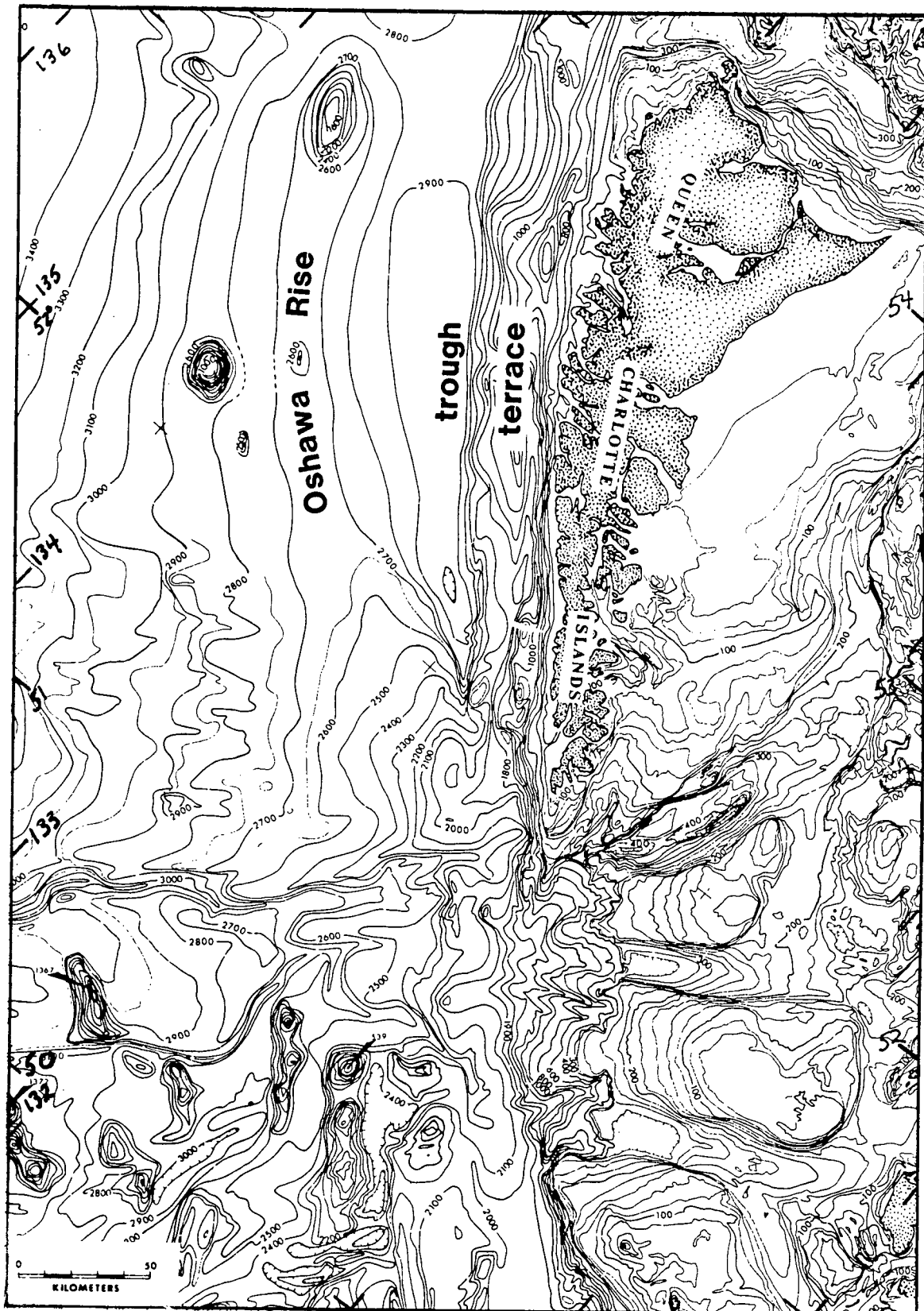
Figure 8 - Bathymetry of the Queen Charlotte Islands
region.

The Oshawa Rise represents a broad gentle bulge in the ocean
floor. The Queen Charlotte terrace is a 25 km wide zone
immediately west of the islands. (after Chase et al., 1975).

Quaternary beach levels. Glacio-isostatic recovery along the coast is not compatible with the contemporary uplift patterns observed (Riddihough, 1982b). Figure 9 and figure 10 show the agreement between the two studies. The pattern of uplift along the Queen Charlotte Islands and landward subsidence is consistent with other oblique zones of compression or subduction around the world (eg. Sangami Trough, Japan; Alpine Fault, New Zealand). The vertical movement (+1 mm/yr) along the Queen Charlotte transform fault is compatible with a position close to a transform or highly oblique convergent plate boundary (Riddihough, 1982b).

The subsidence of Hecate Strait and Queen Charlotte Sound may also be a result of flexure caused by the oblique subduction of the Pacific plate. Yorath and Hyndman (1983) used a series of wells in Hecate Strait and Queen Charlotte Sound to construct a tectonic subsidence history of the basin. They concluded that subsidence began at 6 Ma after a previous period of uplift and therefore, that oblique underthrusting began at that time. This timing is corroborated by a new study indicating that the Pacific plate changed motion to a more convergent direction with respect to North America at 5 Ma (Cox and Engebretson, 1985). They correlated a small bend in the Hawaiian-Emperor seamount chain with geologic evidence for convergence at 5 Ma along the San Andreas Fault. This change in plate motion at 5 Ma could have caused the Pacific plate to begin subducting obliquely beneath the Queen Charlotte Islands.

The Queen Charlotte trough resembles trenchs in areas were
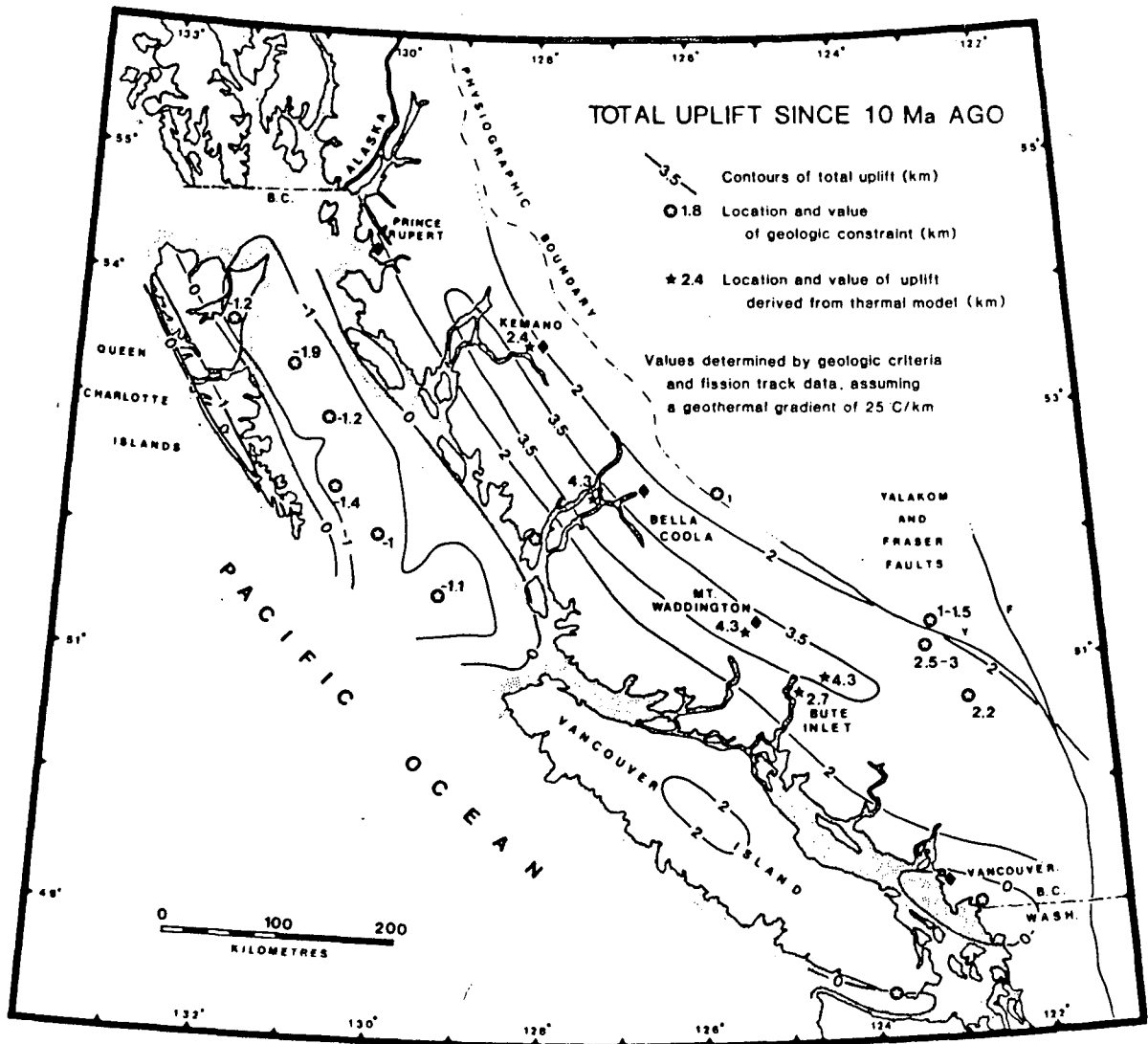
Figure 9 - Total uplift, with respect to sea level, since 10 Ma.

The uplift figures in the northern coast mountains represent maximum values (from Parrish, 1982).
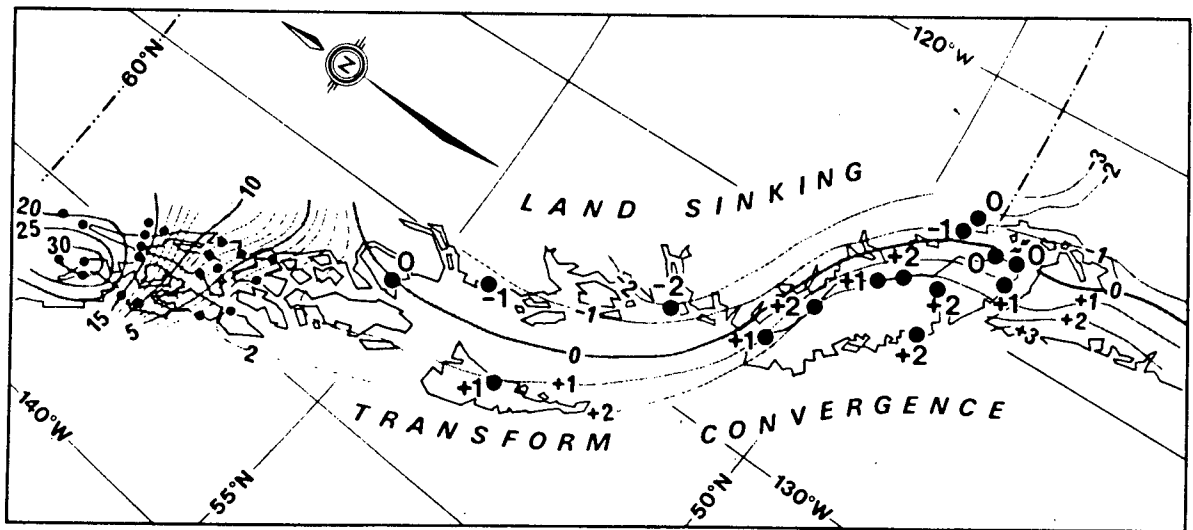
Figure 10 - Contemporary vertical land movements
relative to sea level in mm/yr from tidal stations.

(from Riddihough, 1982b).

shallow subduction is known to occur (eg. Chile-Peru trench). It has been documented both on bathymetry charts and seismic profiles (figure 8 and figure 11). The trough is 300 km long, up to 55 km wide and is between 2.8 to 3.0 km deep (Chase et al., 1975). Seismic profiles across the trough indicate that the oceanic basement dips landward. The basement reflections, however, end abruptly under the terrace. The seismic profiles also indicate that the trough is filled with flat lying sediments which is characteristic of a Chile-Peru type trench.

From the mountain summits on the Queen Charlotte Islands to the trough, the gradient of the continental slope is very constant (about 7°). Even the 25 km wide Queen Charlotte terrace only slightly interrupts this trend. The terrace is a relatively narrow feature and is characterized by two steep scarps - one adjacent to the shore and a second 25 km from the shore that drops to the abyssal deeps (figure 8). Seismic profiles (Chase et al., 1975; Davis and Seemann, 1981) show that the terrace is composed of deformed strata with high amplitude folds (figure 11). A gravity low over the terrace suggests that a thick sedimentary sequence underlies it (Couch, 1969; Srivastava et al., 1971; Srivastava, 1973; Riddihough, 1981; Currie et al., 1980). The Queen Charlotte terrace (figure 7), may be an accretionary sedimentary wedge (Yorath and Hyndman 1983).

A previous refraction survey (Horn et al., 1984; Horn, 1982) crossed the Queen Charlotte fault zone at 52.25°N. The
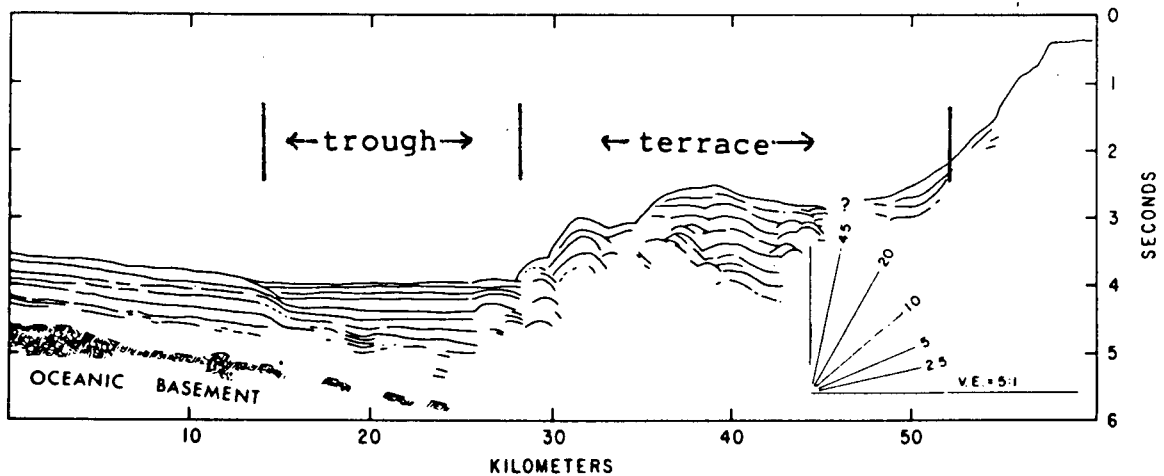
Figure 11 - Reflection seismic profile across the Queen
Charlotte terrace.

This line drawing of a reflection seismic profile shows the
flatlying sediments deposited in the Queen Charlotte trough
created by downwarping of the basement just west of the
terrace edge. The terrace appears to be deformed sediments.
The basement is not visible beneath the terrace (from Chase
et al., 1975).

interpretation is shown in figure 12. This interpretation indicates that the terrace is composed of a thin low velocity high gradient layer (unit 6 in figure 12) overlying a higher velocity lower gradient layer (unit 7 in figure 12) that extends to at least 10 km depth. This is consistent with an accretionary wedge of highly compressed sediments (unit 6) overlying a sheared and fractured oceanic crust (unit 7) (Horn et al., 1984). The model is not well constrained below about 10 km because of the design of the experiment.

Seismicity and heat flow studies conducted in the Queen Charlotte Islands region also indicate that a compressive tectonic regime is active along the Queen Charlotte transform fault adjacent to Moresby Island. Recent microseismicity studies (Hyndman and Ellis, 1981; Berube, 1985) indicate that most of the seismic activity occurs along this scarp of the terrace, indicating that the inner scarp is the active plate boundary. Berube (1985) located about 130 earthquakes from a total of 310 recorded over a 3 month period in 1983. She compiled several composite P-nodal fault plane solutions for clusters of earthquakes (figure 13). The composite solution for the cluster along the Queen Charlotte fault adjacent to Graham Island shows that mostly strike-slip motion is occurring along the northern portion of the fault. One composite solution from an earthquake cluster on the fault adjacent to Moresby Island shows a thrust mechanism. Another solution, from an earthquake swarm in the same location, indicates vertical faulting with the ocean side down. A cluster of events from inland Graham Island,
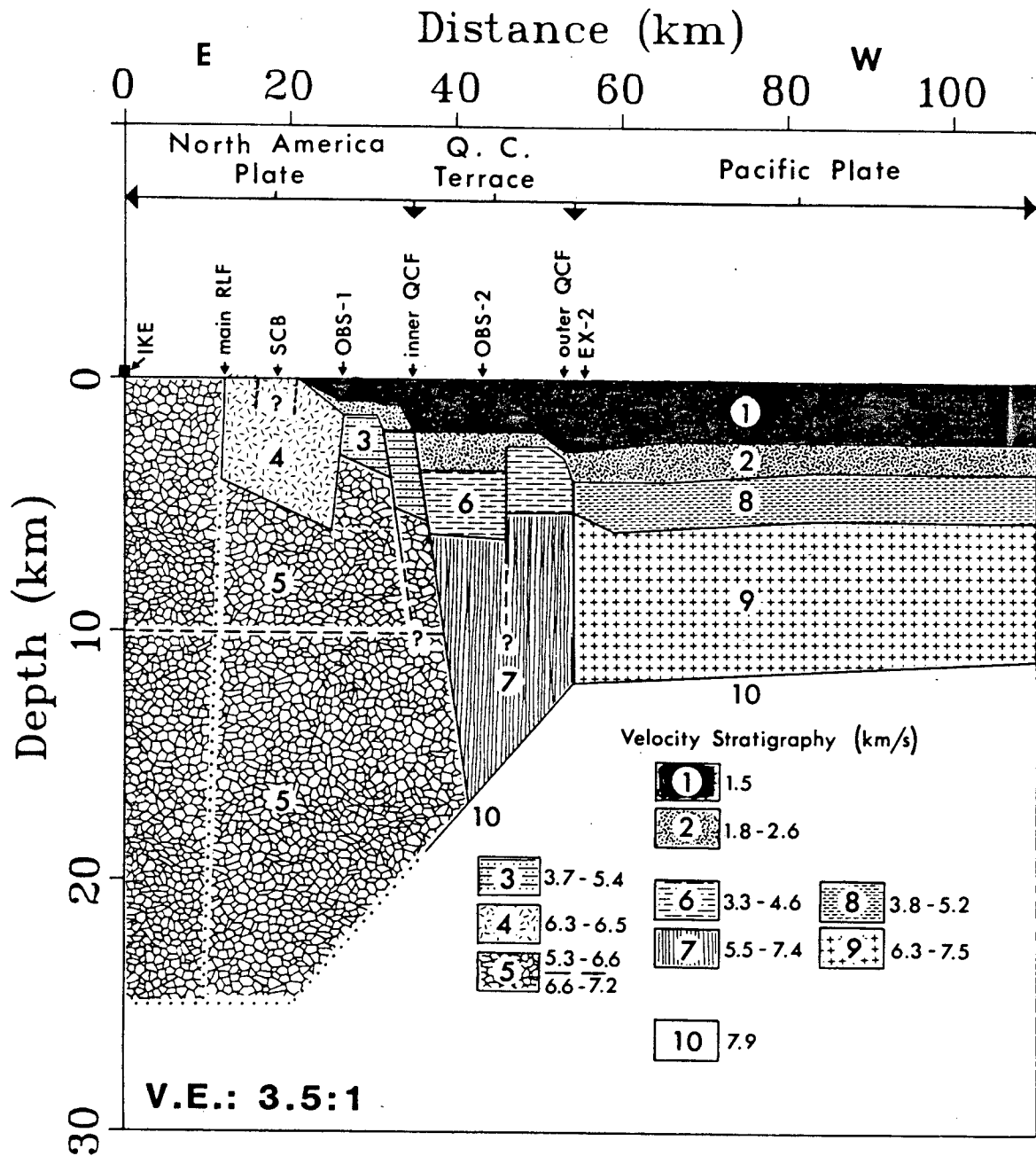
Figure 12 - Crustal structure across the Queen
Charlotte Transform fault.

(from Horn et al., 1984).
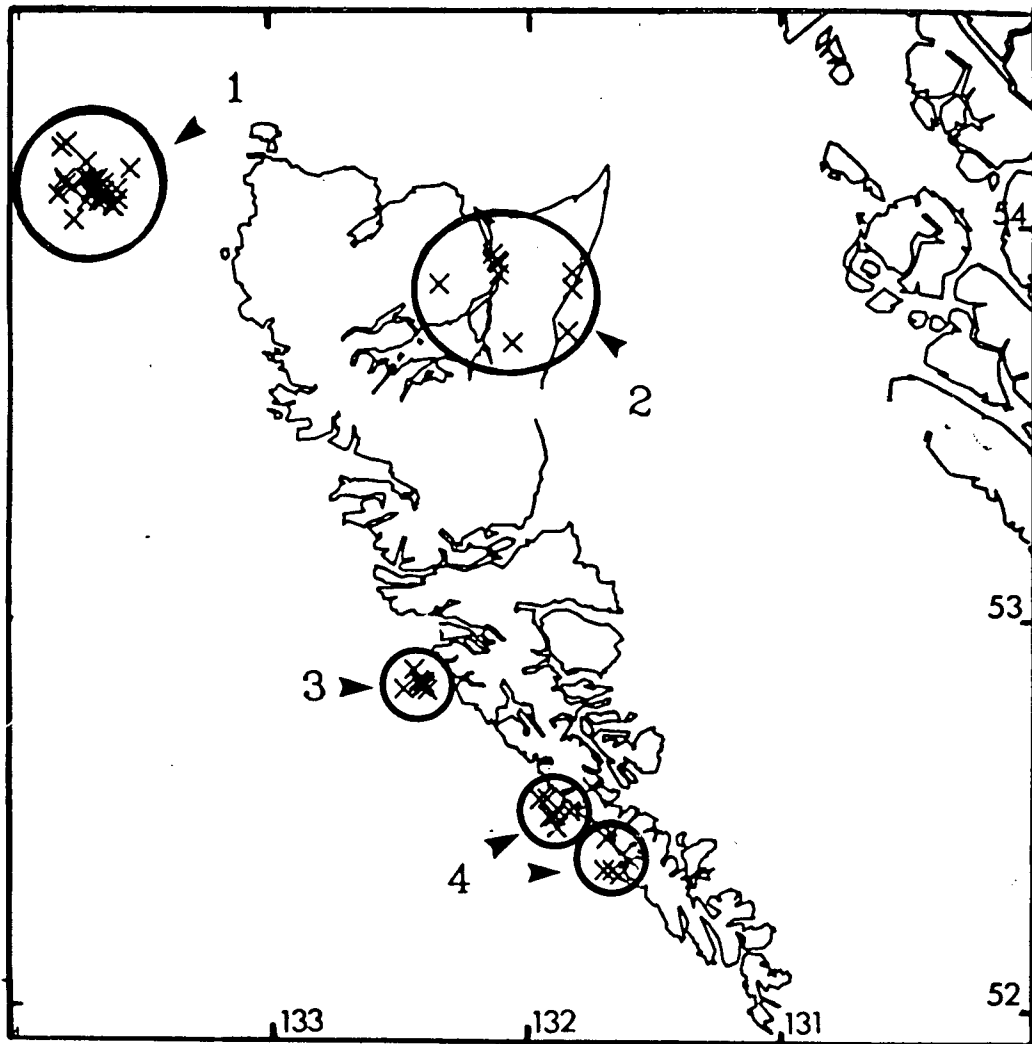
Figure 13 - Location of composite P-nodal fault plane
solutions.

The X's enclosed in circles represent clusters of
earthquakes used to produce composite fault plane solutions
from a microearthquake study. The solutions are:
(1) strike slip motion parallel to the fault zone.
(2) 1 thrust mechanism solution and 1 vertical motion
solution (east side is uplifted) for two clusters of
earthquakes in the same location.
(3) 2 well constrained thrust mechanism solutions.
(4) thrust mechanism solution. (after Berube, 1985).

that cannot be correlated with any known faults, also has a well constrained thrust mechanism. All of the thrust mechanisms indicate a north-south direction of compression, consistent with oblique convergence of the Pacific plate. No earthquakes indicating the presence of a Benioff zone were identified.

Previous studies of large earthquakes indicate that there is convergence or compressive stress across the Queen Charlotte fault zone. Two earthquakes (1949, 1970) have well constrained first motion fault plane solutions. The motion for the 1949 magnitude 8.1 earthquake is mainly strike-slip with a small thrust component (Rogers, 1983). The horizontal motion is parallel to the fault plane (about 15° different from Pacific-North America relative motion). This indicates that the compressive stress was not released in this earthquake (Rogers, 1983). Bostwick (1984) suggests that the first motion fault plane mechanism solutions are not indicative of the character of motion along the rupture. He found a large difference between the aftershock zone and the rupture length suggesting that the displacement offset along the fault was uneven. First motion fault plane solutions from the 1970, magnitude 7.0, earthquake show a thrust mechanism with a dip of 50° to the east. The surface expression of this earthquake has been identified on SEA MARK imaging of the seafloor (G.C. Rogers and E.E. Davis, personal communication, 1985). The newly located fault scarp trends 10° more north-south than the Queen Charlotte fault. This large earthquake indicates a significant component

of convergence (Rogers, 1983).

Recent studies indicate that the present and paleo-heat flow in the Queen Charlotte Islands region are consistent with 6 Ma of subduction. Low heat flow extending 50-200 km inland from the trench axis has been observed in many subduction zones. A continuous transition from high heat flow in the Queen Charlotte trough, to intermediate values on the terrace, to low continental heat flow on the Queen Charlotte Islands was observed by Hyndman et al. (1982). The heat flow values decrease by a factor of three from west to east. The main thermal contrast is located at the seaward edge of the terrace. The average heat flow in the Queen Charlotte trough is close to the theoretical value for the age of the 7 Ma Pacific oceanic crust near the Queen Charlotte Islands. The Queen Charlotte Islands heat flow value (47 mWm^{-2}) is the only measurement on the island but is similar to other areas in the coast Insular Belt (Hyndman et al., 1982). It is also similar to the coastal zone between Cape Mendocino and Vancouver Island which has a uniform heat flow with a mean of 42 mWm^{-2} (Sass et al., 1985). These values are closer to what would be expected above a shallow subduction zone (25-35 mWm^{-2}) than the characteristic heat flow of 70-80 mWm^{-2} within 50-100 km of the San Andreas transform fault (Sass et al., 1985). Numerical modelling by Hyndman et al. (1982) indicates that the observations are consistent with oblique subduction and that a "steady-state" ocean/continent boundary cannot satisfy the data. They suggest that the subducting slab is acting as a heat sink beneath the

Queen Charlotte Islands and Hecate Strait. A new study in southeastern Alaska (Sass et al., 1985), where the plate motion is parallel to the fault strike, indicates that the mean heat flow there is higher (at about 59 mWm^{-2}) than the average value for the Insular Belt (47mWm^{-2}). This may indicate that the northern edge of a subducted Pacific slab does not extend as far as southeast Alaska.

The paleo-heat flow of Hecate Strait and Queen Charlotte Sound has also been studied. Heat flow measurements made in wells drilled in Hecate Strait and Queen Charlotte Sound indicate that the present heat flow is lower in both these areas than in the past. Yorath and Hyndman (1983) have looked at estimates of paleo-heat flow from vitrinite reflectance data from the Hecate Strait and Queen Charlotte Sound wells. Vitrinite is useful because its reflectance is related to its past thermal history. These studies indicate, that at least in Queen Charlotte Sound, the paleo-heat flow was probably twice that of the present day heat flow. According to Yorath and Hyndman (1983), the reduced present day heat flow is a consequence of underthrusting beginning at 6 Ma.

The physiographic, geological, geophysical and tectonic evidence presented in this chapter provides justification for the large onshore-offshore refraction seismic experiment conducted across the fault zone to the mainland of British Columbia in 1983. Much evidence suggests that there is oblique convergence along the Queen Charlotte fault zone, at least along Moresby Island, where the discrepancy between the Pacific-North

America relative motion vector and the trend of the fault is the greatest. The Queen Charlotte fault zone is a complicated area supporting both transcurrent motion and probably some form of compression or underthrusting. The refraction experiment was designed to address some of the questions that have been raised about this enigmatic area.

II. DATA ACQUISITION AND PROCESSING

2.1 Experiment

In August 1983, the Canadian COCRUST group (represented by the University of British Columbia, the Pacific Geoscience Centre and the Earth Physics Branch for this project) carried out an offshore-onshore seismic refraction survey from the deep ocean across northern Moresby Island and Hecate Strait, to the mainland of British Columbia (figure 14). The objectives of this experiment were to determine the lithospheric structure (1) of the Queen Charlotte fault zone, (2) below the Queen Charlotte Islands, and (3) below Hecate Strait. Six ocean bottom seismographs (OBS) were deployed along the refraction line, four east of Moresby Island in Hecate Strait and two west of Moresby Island on the Queen Charlotte terrace. Eight land-based stations were deployed across Moresby Island and three more on the mainland and islands east of Hecate Strait. Twelve 540 km explosive charges were detonated, using timed fuses, every 10 km along a line extending westward from 25 km offshore. In between each 540 km charge, two 60 kg charges were detonated making the shot spacing along the line 3 km. The pelleted TNT explosive NITROPEL® was used for all of the charges. To calculate the time of detonation (origin time) for each shot, the output from a hydrophone towed behind the ship and a geophone placed on the ship deck were recorded along with the WWVB radio time signal on an FM tape recorder and monitored on a chart recorder. A

Figure 14 – Design of the 1983 refraction experiment.

54°

Hecate
Strait

N

Graham
Island

53°

Moresby
Island

Banks
Island

Pitt
Island

▲ Land stations

■ Ocean bottom
  seismographs

✴ Big shots (540 kg)

— Shot line

...... Air gun line

52°

Queen Charlotte
Sound

0 10 20 30 40 50
(km)

134°   133°   132°   131°   130°
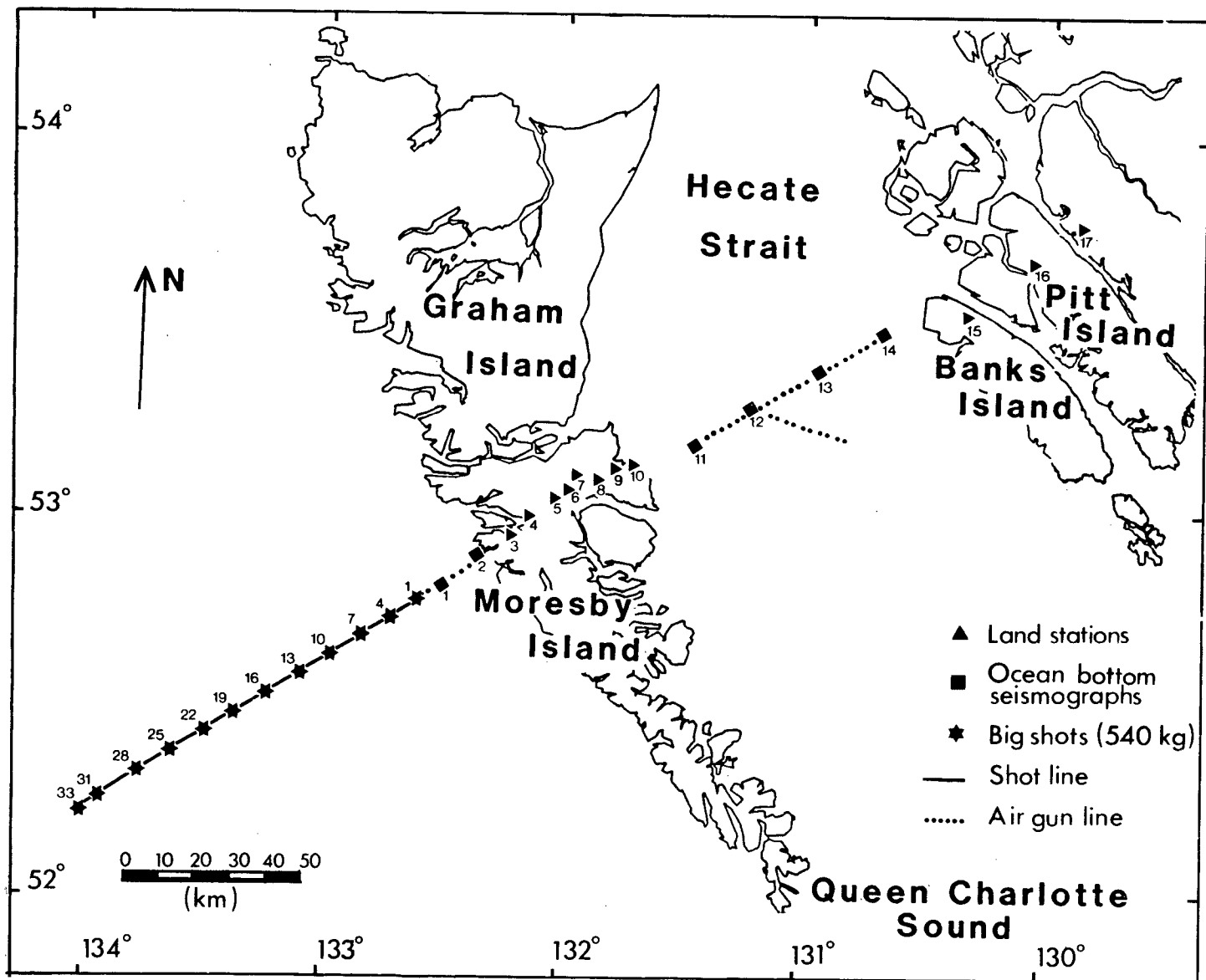
detailed explanation of the origin time calculation is given in Appendix A.

A 32 l (2000 in³) airgun was used to provide 3 additional refraction profiles: (1) over the two OBSs west of the Queen Charlottes, (2) over the OBSs in Hecate Strait, and (3) perpendicular to the OBSs in Hecate Strait. The airgun was fired once a minute at a nominal pressure of 13.8 MPa (2000 psi). When the airgun was deployed the ship steamed at 11 km/hr giving a shot spacing of about 200 m. The experimental pattern was designed to provide good coverage across the Queen Charlotte transform fault and Moresby Island while satisfying environmental constraints which did not allow the detonation of charges in Hecate Strait or in the shallow waters west of Moresby Island.

2.2 Instrumentation

The six OBSs used in this experiment were constructed in the Department of Geophysics and Astronomy after a design from the Atlantic Geoscience Centre (Heffler and Barret, 1979). Substantial technical revisions have been made since the publication of the paper; most notably being a new release mechanism and the use of Benthos® glass spheres for flotation. The OBSs are equipped with two 4.5 Hz seismometers (one horizontal and one vertical) and a hydrophone. The output from these components plus an internally generated clock signal are recorded in direct mode onto a 4 channel cassette tape. To enable sufficiently long deployment the tape speed was set at

0.2 mm/s. The internal time code is an amplitude modulated 10 Hz carrier frequency. The envelope of the high frequency part of the hydrophone channel was superimposed on the time track to help identify the water wave arrival accurately. The frequency response of the whole system (including the playback system) is band limited between 4.5 and 30 Hz (figure 15).

Four of the 11 land-based stations were Teledyne Geotech MCR-600 Microcorders which record in digital format at 60 samples per second (sps). The anti-aliasing filter, with a corner at 9.5 Hz, combined with a Mark Products L-4C 1 Hz vertical component seismometer bandlimits the system between 1.0 and 9.5 Hz. Receiver 9 was a slow speed (15/160 ips - 0.238 mm/s) 7-track Geotech FM analog recorder. The outputs from one vertical and one horizontal seismometer were recorded (each at two gain settings separated by 18 db) on 4 parallel tracks along with the WWVB time code on a fifth track. Both the vertical and horizontal seismometers were Willmore MK II models. The remainder of the seismographs used were EMR Mark II digital instruments (Backpacks) designed and built by the Earth Physics Branch. These recorders sampled at 60 sps and were bandlimited between 2 Hz and 25 Hz. Two Hz Mark Products L4A vertical component seismometers were used with the Backpacks. Table II lists the instrument type for each receiver.
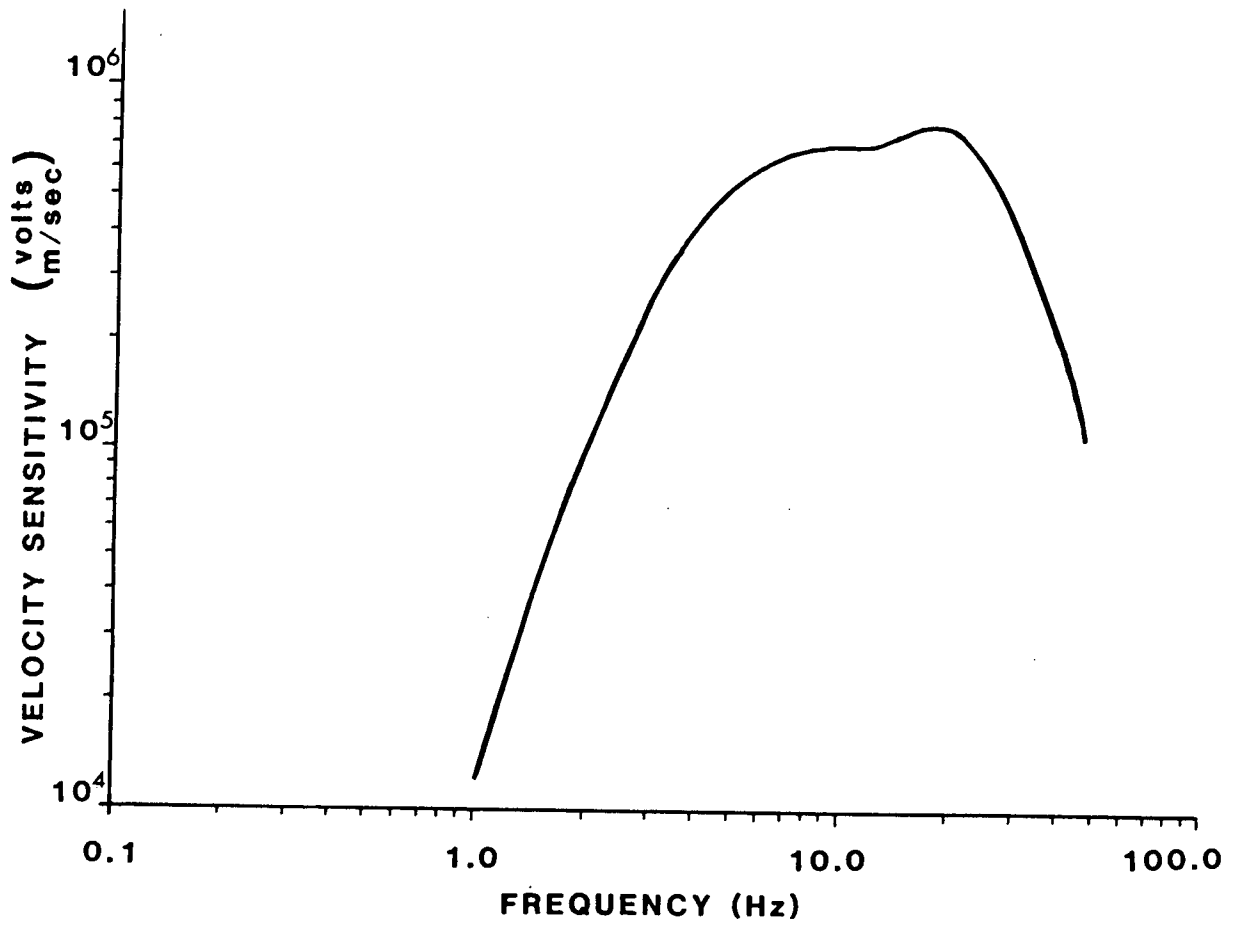
Figure 15 - Velocity sensitivity of the OBSs.

Receiver Number	Instrument Type
1 2 11 12 13 14	OBS (analog)
3 4 6 15 16 17	Backpack (digital)
9	FM (analog)
5 7 8 10	Microcorder (digital)

Table II - Instrument Type

2.3 Initial Data Processing

2.3.1 Digitization

A PDP 11/34 was used to digitize the OBS and FM analog data and to provide plots for quality control. Much of the data handling software was written by the author. The PDP 11/34 data handling package was used to digitize, demultiplex, organize, and plot the data. The OBSs, in particular, presented some problems for digitization.

The OBSs have a very slow tape speed to accommodate long deployment times and recording on a single cassette. The logistics of the 1983 Queen Charlotte Islands experiment required that the OBSs in Hecate Strait be capable of recording data over a period of 6 days. Since the refraction experiment was conducted concurrently with a UBC seismicity study (Berube,

1985) on the Queen Charlotte Islands, it was desirable to have
the OBSs deployed as long as possible. Because of the slow
speed of the OBS tape recorder playing the data back at 47.6
mm/s (1 7/8 ips) on a conventional high quality cassette deck
in the lab would seriously limit the realizable digitization
rate due to the maximum throughput capability of the digitizing
system. Therefore, the field recordings were transferred to 1/4
inch tape using a high quality FM tape recorder giving a final
speed-up factor between the field and lab tapes of 30 times.
Each of the four channels was digitized simultaneously at 120
samples per second (sps) giving a total throughput rate of
14,400 sps. It was felt that the slow OBS tape recorder speed
would introduce significant wow and flutter in the recorded
data. As well, the speed of each OBS tape recorder was set
independently and thus varied from instrument to instrument. To
overcome these problems the digitizing rate for the OBS data was
slaved to the 10 Hz time code carrier frequency, recorded
parallel with the data tracks, using a device designed and built
in the Department of Geophysics and Astronomy. The device is
similar, in principle, to a flutter compensation circuit used in
multi-channel FM tape recorders. By slaving the sampling rate
to the time code, speed variations of up to one Hz are well
corrected and the problems of tape stretch and speed variations
are avoided. Spot checks of the digitized data verify that
fluctuations in sampling rate are less than 0.1 sps. To avoid
aliasing, a 2-pole lowpass analog filter (Sallen and Key circuit
configuration) with a corner at 43 Hz was used to filter the OBS

data before digitizing.

The FM analog data also were digitized at 120 sps using the PDP 11/34 system. The digitizing rate was controlled externally by an accurate frequency generator. Sampling rate fluctuations due to tape stretch and tape speed variations were less than 0.1 sps. The FM analog system itself provided a sufficient anti-aliasing filter for the sampling rate chosen (the response curve is 3 db down at 20 Hz with a rolloff of 30 db/octave).

2.3.2 Time and Distance Corrections

All shot locations and OBS positions were determined from LORAN C navigation supplemented by satellite fixes when available. Relative accuracy of these positions is about 200 m with an absolute accuracy of 300 m (Hyndman et al., 1979). The land receivers were located on 1:50,000 scale topographic maps with an accuracy of about 150 m. Travel time errors introduced by location errors are negligible compared to origin time errors and picking errors.

An important problem in marine refraction studies using timed fuse-detonated explosives is the accurate estimation of shot depth. The timed fuses have a burning rate that increases non-linearly with depth and therefore cannot be used to accurately estimate the depth of detonation. Two independent methods were used to estimate shot depths and are described in detail in Appendix A. The maximum probable error in shot origin times caused by shot depth errors is about ± 0.03 seconds (Appendix A).

The internal clocks in the OBSs and Microcorders were corrected for drift. The OBS clocks were rated just previous to deployment and immediately after recovery. The Microcorder internal clocks were rated before and after each day of shooting. Drift for both the OBSs and the Microcorders was assumed to be linear between ratings. This assumption is probably valid for the OBSs since, once deployed, they are held at a constant temperature by the surrounding seawater. A test of linearity of drift for one of the Microcorders used in the experiment was done by Berube (1985) on the Queen Charlotte Islands just after our experiment concluded. She periodically rated the Microcorder internal clock with WWVB over a period of 12 days and found that the assumption of linear drift was valid. The FM analog recorded WWVB on a track parallel to the seismic channels and thus no drift corrections were necessary. Errors in estimates of the time of first samples of the digitized traces are summarized in Table III.

Receiver	Time of First Sample Error (seconds)
OBS	± 0.013
Microcorder	± 0.006
FM Analog	± 0.006

Table III - Errors in time of first sample

The data from the Backpacks were supplied by Earth Physics Branch without documentation of drift corrections or clock ratings. These errors, as well as picking errors, give total travel time errors of ± 0.05 s to ± 0.10 s for good quality first arrivals. Table IV shows a list of probable maximum errors for different portions of the data set.

Receiver	Travel Time Error (seconds)
1 2 (shots 1 to 16)	± 0.01
3 4 5 6	± 0.05
7 8 9 10	± 0.100
15 16 17 (shots 1-8)	± 0.300
15 16 17 (shots 9-33)	± 0.100

Table IV - Travel time errors

2.3.3 Data Quality and Filtering

The land stations located on the Queen Charlotte Islands recorded very good data. An exemplary power periodogram (figure 16) shows that the seismic signal is bandlimited between 1.5 Hz and 6 Hz with a peak at about 3 Hz. The three land receivers on the mainland recorded good data with the same
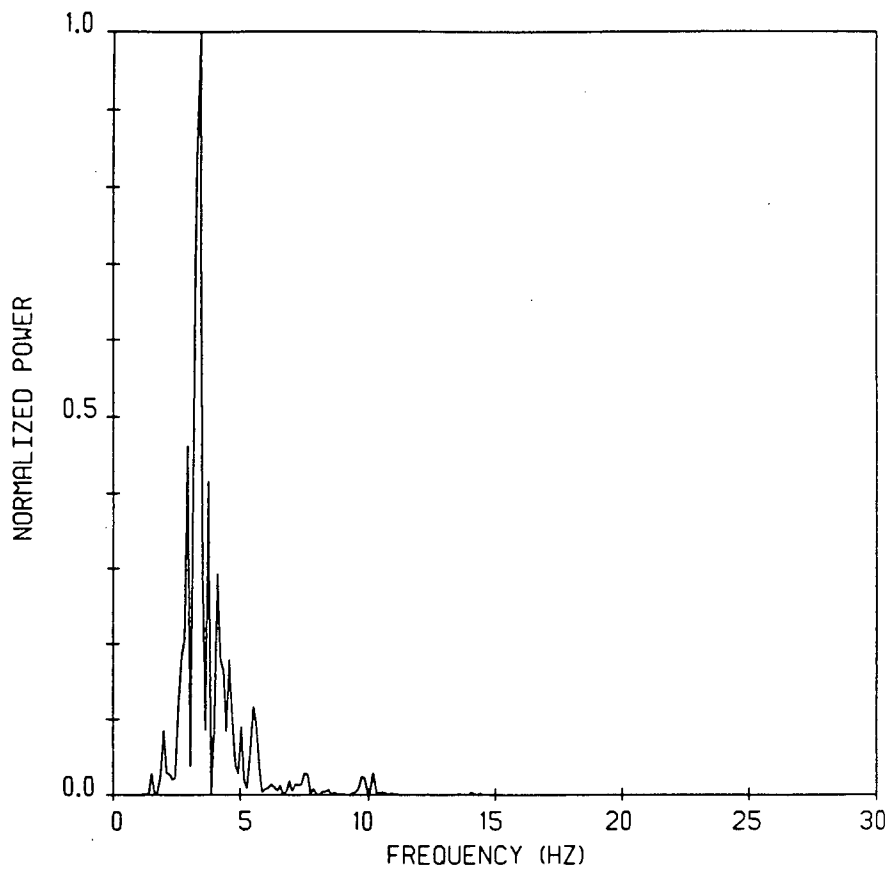
Figure 16 - Periodogram power for a land station.

This power spectrum was calculated over a 2 second window of the seismic signal recorded on Receiver 3.

frequency characteristics as the island receivers. The low frequency of the seismic signal was a characteristic of all the land receiver data. The 60 kg charges at far offsets were not well recorded. Receivers 7,8,9, and 10 were close enough to the water to record ocean induced microseisms. The frequency of the noise was below 1.5 Hz and was easy remove with filtering. All first arrival picks were made on unfiltered data with the aid of filtered sections.

The two OBSs west of the Queen Charlotte Islands recorded good quality data to a distance of about 85 km. Past this distance first arrivals were below the noise level (see record section in Appendix B). Prominent secondary arrivals are visible on receiver 1 for all shots. Filtering of these data did not improve the section beyond a distance of 85 km. Figure 17a shows the power periodogram for a 2 second interval of seismic signal and 17b the same for a portion of background noise. A comparison of these two spectra indicates that most of the seismic energy is below 5 Hz. This is consistent with the frequency characteristics of the seismic energy recorded on the land receivers. There is a significant amount of power at higher frequencies due to background noise which is visible on all of the OBSs. Eight pole zero-phase Butterworth filters with different frequency limtis were applied to the data from receiver 1. A bandpass from 0.1-15 Hz provided the best enhancement for this data set. Attempts to filter out the noise peak at 7 Hz degraded the first breaks past 85 km too much to be acceptable.
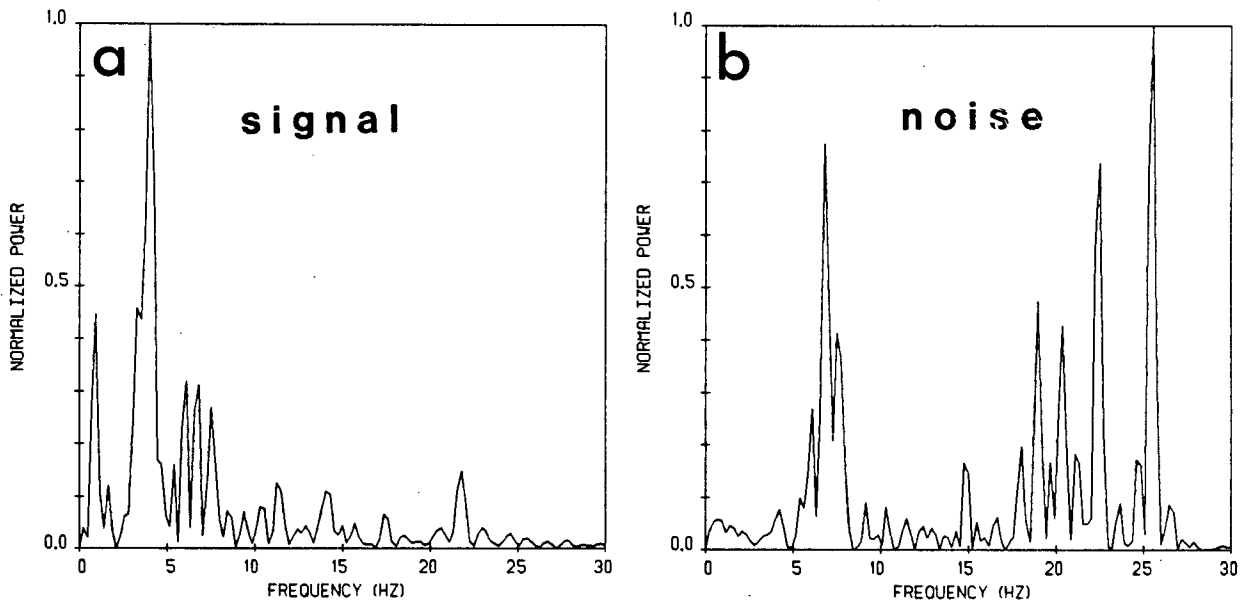
Figure 17 - Power spectra of noise and signal for an
OBS.

These periodograms were computed from data recorded on
Receiver 7 over a two second window of seismic signal (a),
and background noise (b). The seismic signal is band
limited between about 1 to 5 Hz. There is significant noise
in the 5 to 10 Hz range.

The OBSs deployed in Hecate Strait did not record any data except for some strong events observed on the vertical seismometer channel of receivers 12, 13, and 14. The very poor data quality in Hecate Strait is thought to be caused by the environment of the instruments. Hecate Strait is a very shallow body of water with a soft sediment bottom and it is believed that tidal currents and perhaps ship induced noise obscured the seismic signal. Figure 18 shows sample power periodograms from receivers 11 and 12 over 2 second windows of both background noise and signal. The spectra for receiver 12 indicate that the signal is recoverable. There is significant energy between 1.5 and 5 Hz on the 'signal' spectrum that is absent on the 'noise' spectrum, a band consistent with observed seismic signals on land stations and the OBSs west of Moresby Island. An 8-pole zero-phase Butterworth filter was used to attempt to recover the signal on the Hecate Strait OBSs. A very narrow bandpass of 1 Hz to 5 Hz was successful in recovering the strong events, corresponding to shots 1 through 4, on receiver 12, 13, and 14 but no other recognizable seismic energy was recovered. The OBS response is not good below 4.5 Hz (figure 15), mainly because of the 4.5 Hz seismometers used. Thus energy in the frequency range of interest is attenuated relative to the higher frequency noise recorded on all of the Hecate Strait OBSs. This is a problem that is significant on all the other OBSs and is well illustrated by the spectra of receiver 11 (figure 18 c and d). The 'noise' and 'signal' spectra for receiver 11 are almost identical and contain little energy below 5 Hz. Both have the
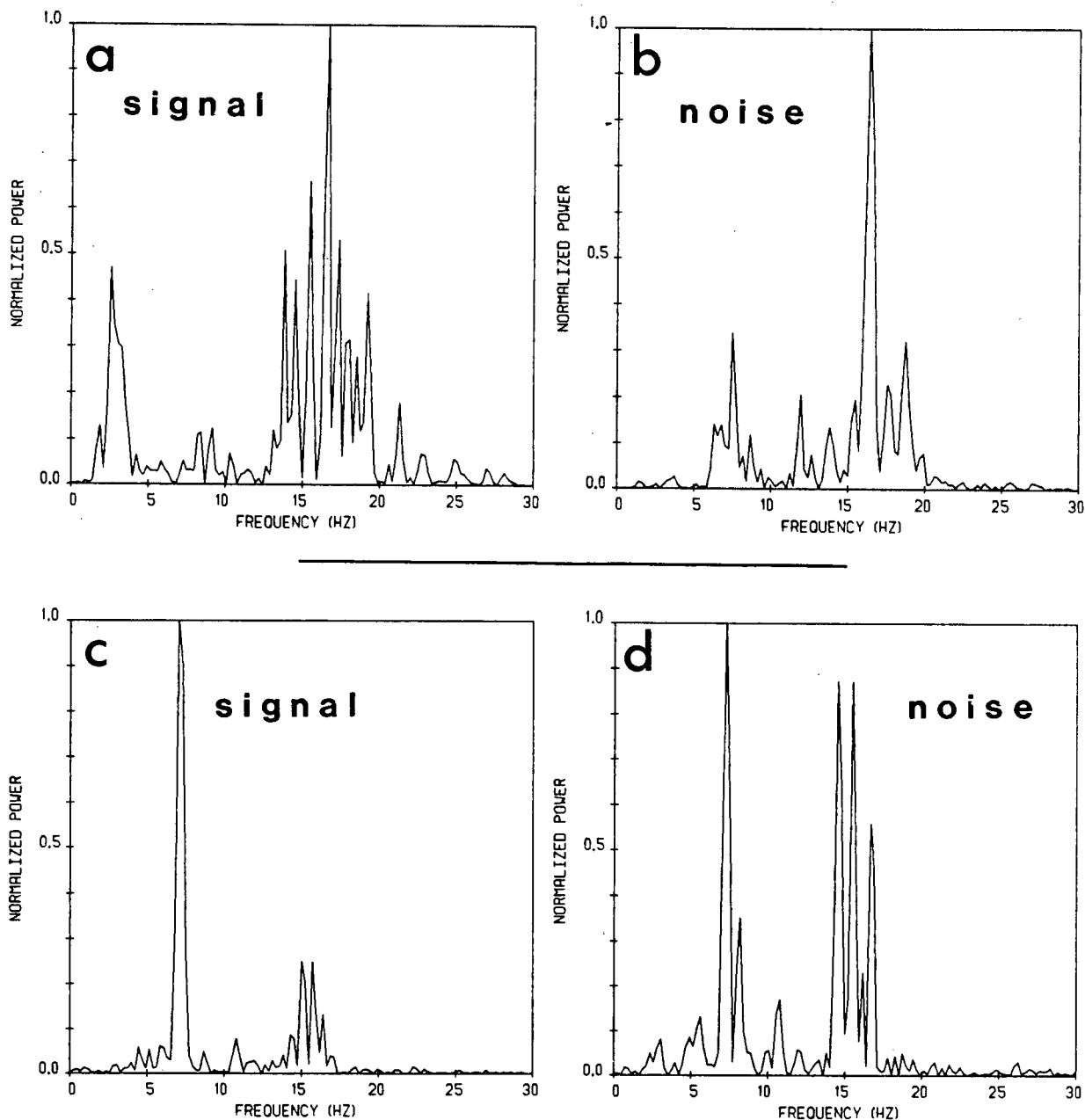
Figure 18 - Power spectra signal and noise for Hecate
Strait OBSs.

These periodograms were computed over a 2 second window of
data.
    (a) Receiver 12 - seismic signal
    (b) Receiver 12 - background noise
    (c) Receiver 11 - seismic signal
    (d) Receiver 11 - background noise
The seimic signal recorded on receiver 12 is band limited
between 1 and 5 Hz (a). There is significant noise above 5
Hz (b). A bandpass filter of 1-5 Hz was necessary to
recover any recognizable seismic signal.
Filtering the data from receiver 11 did not improve the
quality. The similarity of c and d indicates that any
seimic signal present is completely obscurred by background
noise.

same two peaks, one between 15 and 20 Hz and another between 5 and 10 Hz. The same filter as above was applied with varying frequency limits but no observable seismic energy was recovered.

2.4 Summary

Except for the 4 OBSs deployed in Hecate Strait all of the receivers yielded good quality data. The land stations deployed on Moresby Island recorded excellent data while the mainland stations were noisier because of the far offset from the sources. The two OBSs west of Moresby Island also recorded good data. Some seismic signal was recovered from the Hecate Strait OBSs by filtering the data using a very narrow bandpass. The full data set is described in an open file report (Clowes, 1984). All of the explosion data are presented as common receiver record sections in Appendix B.

III. INTERPRETATION

3.1 Modelling and Uniqueness

A forward modelling process was used to calculate two-dimensional synthetic seismograms that matched the data. Although it is possible to construct a model that fits the data using such a modelling technique there exists an infinite number of other models that will also satisfy the data. The seismic refraction problem is very non-unique even though the data constraints often outnumber the parameters. This non-uniqueness stems from the lack of constraints on a few parameters in the model. For example, if no turning rays or reflections from the lower boundary exist in a layer the velocity gradient for that layer is not well constrained. It is necessary, therefore, to employ all of the constraints that one can muster. First and foremost, the model must be geologically reasonable. Obviously, any other available concrete data must be used to further restrict the non-uniqueness of the problem.

The problem of non-uniqueness must also be addressed in the data acquisition process. By choosing the optimum array of shots and receivers it is possible to reduce the number of poorly constrained parameters in the model. The reversed seismic refraction profile is a common example of such an experimental design technique. It allows both the dip of the refracting interface and the velocity of the layer below the refracting interface to be determined uniquely. Because of

environmental regulations it was not possible to reverse the 1983 refraction line by shooting in Hecate Strait (figure 14). An attempt to alleviate this problem was made by detonating many explosions at increasing offset from the linear array of receivers. This, in effect, reverses the line over some of its length. This 'pseudo-reversal' is exploited by modelling the data in both common shot and common receiver gathers that sample the same area of the earth. The line is not reversed in the usual sense; however, it is necessary to satisfy both the common shot and common receiver profiles with an identical model. Each record section or profile is modelled separately until a common model fits the data sufficiently well.

The forward modelling technique, applied to such a complicated data set, has two main drawbacks. It is impossible to alter each model in a consistent manner while attempting to fit the data. This lack of consistency may affect the final model in unknown ways. The method is impractical for large data sets. Perhaps a more satisfying approach would be to construct a model using a two-dimensional inversion technique. This would ensure that the final model fits the total data set in some consistent manner. The two-dimensional inverse problem applied to seismic refraction is, for the reason stated previously, very non-unique and therefore unstable. Spence (1984) applied two-dimensional travel time inversion techniques to a refraction data set similar in design to the 1983 Queen Charlotte Islands experiment (multiple shots recorded on multiple receivers). He found that because the problem is unstable it can be used only

to 'fine tune' a model that has largely been constructed by forward modelling methods. Because of time constraints, two-dimensional travel time inversion was not attempted as part of this thesis.

It is also important to note that it is difficult to objectively determine how well the model should fit the data. This is particularly true if the model is parameterized non-uniformly such as in this thesis. In this case the characteristics of the final model are biased by the initial model in unknown ways. In any forward modelling or iterative inversion procedure it is difficult to objectively determine which features of the model are required by the data. The goodness of fit thus becomes subjective. Noting these concerns we will proceed in a careful manner.

3.2 Description of the Modelling Algorithm

All models were constructed using a ray method synthetic seismogram algorithm for laterally inhomogeneous media (Spence, 1984; Spence et al., 1984). Ray paths and travel times are calculated using a modified version of the Whittall and Clowes (1979) ray tracing program; amplitudes are computed using asymptotic ray theory. The model is parameterized as a series of large blocks with the velocity and linear velocity gradient defined at the top of each block. The ray paths are then traced as arcs of circles with a radius defined by the value of the gradient (see Gebrande, 1976). Snell's Law determines the behaviour of rays crossing boundaries. Because this is a ray

method, all the limitations of ray theory apply to the modelling algorithm, except that "pseudo" head waves can be generated as described by Whittall and Clowes (1979) and Spence et al. (1984). Thus turning rays, pre- and post-critical reflections, multiple reflections and head waves can be invoked if desired. The algorithm is fast and efficient allowing the user to easily and economically test many variations of a model.

3.3 Interpretation of Individual Profiles

3.3.1 The Final Model - A Preview

The final model (figure 19) was constructed by modelling 5 common receiver and 2 common shot profiles. A short description of the final velocity model will aid in placing the interpretations of each profile in perspective. The main feature of the model is the lateral change from a typical oceanic crust to thicker crust beneath the Queen Charlotte Islands and Hecate Strait. The Queen Charlotte terrace separates these two regions. In the model, the velocity structure of the lower oceanic crust is very similar to that of the lower terrace region and the lower crust east of the fault zone, although this may represent limitations of the data set and modelling procedure. The oceanic Moho is at about 10 km depth. Beneath the terrace and further east, the Moho dips at 5° to the east reaching a depth of 35 km beneath the mainland coast.

The shallow oceanic sediment layer (1.8 km/s) is constrained in depth by a continuous seismic reflection profile
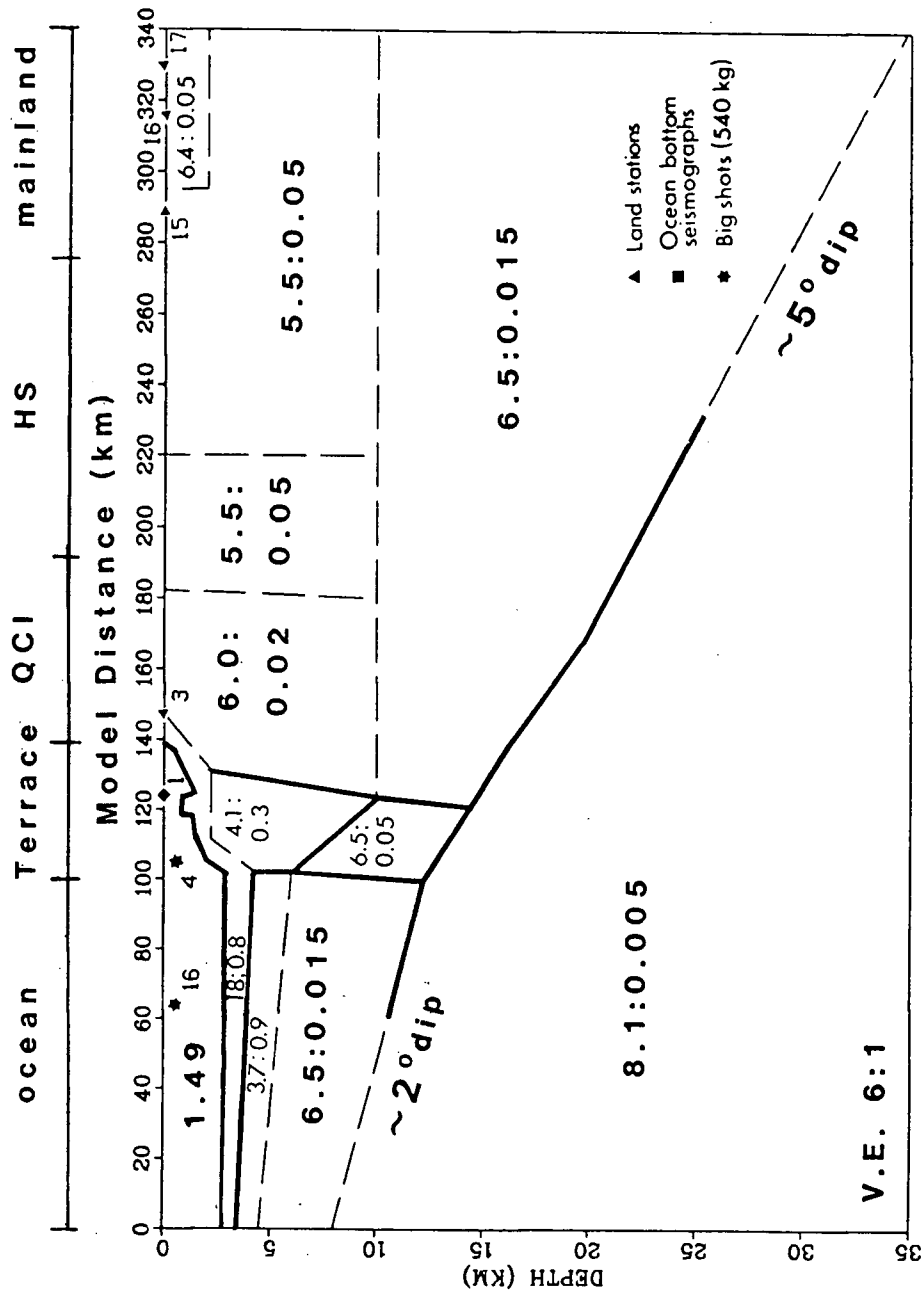
Figure 19 - The final velocity model.

Solid lines indicate boundaries that are well constrained by the data. Dashed lines indicate boundaries that are not well constrained. The first number in each block is the velocity (in km/s) at the top boundary of the block. The second number is the velocity gradient (in km/s/km). The model distance is plotted across the top of the figure. Positions of shots and receivers used in this study are superimposed on the model. QCI = Queen Charlotte Islands. HS = Hecate Strait.

collinear with the offshore section of our refraction line (Davis and Seemann, 1981). The layering below this sediment zone is not well constrained by our data set. The oceanic structure from a seismic refraction profile (Horn et al., 1984 and Horn, 1982) parallel to the Queen Charlotte fault zone and south of our survey was the basis for choosing the ocean structure in our model. The lack of any near surface details for the Queen Charlotte Islands eastwards in the final velocity model results from the design of the experiment. More shots near the island and mainland stations would be needed to provide the constraints to construct an upper crustal model for this region. The refraction models of Johnson et al. (1972) and Forsyth et al. (1974) provided some constraints as to the approximate velocity structure and depth to mantle in the mainland region east of the Queen Charlotte Islands. Neither of these surveys was adequate to provide a detailed velocity model of the crust in this area.

3.3.2 The Choice of Data Sets for Modelling

For the purposes of this thesis, only a portion of the entire data set was fully interpreted. The objective of this research was to study the deep crustal structure beneath the Queen Charlotte Islands and Hecate Strait and the data set was chosen accordingly. The criteria used in choosing the profiles to be modelled were:

(1) the data must sample the part of the earth that is to be studied,

(2) the data must take advantage of the 'pseudo-reversal' of profiles, and

(3) the data must be of sufficient quality to interpret. After preliminary modelling of every common receiver profile it became apparent which ones best met the above criteria. Common receiver profiles 1, 3, 15, 16, 17, and common shot profiles 4, and 16 were chosen for modelling. Except where noted, all distances referred to in this chapter are shot-receiver distances and, where applicable, are followed by model distances in parentheses. A discussion of the interpretation of each profile follows.

3.3.3 Common Receiver Profile 1

Receiver 1, an OBS, is the most westward receiver along the line (figure 14). It was deployed on the Queen Charlotte terrace, in 900 m of water. It is possible to correlate shot-receiver distance to model distance by viewing the appropriate figure displaying both data and synthetics. The data are of good quality to a distance of 80 km beyond which the first arrivals are not visible (figure 20). The first arrivals to 49 km have errors less than ±0.05 s; arrivals past 49 km are more uncertain and the estimated travel time errors are in the order of ±0.1 s. The data have been corrected for spherical spreading (by multiplying the data by r^2 where r is the shot receiver distance) and for shot size by assuming that the recorded amplitudes are proportional to $W^{2/3}$, where W is the weight of the shot in kilograms (O'Brien, 1960). This did not correct the

Figure 20 - Comparison of the data and synthetics for
Profile 1.

The data for common receiver profile 1 (a) is compared with
the synthetic seismogram (b) computed using the final model.
Arrowheads on (a) denote first arrival picks of mantle
refracted rays. The shot-receiver distance is plotted along
the top of (a). The model distance is plotted along the
bottom of (b) and between (a) and (b). The data are plotted
with a reducing velocity such that arrivals with an apparent
velocity of 8 km/s appear horizontal.
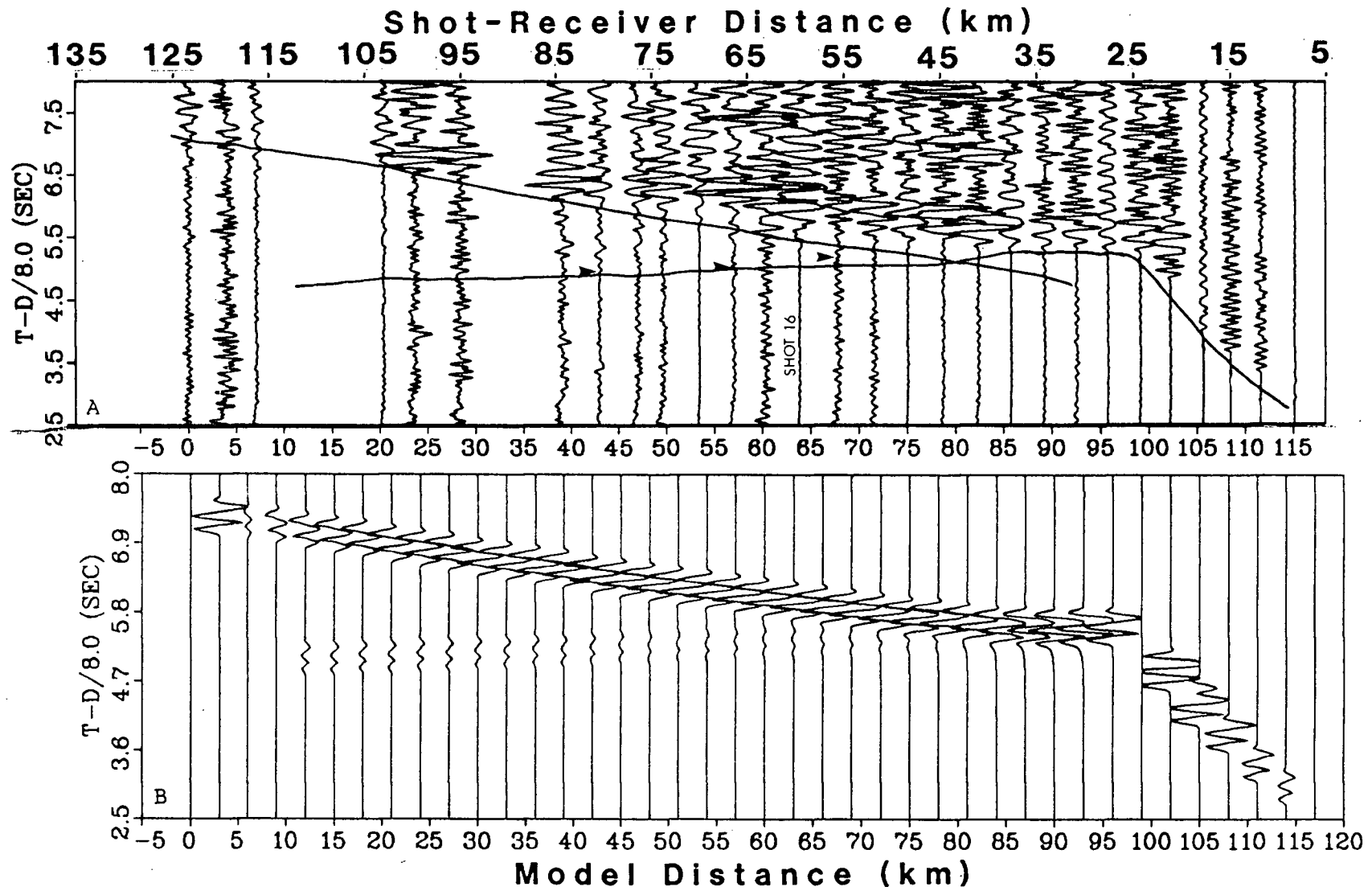
close shots for receiver 1 well as is indicated by the amplitude
variation over the first six traces (every fourth trace is a 540
kilogram shot).

Some features of this profile are very important. The
sharp break from crustal arrivals to mantle refractions
occurs at 25 km, providing an estimate of the depth to the
mantle. The low apparent velocity of the crustal arrivals are a
result of slower crustal material and the effect of topography
of the Queen Charlotte terrace. The Pn mantle refractions have
an apparent velocity slightly over 8 km/s but they are very weak
and die out by 85 km. The high amplitude secondary arrivals
from 40 km to 125 km have an apparent velocity of 6.8 km/s.
These arrivals merge with the Pn arrivals at about 40 km which
corresponds to the critical point.

The modelling procedure entailed fitting the travel times
and then modelling the amplitude characteristics of the data.
Altering the model to fit amplitude characteristics often
degraded the travel time fit. Both travel times and amplitude
fits were then modelled in conjunction until a satisfactory
model resulted.

The data from receiver 1 samples the oceanic and terrace
regions west of the Queen Charlotte Islands. Figure 21 shows
ray tracing through this portion of the final model. The
synthetic seismogram for this profile and the data are presented
in figure 20. The rays arriving between 8(117) km and 25(99) km
are traced through the low velocity - high gradient upper
terrace region. A low velocity and high gradient were necessary
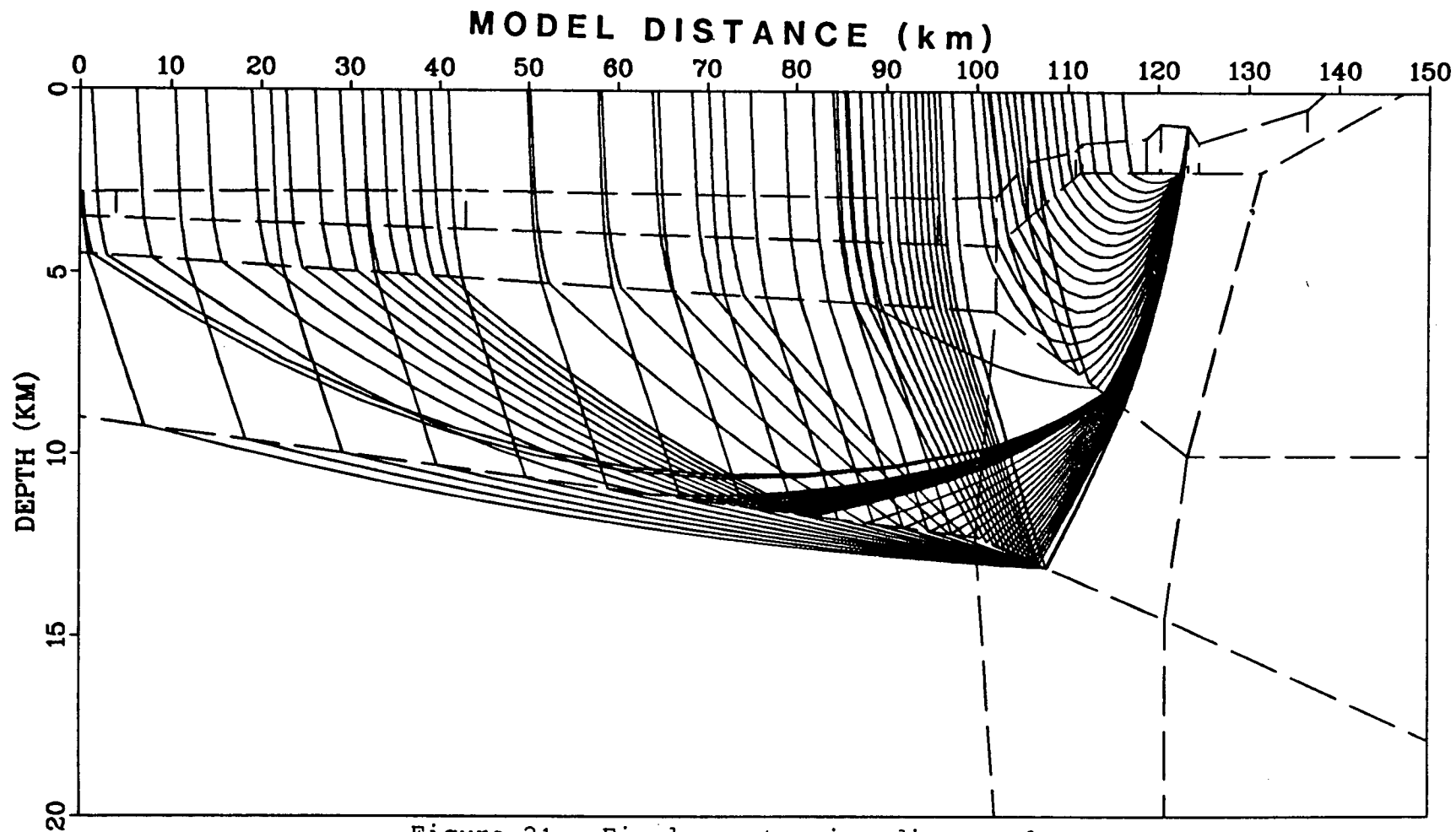
Figure 21 - Final ray tracing diagram for
Common Receiver Profile 1.

(see text for explanation).

to fit both the travel time and amplitude characteristics for these arrivals. The synthetic amplitudes increase from 8(117) km to 25(99) km where they merge with the strong secondary arrivals at 30(95) km. The mantle refractions have an apparent velocity controlled by the mantle velocity, and the dip on an upper oceanic layer beneath the shots. In other words, the $2°$ eastward dip of the oceanic Moho in the model is not well constrained. It may indeed be horizontal and a more shallow structure may account for the apparent velocity of these arrivals. The strong secondary arrivals from 30(90) km to 125(0) km are interpreted as post-critical reflections from the Moho (figure 21). The travel time and amplitude fit is good (figure 20). These arrivals constrain the average velocity above the Moho and thus allow the approximate depth to the Moho to be determined. Variations in the upper oceanic layers, which are not well constrained, could influence the depth to the Moho. For example, a change in velocity of the 3.7 km/s layer to 4.2 km/s would force the oceanic Moho to be about 2 km shallower. These secondary arrivals also constrain the velocity gradient in the lower oceanic crust to be very low (0.015 km/s/km) in order to propagate energy from the farthest shot to the receiver. The thickness of the 1.8 km/s layer, representing unconsolidated sediments, is constrained by continuous seismic profiles in the area (Davis and Seemann, 1981). The oceanic structure of the final model is very similar to that of Horn et al. (1984).

The terrace region was divided into an upper block and a lower block. The position of the boundary separating the upper

and lower terrace regions is not well constrained. The lower block must have a much smaller gradient than the top block in order for the wide-angle reflections to reach the receiver. The velocity structure of this block is suspiciously similar to the lower oceanic layer.

3.3.4 Common Receiver Profile 3

Receiver 3 is located just east of the Queen Charlotte fault zone and is the most westward land station on the Queen Charlotte Islands (figure 14). This profile was chosen because it exhibited a marked lack of the strong secondary arrivals so prominent on receiver 1. The data quality is excellent (figure 22 a). Estimated travel time uncertainties are less than 0.05 s. The secondary arrivals visible at far offset on receiver 1 are not evident on any of the receivers east of the Queen Charlotte fault zone (see Appendix B). This suggests there is a significant lateral change in the crust across the terrace region. The first arrivals on receiver 3 are similar in character to receiver 1. The crustal arrivals break over at about 45 km to Pn refractions with an apparent velocity slightly greater than 8 km/s. The large amplitude arrivals from 45 km to 68 km are significant and correspond to energy that has travelled through the terrace region. First arrivals from 33(115) to 45(107) km have travelled through the upper terrace block with its high velocity gradient. Consequently the amplitudes are large and increase with offset. Traces 1 and 4 (at 33 and 42 km) of the data illustrate this effect. Traces 2

Figure 22 - Comparison of data and synthetics for
Common Receiver Profile 3.

(a) data.
(b) synthetics produced from final ray tracing diagram.
The travel time curves from the synthetic arrivals are drawn
over the data section. See Figure 20 for an explanation of
distance and time axes.

and 3 were from 60 kg charges, and as noted previously, it is believed that the standard charge-size correction has not worked well at near offset distances. At 45(105) km distance these arrivals merge with another set of large amplitude arrivals for which the apparent velocity is about 6.8 km/s. They continue to about 68(78) km. This phase has been interpreted as reflections from the Moho beneath the terrace. It ends abruptly because of the change in dip of the Moho beneath the outer terrace scarp (figure 23). The synthetic seismograms mimic well these amplitude characteristics (figure 22). First arrivals extending from 58(90) km to 148(0) km are due to rays refracted through the upper mantle. The observed and synthetic travel times and amplitudes agree well for this phase. A secondary arrival from 80 to 112 km (model distance) on the synthetic section is due to rays turning in the lower oceanic crust. Such a prominent phase is not observed on the data section although there is substantial energy in the coda of observed traces over this distance range.

3.3.5 Common Receiver Profile 15

Receiver 15 is the most westward mainland station (figure 14). This record section, and those of receivers 16 and 17, were chosen because they were distant from the shots (therefore ray paths to them sampled deepest into the earth) and because they exhibited strong secondary arrivals (figure 24 and Appendix B). The first arrivals from shot-receiver distance of 175 to 195 km are very weak and emergent. Because of their
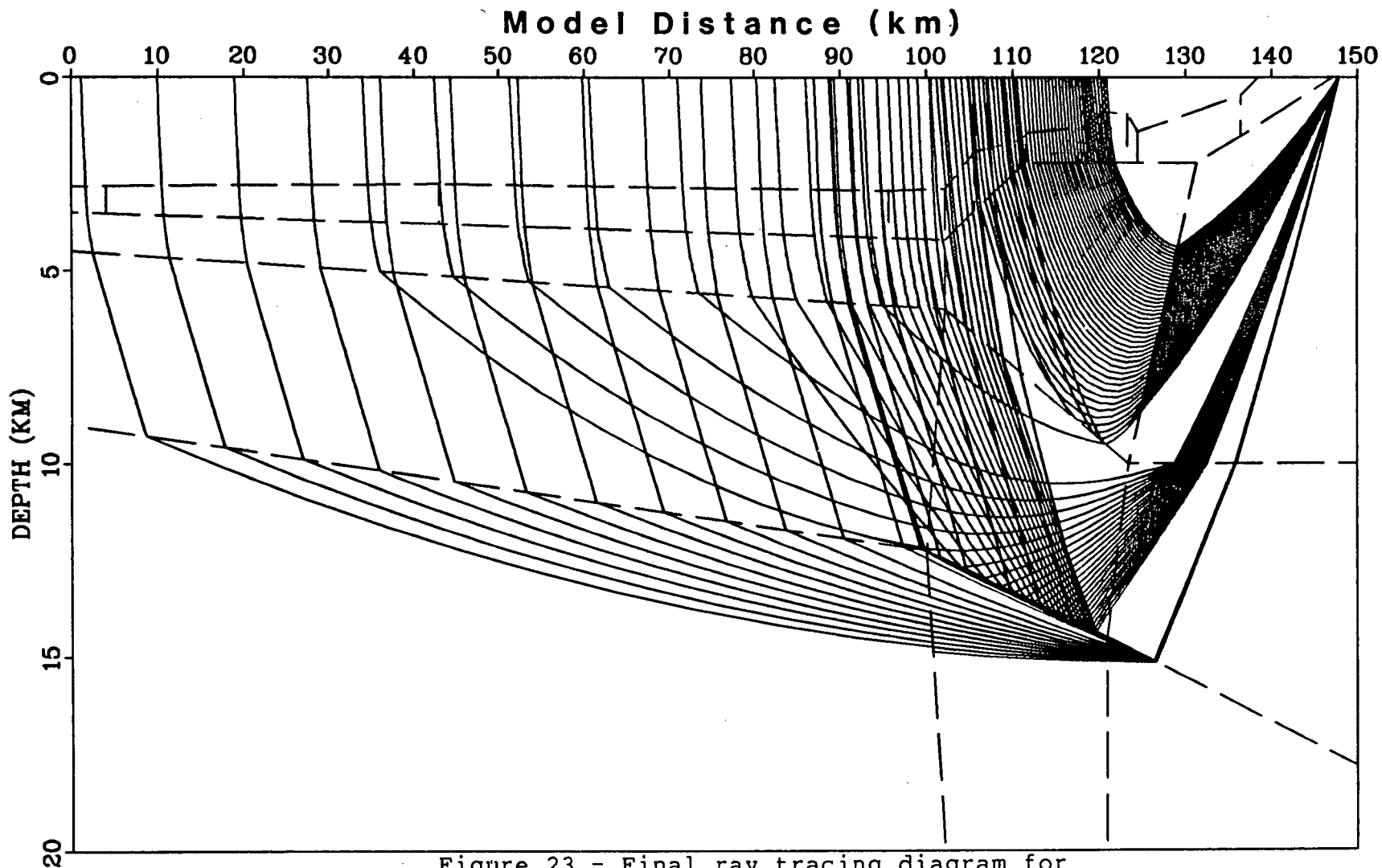
Figure 23 - Final ray tracing diagram for
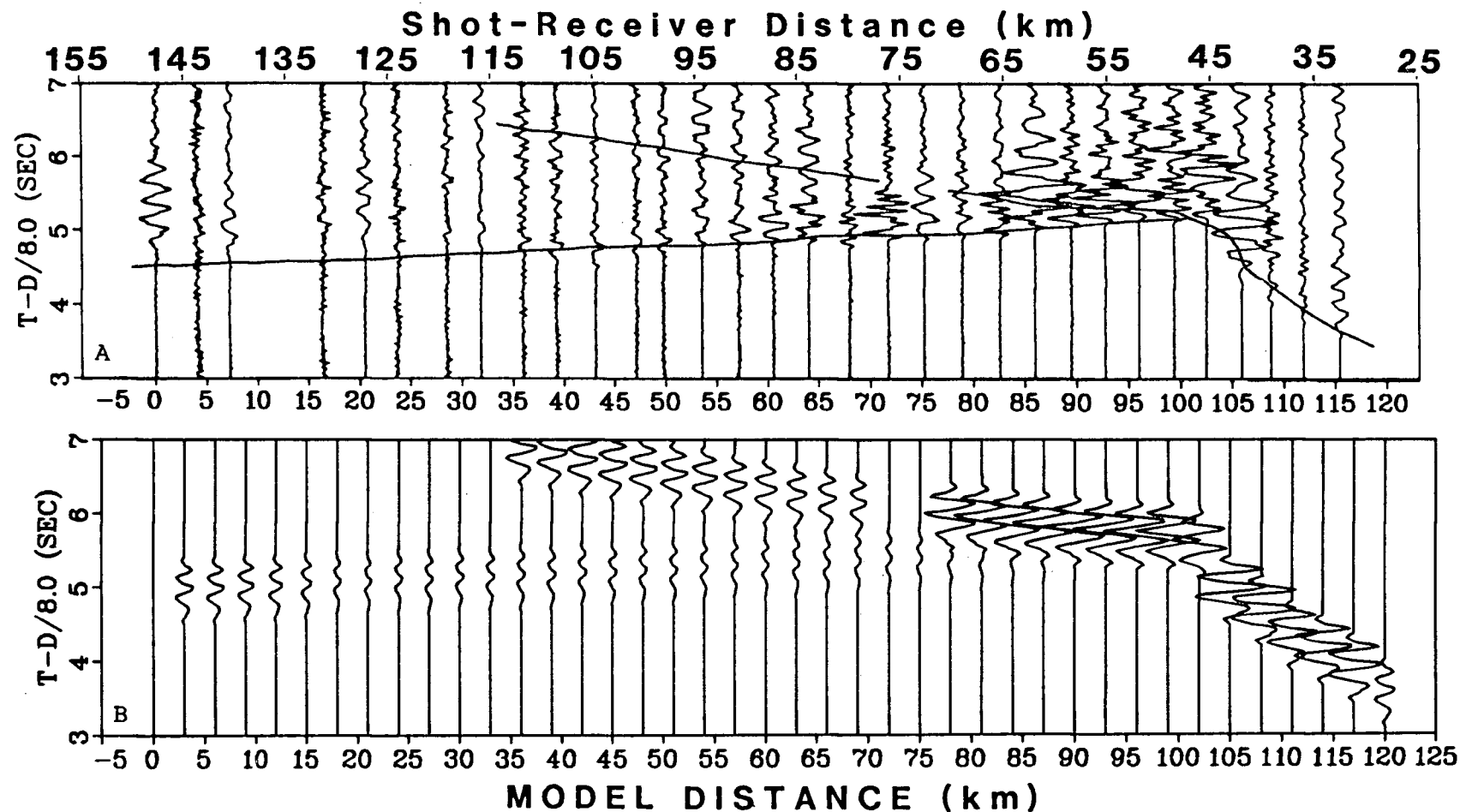Common Receiver Profile 3.

(see text for explanation).
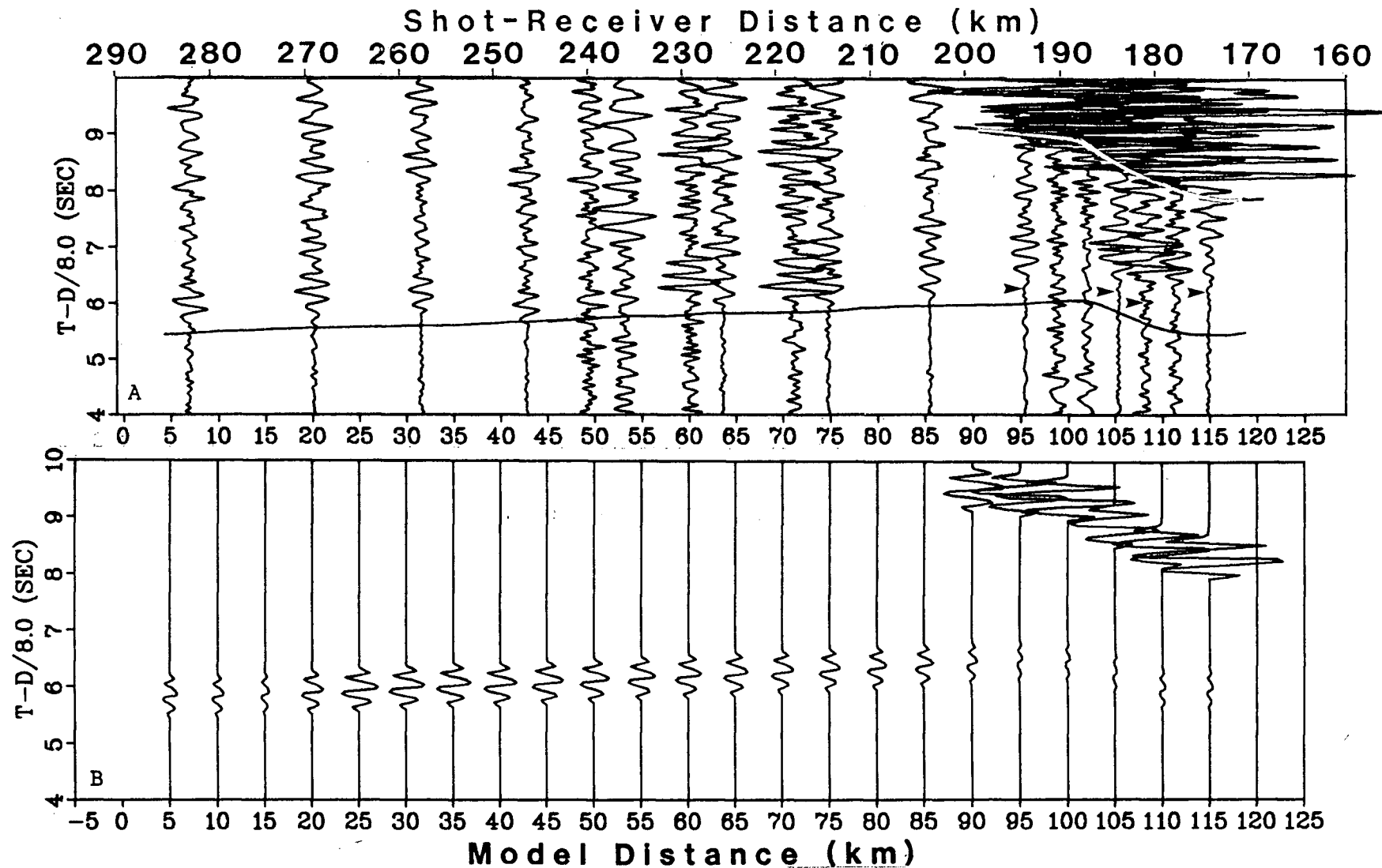
Figure 24 - Comparison of data and synthetic for
Common Receiver Profile 15.

(a) data.
(b) synthetics produced from final ray tracing diagram.
The travel time curves from the synthetic arrivals are drawn over the data section. The arrowheads mark first picks for mantle refracted arrivals. See figure 20 for an explanation of distance and time axes.

emergent nature and small amplitudes travel time picks were difficult to accurately determine and it is possible that the picks do not represent the actual first breaks. From 200 km to 285 km the first arrivals (Pn phase) are clearer with an estimated travel time uncertainty of about ±0.10 s. The mainland data (figure 24) are noisier than the Queen Charlotte Islands data (figure 22) because of the large shot-receiver distances. All of the travel time picks were made on unfiltered data with the aid of the filtered sections. The apparent velocity of the Pn arrivals past 210 km is about 8.5 km/s. The very strong secondary arrivals at about 8.0 s end abruptly at 190 km. These strong arrivals occur only for shots that were detonated over or very close to the Queen Charlotte terrace. The data recorded on receivers 16 and 17 are very similar to this profile.

The final model with traced rays is shown in figure 25. The strong secondary arrivals have been interpreted as post-critical reflections from the Moho beneath the Queen Charlotte Islands. The travel times fit well but the amplitudes are slightly small. Nonetheless, the secondary reflection events do have a much larger amplitude than all other arrivals on the synthetic section. The abrupt end of these reflections is modelled correctly by a combination of the change in dip of the Moho at 100 km (model distance) and the high gradient upper terrace region.

The very weak mantle refractions for shot-receiver distances from 175(115) km to 190(95) km are modelled well in
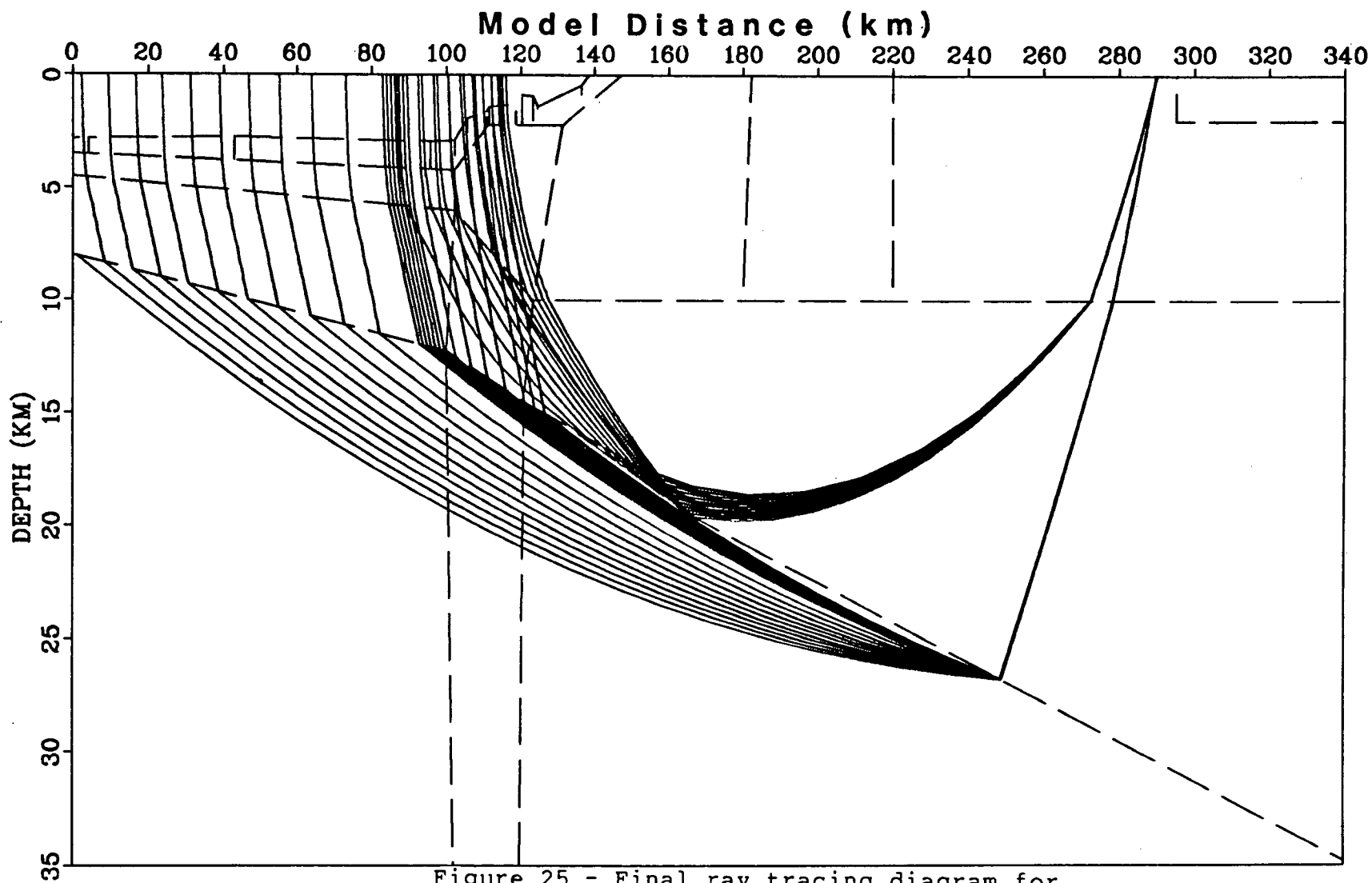
Figure 25 - Final ray tracing diagram for
Common Receiver Profile 15.

(see text for explanation).

amplitude. The eastward dip of the Moho beneath the terrace and the low gradient in the mantle contribute to the small amplitude arrivals. The model travel times are earlier than the picked arrivals by as much as 0.3 s on some traces. Synthetic travel times for receivers 16 and 17 exhibit this same characteristic. These weak arrivals are very emergent and the picks are not reliable as they are at the level of the background noise. Other arrivals on this data section and other sections sample the terrace region and fit the model well, indicating that this misfit is not due to local structure beneath the shots over the terrace. The velocity structure of the terrace region is reasonably well constrained by receivers 1, 3, and common shot gather 4. The wide-angle reflections recorded on receiver 15 also sample the same region as the weak arrivals. Forcing the weak arrivals to fit the data travel times makes the reflections late with respect to the data. To correct this an 18 to 20 km deep Moho beneath the the terrace region would be required. This model has been tested and is inconsistent with the data. It would require a steeply dipping segment of Moho joining the ocean crust to the terrace crust. This in turn creates a large shadow zone west of 200(90) km where no mantle refractions can penetrate to the surface. This is not observed on the data. The mantle refractions on receiver 15 from 205(90) km to 285(0)km constrain the Moho to be dipping gently from the edge of the oceanic crust eastward. For the above reasons it is felt that the misfit may be a result of not being able to pick the first arrivals because they are below the background noise level

and not due to structure in the terrace region.

The increase in amplitude of the mantle refractions at 225(85) km is modelled with a change in dip of the Moho beneath the outer edge of the terrace. These arrivals have larger amplitudes than the weak energy recorded from 175(115) km to 195(90) km because the Moho boundary is more horizontal.

3.3.6 Common Receiver Profiles 16 and 17

Profiles 16 and 17 are very similar to one another. Receiver 16 is located on Pitt Island just west of the mainland coast (figure 14). Receiver 17, located on the mainland, is the most eastward station. Profile 16, a common receiver gather, is displayed in figure 26 and Appendix B. Profile 17 data, also a common receiver gather, is found in figure 28 and Appendix B. The data are very noisy because of the high gain required at such long shot-receiver distances. The data recorded on receiver 17 are of marginal quality. Arrivals between 245 km and 325 km have an estimated uncertainty of ±0.3 s. First arrivals between 215 km and 235 km are very weak and emergent and have even larger uncertainties. Receiver 16 has better quality data. The weak emergent arrivals between 195 km and 222 km have an estimated error of about 0.3 s. The arrivals between 225 km and 302 km have uncertainties of about 0.15 s. Since the characteristics of these two profiles are very similar they will be discussed together.

These data were modelled to help constrain the position of the Moho further downdip beneath Hecate Strait. The final model

Shot-Receiver Distance (km)
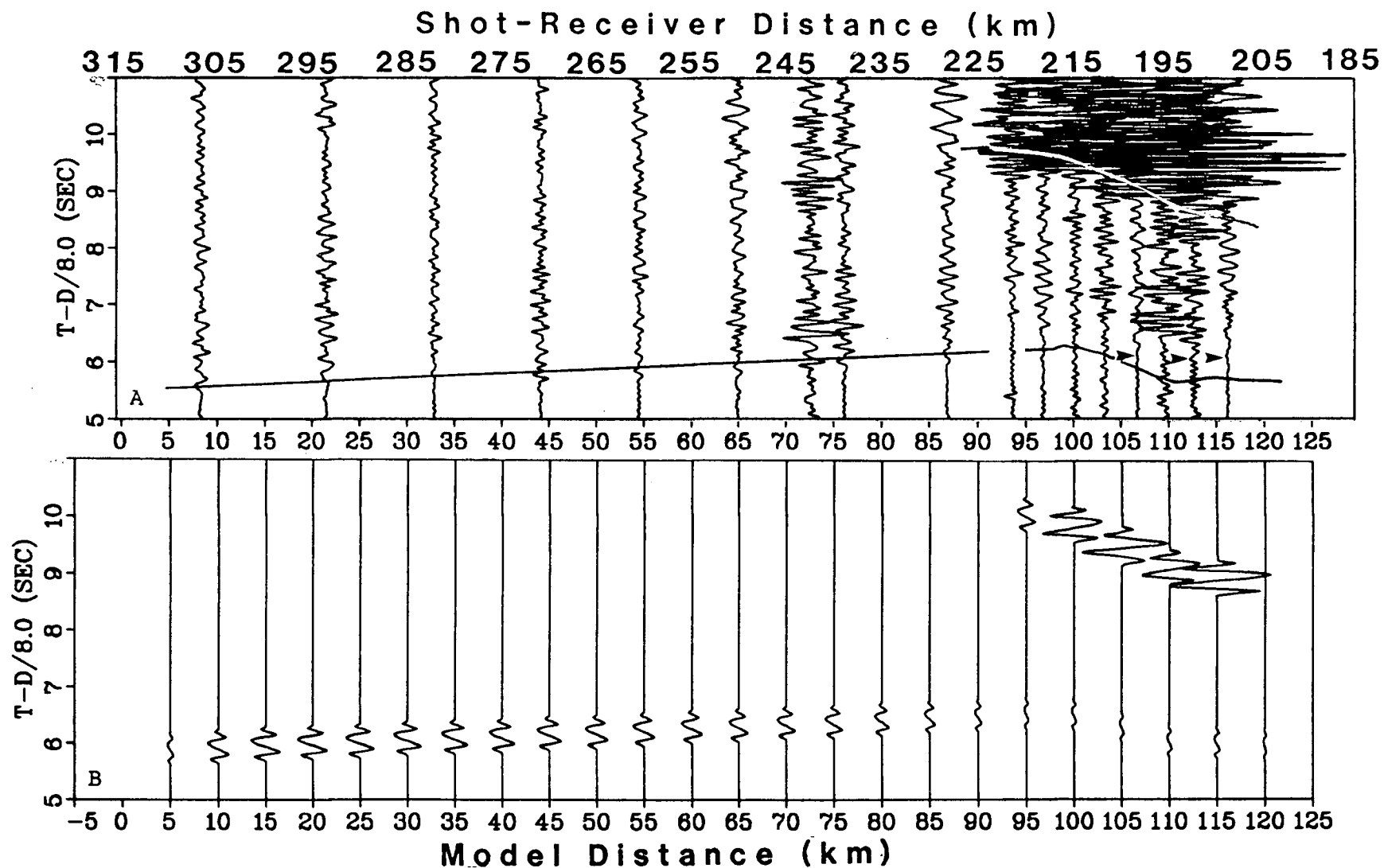
Figure 26 - Comparison of data and synthetic for
Common Receiver Profile 16.

(a) data.

(b) synthetics produced from final ray tracing diagram.
The travel time curves from the synthetic arrivals are drawn

over the data section. The arrowheads mark first picks for
mantle refracted arrivals. See figure 20 for an explanation
of distance and time axes.
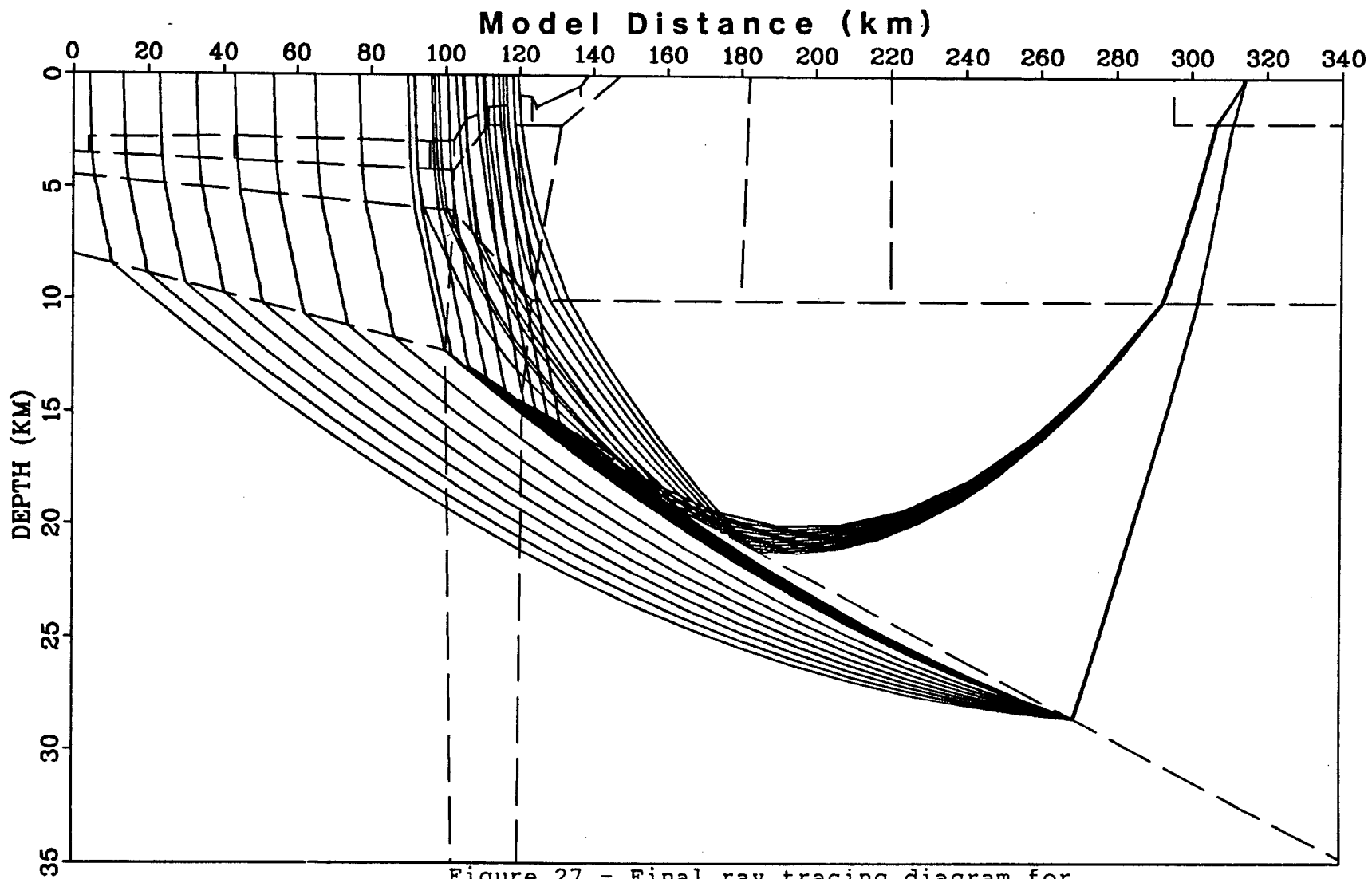
Figure 27 - Final ray tracing diagram for
Common Receiver Profile 16.

(see text for explanation).

with traced rays (figure 27 and figure 29) is very similar to
figure 25 except that the crust is sampled farther to the east
than receiver 15. The amplitudes of the weak emergent arrivals
at the shorter offset distances were modelled well but the
travel times were too early(figure 26 and 28), as was the case
for receiver 15. However, the misfit is in the order of the
travel time uncertainties. The strong, wide-angle reflections
are modelled well in amplitude and travel time. These rays
reflect the Moho further downdip and help to define its eastward
slope to a distance of 200 km (model distance). The amplitudes
and travel times of the mantle refractions up through the
oceanic layers (west of the terrace region) are modelled well.
The increase in amplitude beyond 225(89) km on profile 16 and
240(90) km on profile 17 corresponds to the change in dip of the
Moho at the outer terrace edge and fits the data well. The lack
of a shadow zone for these refracted arrivals surfacing just
west of the terrace region further indicates that the Moho dips
gently eastward beneath the terrace region.

It was found that all model arrivals on receivers 16 and 17
were too late without the small 6.4 km/s block immediately
beneath the stations (figures 19 and 27). The same effect could
be caused by a shallower Moho beneath the receivers but the
corner introduced by bending the Moho creates a shadow zone for
mantle arrivals at far offset. This effect is not observed in
the data. The low gradient in the mantle (0.005 km/s/km) is
constrained by the amplitudes of Pn arrivals at long
shot-receiver distances on these three receivers. The

Shot-Receiver Distance (km)

335   325   315   305   295   285   275   265   255   245   235   225   215   205

Model Distance (km)
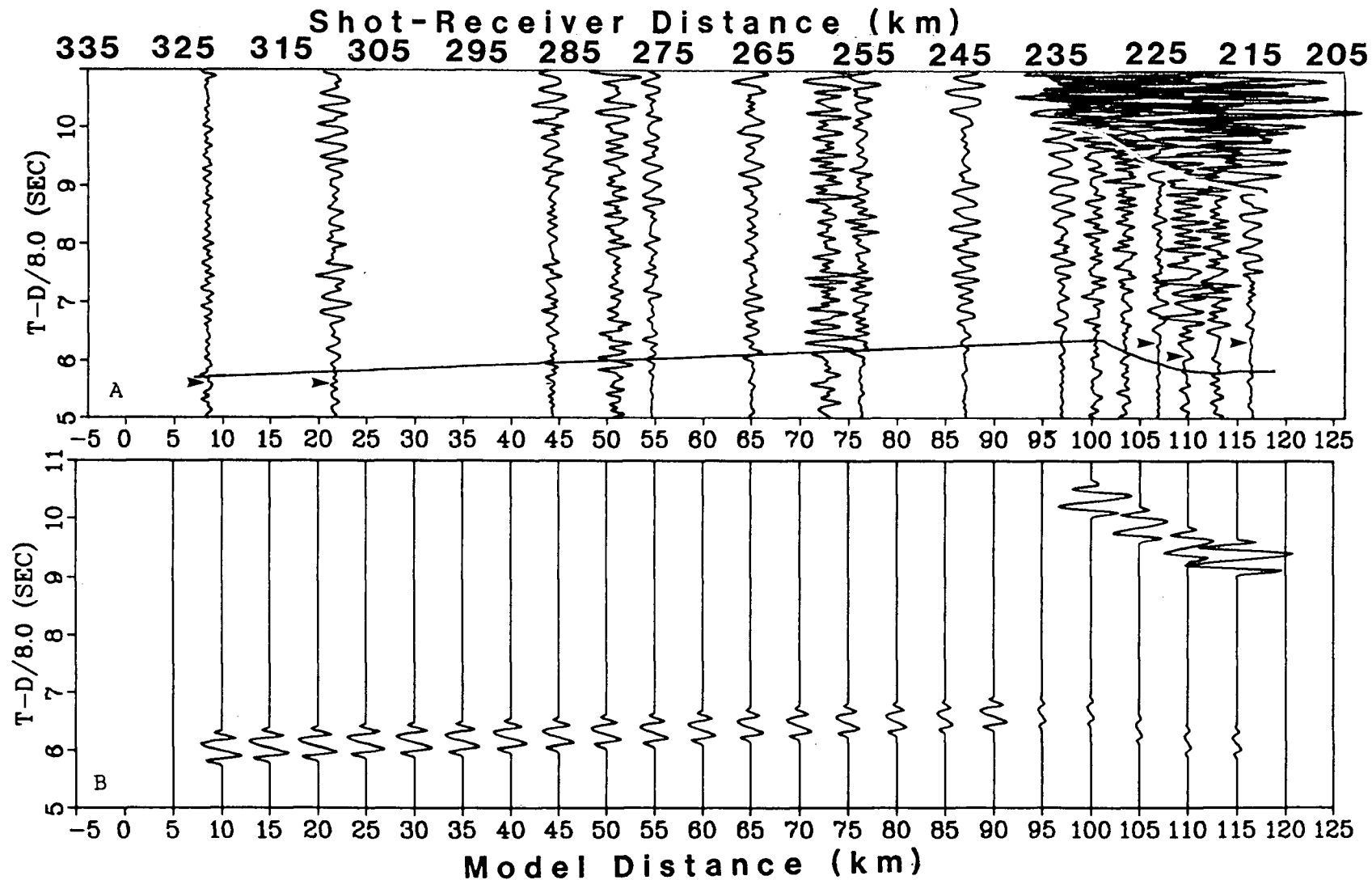
Figure 28 - Comparison of data and synthetic for
Common Receiver Profile 17.

(a) data.

(b) synthetics produced from final ray tracing diagram.
The travel time curves from the synthetic arrivals are drawn
over the data section. The arrowheads mark first picks for
mantle refracted arrivals. See figure 20 for an explanation
of distance and time axes.
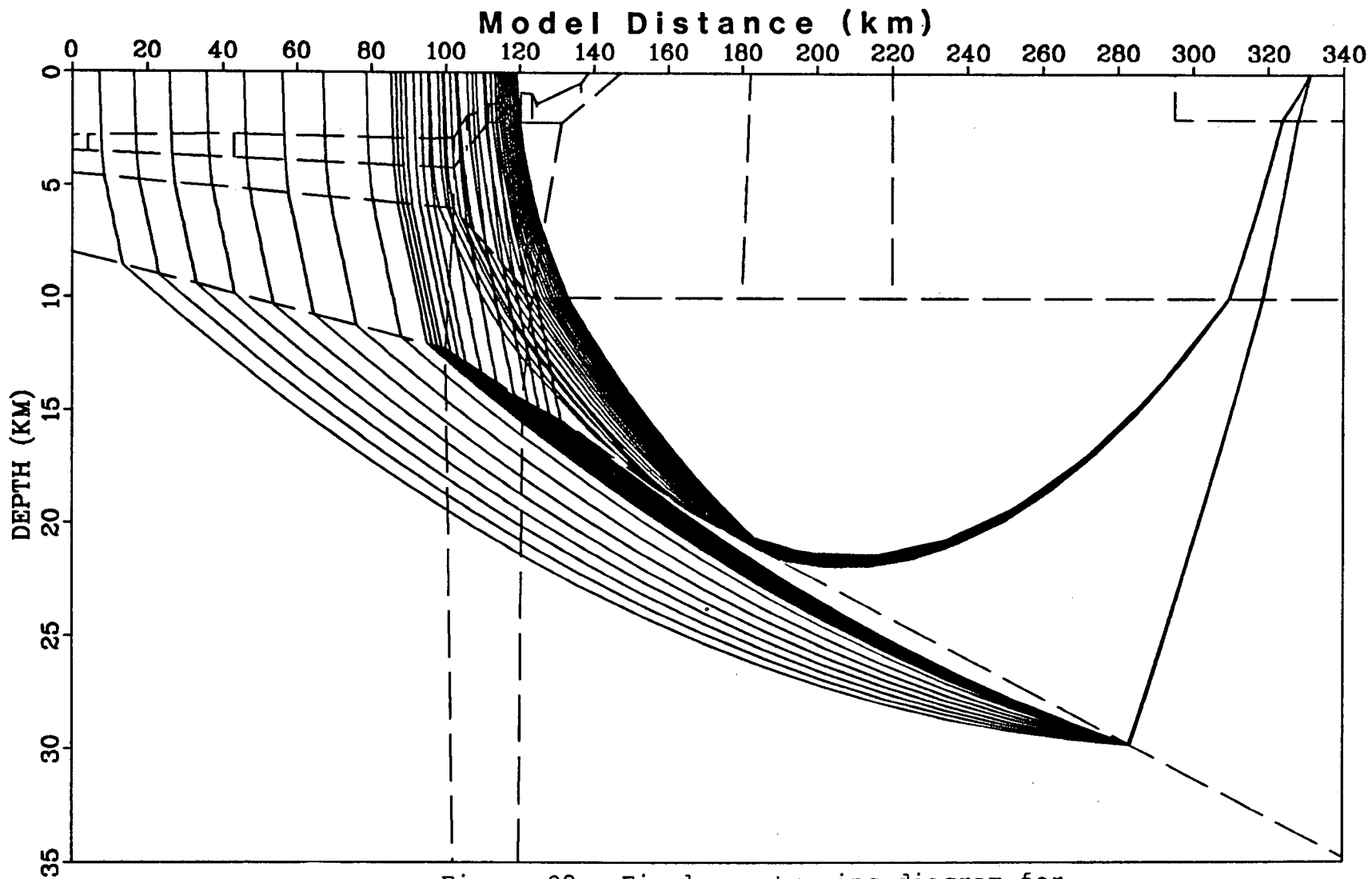
Figure 29 - Final ray tracing diagram for
Common Receiver Profile 17.

(see text for explanation).

amplitudes of these arrivals are very sensitive to changes in the gradient because of their long mantle path. A gradient higher than 0.005 km/s/km results in much larger amplitudes at the farthest distances. Even with this small gradient the amplitudes are a little larger than desired. However, a smaller gradient does not allow shots at far offset to propagate energy to the mainland.

3.3.7 Common Shot Profile 4

This profile represents shot 4 recorded on all receivers. The data are shown in figure 30. The amplitudes have been corrected for the response of the different instruments that were deployed along the line. Because several types of instruments with different response functions were deployed, the trace to trace amplitude variation is sometimes large. Localized structure beneath a receiver may also account for amplitude variations. The first two traces, corresponding to data from the two OBSs west of Moresby Island (figure 14), have amplitudes very much smaller than the land receivers. This variation is thought to be a result of the coupling of the OBS

Shot-Receiver Distance (km)

Model Distance (km)
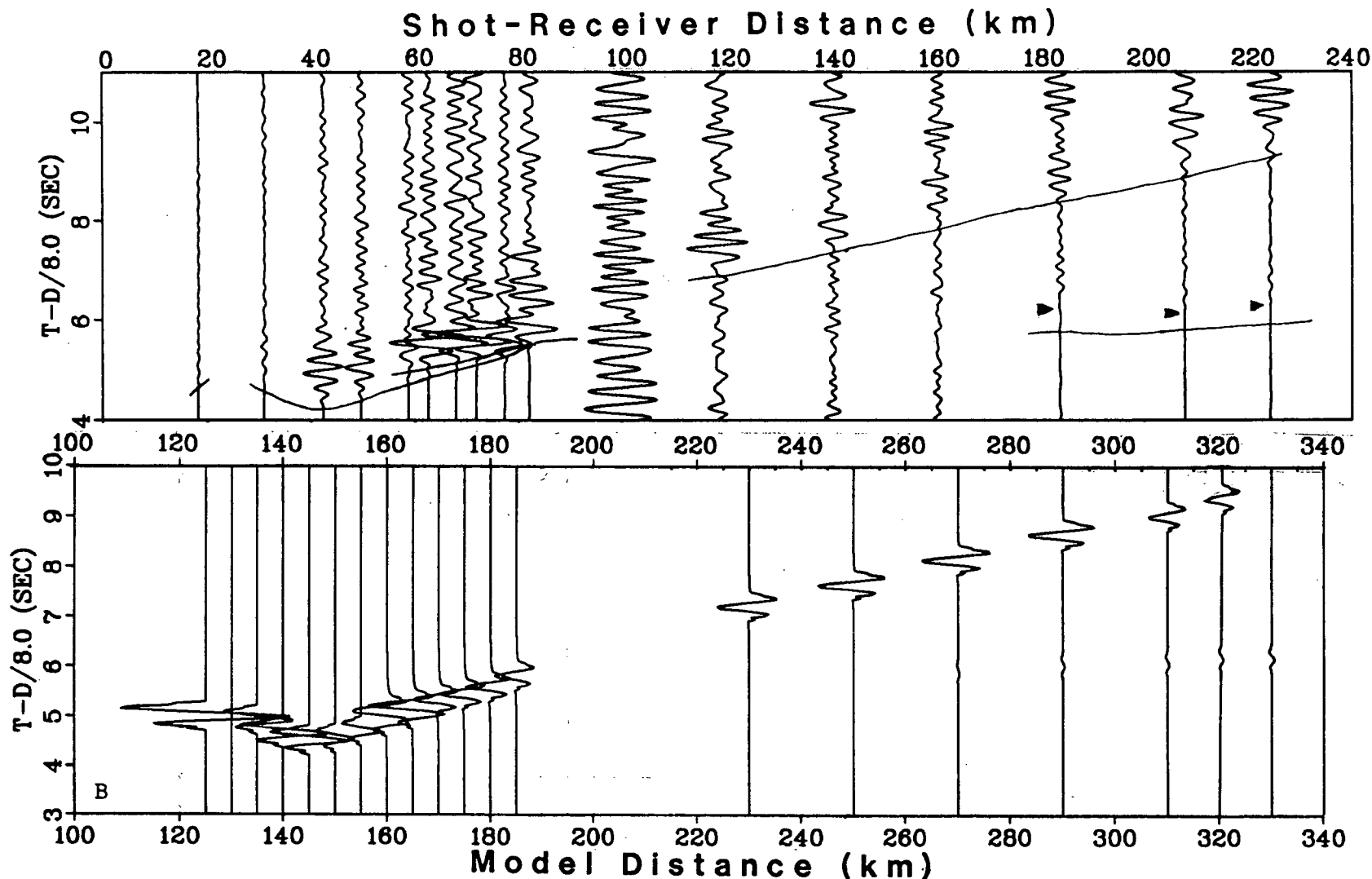
Figure 30 - Comparison of data and synthetic for
Common Shot Profile 4.

(a) data.
(b) synthetics produced from final ray tracing diagram. The travel time curves from the synthetic arrivals are drawn over the data section. Arowheads denote mantle refracted arrival first picks. The data were bandpass filtered from 1 - 5 Hz. Except for the data between 120 km and 160 km shot receiver distance the first picks were made on unfiltered data. See figure 20 for an explanation of distance and time axes.

with the ocean bottom and the instrument response. It is most likely that the OBSs were sitting on soft sediments while the land stations were placed on bedrock. As well the OBS is equipped with 4.5 Hz seismometers while the land stations are equipped with 1 or 2 Hz seismometers. Thus energy recorded below 4.5 Hz on the OBSs is greatly attenuated (figure 15). As indicated in Chapter II, most of the seismic energy is below 5 Hz and thus it is partially attenuated by the OBS itself (figures 16 and 17a). The travel times for the first two receivers have been corrected to effectively place the OBSs on the ocean surface.

The first arrivals before 82 km (shot-receiver distance) are of excellent quality with travel time uncertainties in the order of 0.05 s or less. First arrivals beyond 82 km are very weak and emergent and correspond to shot 4 (the fourth trace from the near-offset end) on each of the common receiver gathers 15, 16, and 17 (figure 24, 26, and 28). These arrivals have an apparent velocity of about 8 km/s. The strong secondary arrivals between 120 km and 230 km have an apparent velocity of 6.6 km/s.

The final model, with traced rays, is shown in figure 31. This profile is the 'pseudo-reversal' for receivers 1 and 3. (figure 21 and figure 23). Arrivals before 80(185) km are rays that have traversed the terrace region. The arrivals out to 65(170) km are modelled as turning rays through the upper high gradient terrace block. Arrivals between 65(170) km and 80(185) km are modelled as reflections from the Moho beneath the
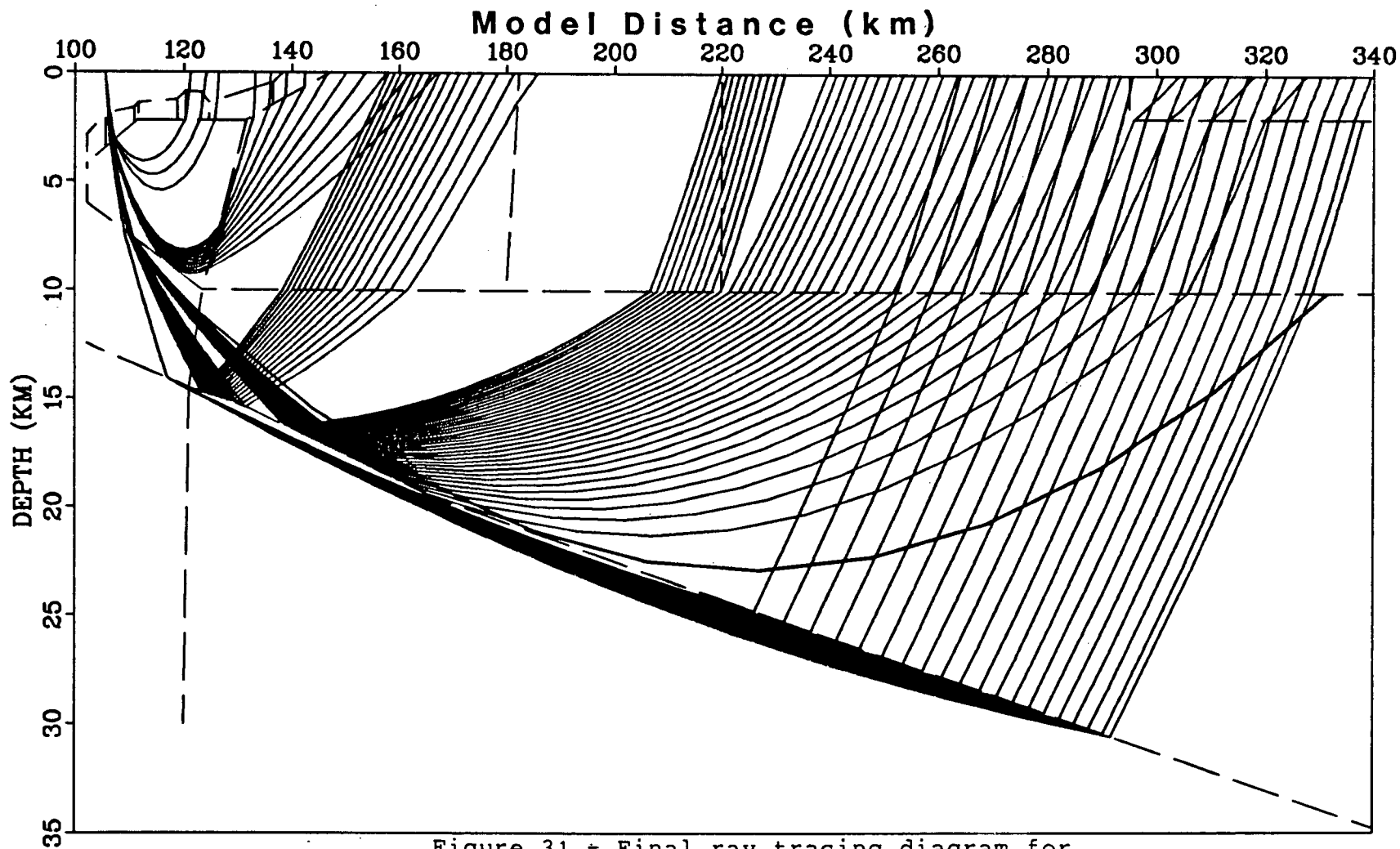
Figure 31 - Final ray tracing diagram for
Common Shot Profile 4.

(see text for explanation).

terrace. The model travel times and amplitudes fit the data well. Two different types of rays (refracted and reflected) to model these arrivals were chosen because of the location of the boundary separating the upper and lower terrace blocks. The weak first arrivals from 180(285) km to 230(335) km 'reverse' the mantle refractions of receivers 15, 16, and 17. The amplitudes of the synthetics match the data well but the travel times are slightly early. It is considered that this misfit may be data related rather than model related and is discussed fully with the interpretation of receiver 15. The large amplitude secondary arrivals from 120(225) km to 230(335) km have been interpreted as post-critical reflections from the Moho beneath the Queen Charlotte Islands and Hecate Strait. Both the amplitudes and travel times are well modelled by the synthetics seismograms. These arrivals help constrain the dip of the Moho in the interval between 140 km and 185 km (model distance).

3.3.8 Common Shot Profile 16

Common shot profile 16 (figure 32) gathers data from a far shot recorded on all receivers. Amplitudes have been corrected for receiver response. Receivers 1 and 2 were effectively placed on the surface of the ocean by ray tracing through the water column. The amplitudes of these two arrivals (marked on figure 32 with arrowheads) are very much smaller than arrivals recorded on the land stations. This is considered to be related to the OBS-ocean bottom coupling and the poor response of the OBSs at frequencies below 5 Hz. This is discussed in more
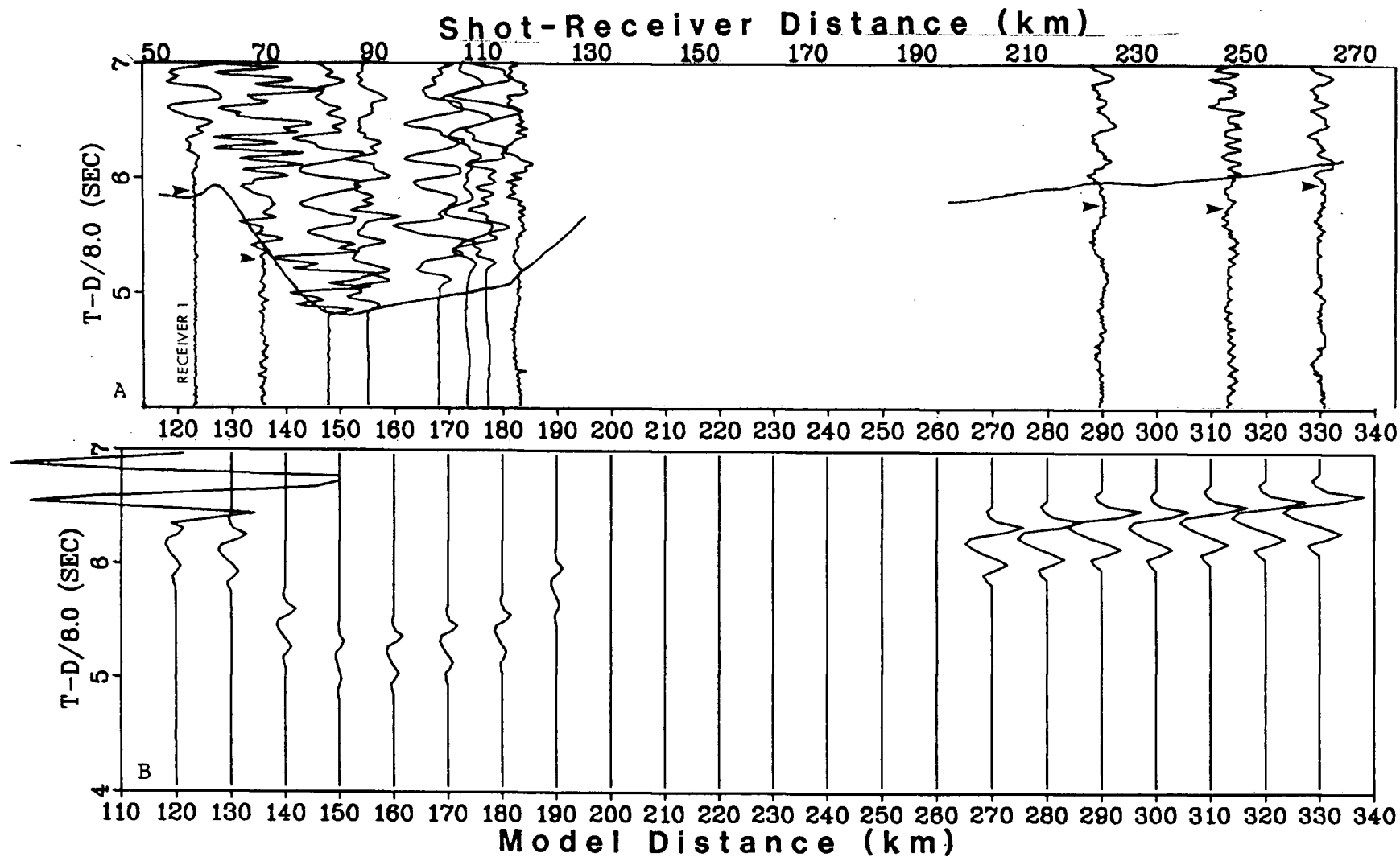
Figure 32 - Comparison of data and synthetic for
Common Shot Profile 16.

(a) data.
(b) synthetics produced from final ray tracing diagram.
The travel time curves from the synthetic arrivals are drawn
over the data section. Arrowheads denote first picks. See
figure 20 for an explanation of distance and time axes.

detail with the interpretation of shot 4 common receiver gather. The travel time uncertainties for these two arrivals is in the order of 0.1 s. The first arrivals between 80 km and 125 km have uncertainties of about 0.05 s. This energy was recorded on stations deployed across the Queen Charlotte Islands. The gap in the data between 130 km and 220 km represents the four OBSs (receivers 11, 12, 13, and 14) that were deployed in Hecate Strait. Due to a source or sources of unknown high amplitude noise, they did not record any visible seismic energy from shot 16. The three arrivals beyond 220 km correspond to the mainland stations and have an apparent velocity of slightly less than 8 km/s although it is hard to estimate this accurately with only three points.

All first arrivals have been modelled as mantle refractions (figure 33). The only secondary arrival observed on this common shot profile at 60 km and 6.3 s corresponds to receiver 1. This wide angle reflection from the oceanic Moho is observed on common receiver profile 1 (figure 20 pg. 58). Wide angle reflections from shot 16 are identifiable only on receiver 1 because the change in Moho dip at the outer terrace edge (at a model distance of 100 km in figure 33) and the high gradient upper terrace do not allow energy to propagate eastward through the terrace region. It is for this reason that all first arrivals were modelled as mantle refractions.

The model travel times and amplitudes fit the data well for arrivals out to 130(190) km. This profile helps to constrain the Moho dip in this region and the average velocity structure
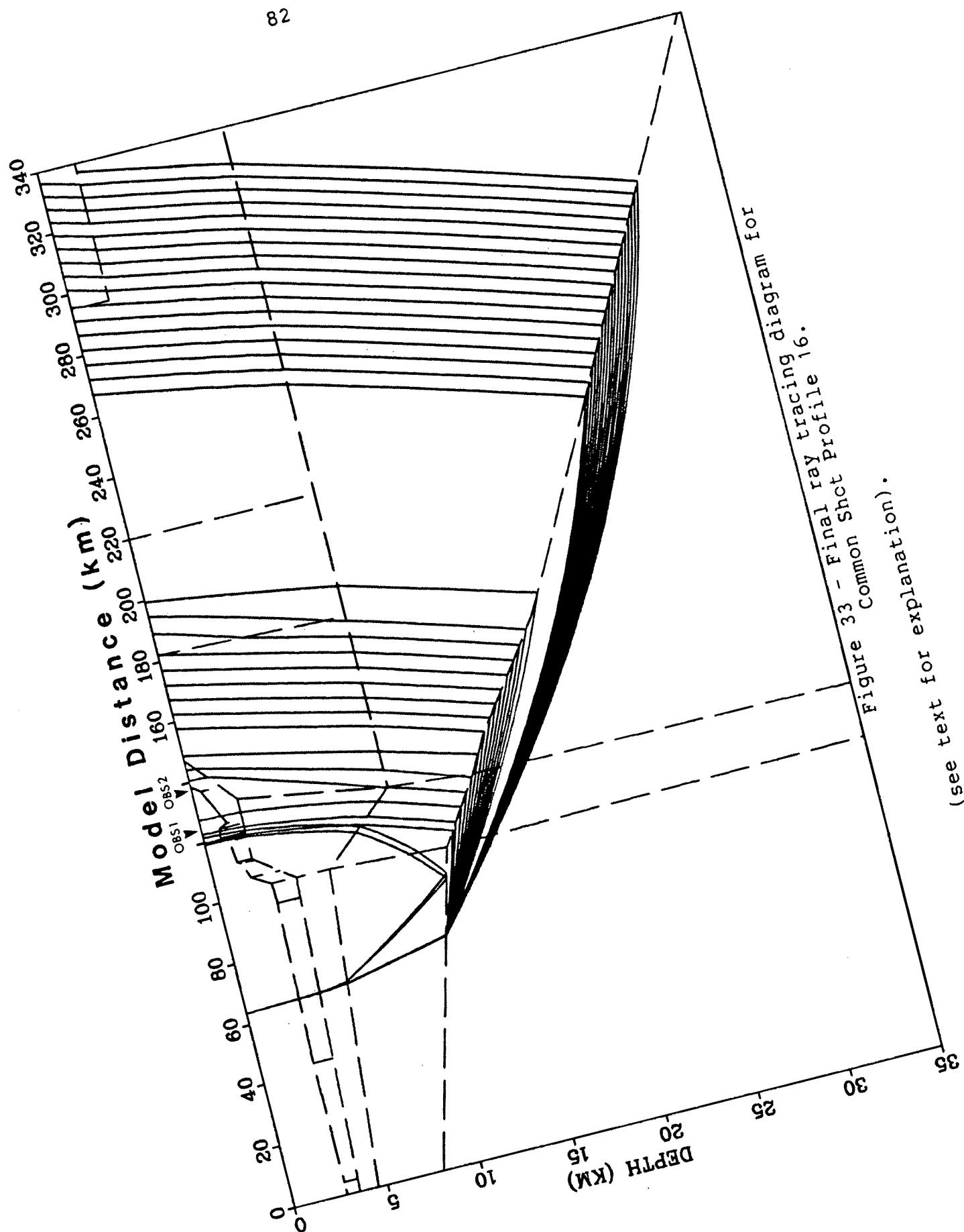
Figure 33 - Final ray tracing diagram for
Common Shot Profile 16.
(see text for explanation).

above the Moho. A small bend in the Moho beneath the Queen Charlotte Islands was used to model the apparent velocity variations between 80(140) km and 130(190) km. Whether this bend in the Moho or structure at a shallower depth is the cause of this variation is not constrained by this data set. These arrivals 'reverse' common receiver gathers 15, 16, and 17 for rays that cross the Moho beneath the Queen Charlotte Islands. This 'pseudo-reversal' helps constrain the dip of the Moho.

The model fit at far offsets is not quite as good. The travel times are late and the amplitudes much too large. Because the arrivals are the only data points in that region it is difficult to determine whether the amplitude variations are caused by local site-dependent structure or features at lower crustal depths. The uncertainties of the travel time picks are large because of the noise. It is felt that these arrivals are fit as well as the data quality requires. The amplitudes would be lowered by a smaller gradient in the mantle although this is inconsistent with receiver gathers 15, 16, and 17. With a gradient below 0.005 km/s/km, a shadow zone in the terrace region for mantle refracted rays is created for these common receiver gathers.

3.4 The Final Model - A Recap

The final model has several features which are well constrained by the data. The terrace region, the change in dip of the Moho beneath the outer edge of the terrace, and the shallow crust beneath the Queen Charlotte Islands and Hecate

Strait will be discussed. The 1.8 km/s layer, representing unconsolidated sediments, is constrained by a continuous seismic profile (Davis and Seemann, 1981) along the refraction line. The oceanic structure is very similar to Horn et al. (1984). Other refraction studies (Johnson et al., 1972; Forsyth et al., 1974) indicate that the crust is about 30 km thick along the west coast of the mainland.

The terrace region has been divided into two blocks: an upper unit with low velocity (4.1 km/s) and high gradient (0.3 km/s/km) and a lower unit with a much higher velocity (6.5 km/s) and a low gradient (0.05 km/s/km). Exactly where this change takes place is constrained only between 6 and 10 km. The high gradient in the upper block is necessary to explain amplitudes of close arrivals on receivers 1 and 3. The lack of any wide-angle reflections from the oceanic Moho that are so prominent on receiver 1 (but not observed on any receivers east of the Queen Charlotte fault zone) is also explained by this block which focuses the energy to the surface. The high gradient also contributes to the abrupt end of the Moho reflections visible on receivers 15, 16, and 17. The lower terrace unit, with a gradient of 0.05 km/s/km, is required by the wide angle reflections on receiver 1. A higher gradient does not allow the energy to reach the station. The refractions and wide-angle reflections at far offset on shot gather 4 also require a region of low gradient in the lower terrace. The average velocity of the terrace region is constrained by first arrivals through the terrace (figure 33, figure 21 and figure 23).

The 5° eastward dip of the Moho shown in the final model is reasonably well constrained out to 200 km model distance (figure 19). Wide angle reflections recorded on receivers 15, 16, and 17 help fix the depth of this boundary at points progressively eastward. The change in dip of the Moho from an almost horizontal discontinuity beneath the ocean to a dipping interface beneath the terrace is the major factor controlling the abrupt termination of these wide-angle reflections (eg. figure 24). The wide-angle reflections on shot gather 4 provide a 'pseudo-reversal' of reflections on receivers 15, 16, and 17. Variations in the shallow structure of the model above the dipping Moho can influence its dip. If the 5.5 km/s block from 220 km to 340 km, model distances, (figure 19, page 53) were replaced with a 6.65 km/s block the dip of the Moho would have to be increased to 9° in order to satisfy the travel time fit.

A shallow Moho beneath the terrace region is required by the continuity of mantle refraction first arrivals on receiver gathers 15, 16, and 17. A steeply dipping boundary joining the oceanic Moho to a deep continental Moho, such as shown in figure 12 (page 27), would block the mantle rays and create a shadow zone east of the terrace region. None of the energy from shots in the shadow zone would reach receivers 15, 16, or 17.

The average velocity of the ocean crust and the depth of the oceanic Moho are well constrained by the wide-angle reflections recorded on receiver 1. Since all other rays travel vertically through the oceanic region the upper layers are poorly constrained and could easily be represented by one layer.

The oceanic structure used was taken from Horn (1982) and Horn et al. (1984), who also modelled a refraction line shot parallel to the Queen Charlotte fault zone. The mantle refractions through the terrace region recorded on receivers 1 and 3 help constrain the depth to the Moho in that region.

The solid boundaries in figure 19 (page 53) are well constrained by the data. The dashed lines represent boundaries that are not well constrained by the data set. The modelling procedure has provided us with a velocity structure that has some well constrained and significant features. The terrace region and a gently dipping and shallow Moho beneath the Queen Charlotte Islands and western Hecate Strait are such features. What is the tectonic significance of this velocity structure? The slow velocity and high gradient of the upper terrace is diagnostic of highly sheared and deformed sediments. Could this be an accretionary sedimentary wedge? Is the very shallow Moho beneath the Queen Charlotte Islands continental crust or underthrusted oceanic material? In the following chapter, an attempt to answer these questions is made.

IV. DISCUSSION AND CONCLUSIONS

This seismic refraction study was planned to obtain more information on the Queen Charlotte Islands region. To meet this objective of the study, it is necessary to take the final velocity model derived from the data and interpret it in a tectonic sense. Only the features of the model that are both significant and well constrained will be considered. These features are: (1) the thin crust beneath the Queen Charlotte Islands and Hecate Strait; (2) the gentle eastward dip (5°) of the Moho starting at the outer edge of the terrace; and (3) the terrace region itself which separates different material on either side. Two different models, one with subduction and one without, will be discussed in this chapter. Both of these models are shown in figure 34.

Evidence indicating the possible underthrusting of the Pacific plate beneath North America at the Queen Charlotte Islands was discussed in Chapter I as justification for the refraction experiment. The data analyzed do not delineate a structure that could be unambiguously identified as a subducting slab; however, the model does indicate that the crust is not comprised of normal continental material. The gentle transition from oceanic crust to the crust beneath the Queen Charlotte Islands is also not indicative of a transition from standard ocean crust to standard continental crust where a large change in thickness can be expected over a small distance. Thus the Moho defined by the refraction data beneath the Queen Charlotte Islands and Hecate Strait may be the bottom edge of an
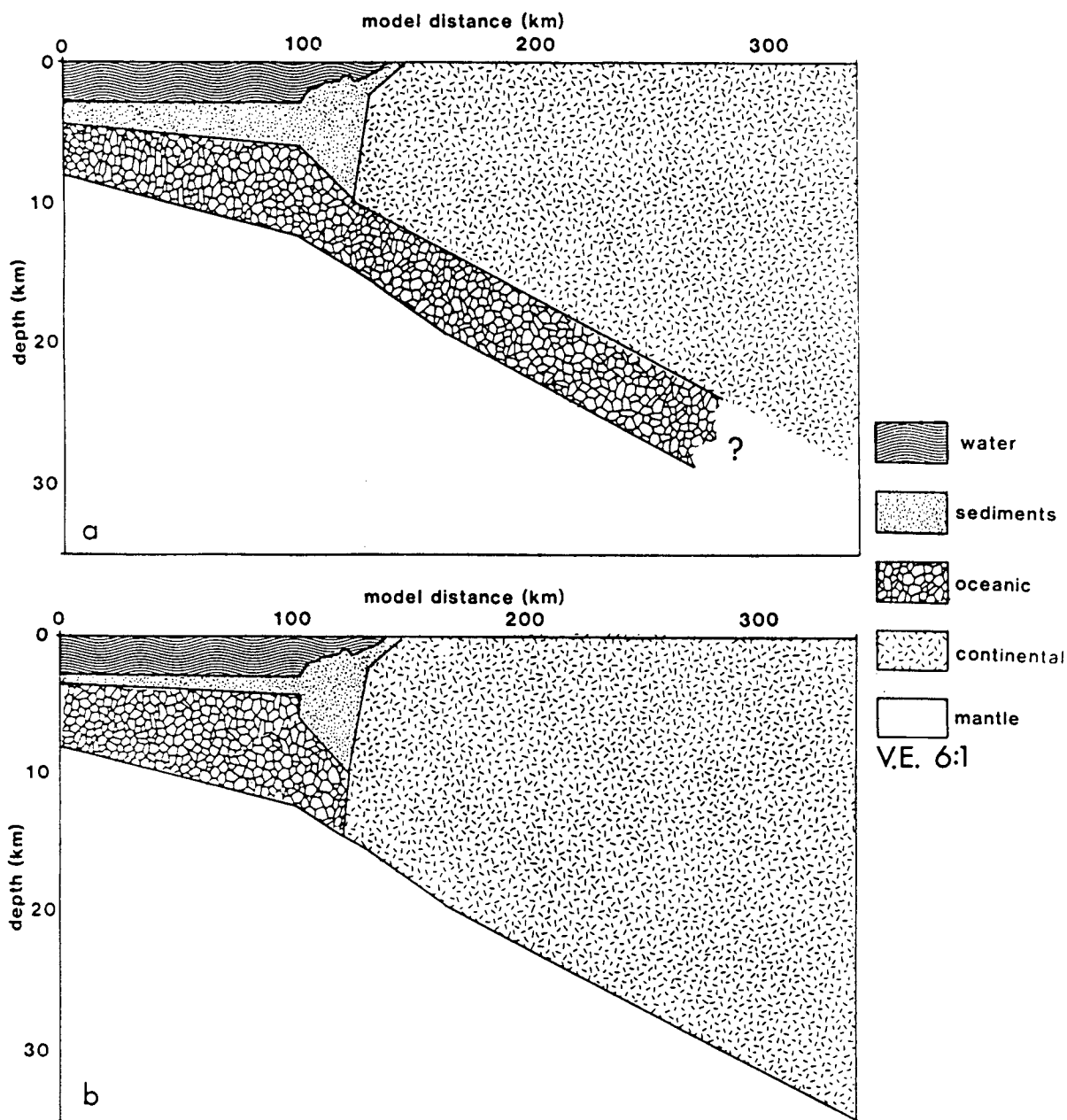
Figure 34 - Two possible models of the tectonic regime
at the Queen Charlotte Islands

These two drawings are schematic representations of (a) a
subduction tectonic regime and (b) a non-subduction regime
at the Queen Charlotte Islands. The top of the subducting
slab drawn in (a) is not seen by the refraction data and is
shown here just as a possible model. Vertical exaggeration
is 6:1.

underthrust Pacific plate.

Further credence to this interpretation is provided by the lower terrace unit which is very similar in velocity structure to the oceanic plate to the west and the crust beneath the Queen Charlotte Islands to the east. This indicates that oceanic crust most likely underlies the compressed sediments of the terrace region. The upper terrace region with its low velocity and high gradient (4.1 km/s; 0.3 km/s/km) probably represents compressed sediments. Von Huene et al. (1985) report a velocity of 1.7-2.0 km/s at the front of the accreted sediments and 5.6 km/s for older more compressed accreted sediments in central Peru. The terrace, from both seismic reflection (Chase and Tiffin, 1972 and Chase et al., 1975) and seismic refraction work (Horn et al., 1984 and this study) appears to be composed of highly deformed compressed sediments. The step-like profile of the terrace is similar to many known subduction zones that are accreting sedimentary material (see Karig, 1977). The model in this study indicates that this thick sequence of material closely resembles accretionary sedimentary prisms that are prominent in shallow subduction zones (Seely, 1979; Uyeda and Kanamori, 1979 and others). The eastward sloping boundary between the upper and lower terrace regions is not well enough constrained by the data to claim it represents the top of an underthrust Pacific plate. In the trough region the oceanic Moho bends downward from being almost horizontal beneath the ocean to an eastward dip of about 5°. The bend in the Moho is well constrained by the abrupt end of reflections from this

horizon on any receivers east of the terrace (receivers 3 to 17). The gentleness of the dip and its extension below Hecate Strait is also well constrained. This feature correlates well with an underthrust shallow slab where a gentle dip would be expected. The lack of ability to distinguish the slab beneath the Queen Charlotte Islands and Hecate Strait from the continental material above it may due to the data set or in-situ physical properties of the slab or the continental crust above it. All raypaths pass through the proposed slab (no rays have turning points in the slab) and thus it is not readily distinguishable from material above it.

The extremely shallow subduction of the Pacific plate is not surprising. The Pacific plate at the Queen Charlotte Islands is about 7 Ma old. Ruff and Kanamori (1980), and Vlaar and Wortel (1976) note that there is a strong inverse correlation between lithospheric age and depth of penetration of the slab. The young, hot, and buoyant slab tends to resist subduction into the mantle. Uyeda and Kanamori (1979) note that in places where the overthrusting plate has a higher absolute velocity toward the trench (assuming the trench is fixed in the mantle) than the underthrust slab, the subduction is shallow. This is observed in the Chilean ($10°$-$30°$ dip), Peru ($10°$), and North Honshu Japan ($35°$-$40°$) subduction zones (see Uyeda and Kanamori 1979 and Wortel, 1980). The absolute motion of model AM1 (Minster et al., 1974) indicates that from the hotspot reference frame North America is moving in a southwest direction at about 2.7 cm/yr. The Pacific plate is moving almost north-

northwest at 5.6 to 6.1 cm/yr. Thus North America is overthrusting the trench while the Pacific plate is moving mostly parallel to the trench. The overthrusting plate having the larger component of convergence indicates that shallow subduction should be occurring.

Time constraints did not allow a gravity interpretation of the final velocity model but preliminary modelling of gravity data across the southern tip of Moresby Island indicates that a shallowly subducting slab is consistent with the data (S. Carbotte, personal communication, 1985). The gravity model is shown in figure 35. It indicates that the Moho dips between $4°$ and $9°$ beneath the terrace region and western Hecate Strait. In eastern Hecate Strait the Moho is flat lying reaching a maximum depth of 22 km. Crustal thickness below the terrace region is about 12 to 15 km agreeing well with the refraction velocity model. This gravity model is consistent with very shallow subduction of the Pacific plate beneath the Queen Charlotte Islands.

There are many places in the world where very shallow subduction has been documented. Focal mechanisms of seismicity indicate that beneath central and northern Peru the slab dips between $10°$ and $15°$ (Stauder, 1975). Cockerham (1984) reports that the Gorda plate dips at $10°$ for a length of 120 km to a depth of 30-35 km where it steepens to a dip of $25°$. Closer to home, the Juan de Fuca plate also exhibits shallow subduction. Preliminary analysis of the Lithoprobe seismic reflection profiles across southern Vancouver Island indicates that
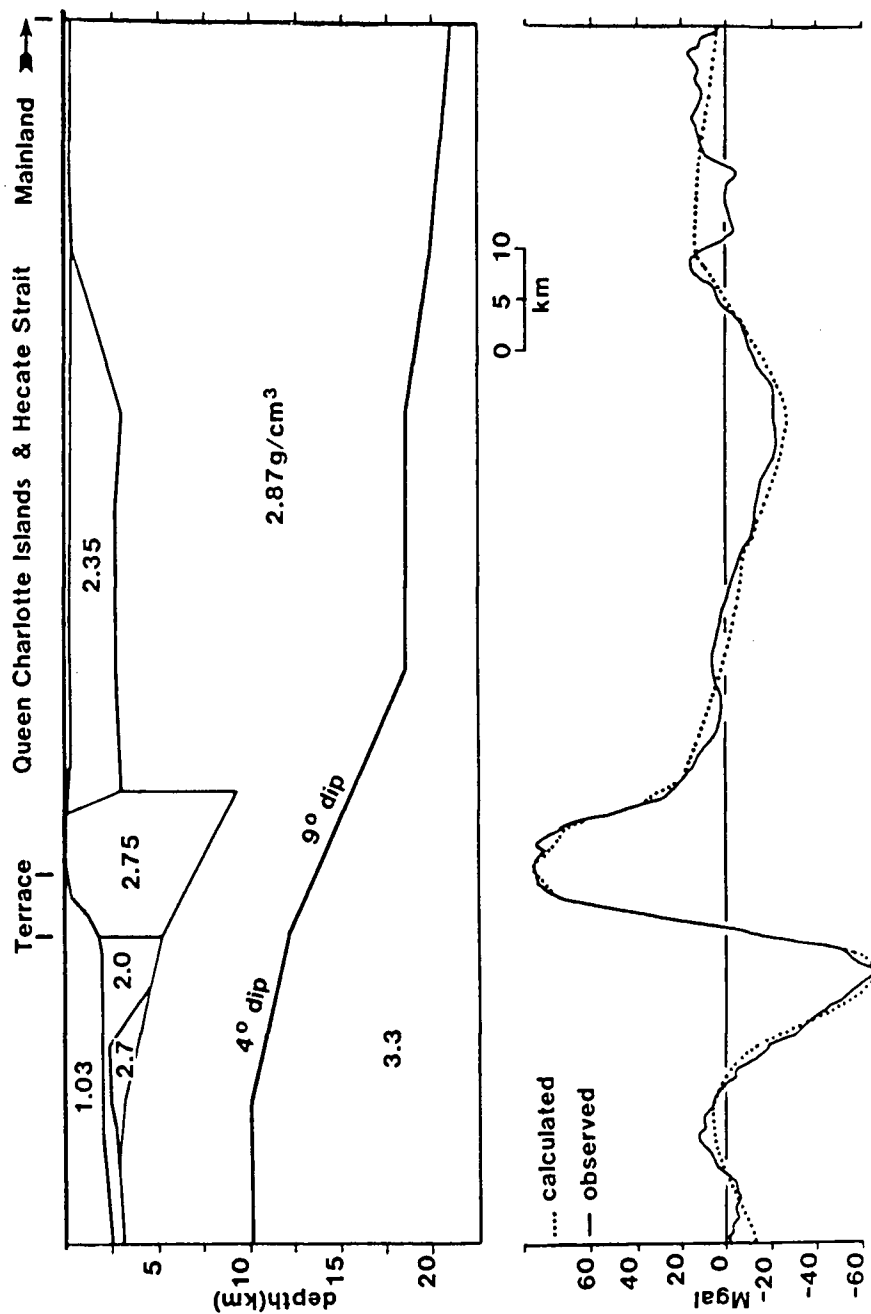
Figure 35 - Preliminary gravity model across the
southern tip of Moresby Island

(S. Carbotte, personal communication, 1985).

Wrangellia is between 15 and 20 km thick and is underlain by a zone of possibly underplated allocthonous material or an old slab, beneath which lies the actual subducting slab (Yorath et al., 1985).

The model of shallow subduction is consistent with other phenomena observed in the Queen Charlotte Islands region, discussed previously in Chapter I. The broad gentle offshore topographic bulge and associated gravity high is observed here. The Queen Charlotte trough is shallow and filled with 2-3 km of flat-lying sediments resembling trenches associated with a shallow angle of subduction such as central and northern Peru, the Aleutians, and others. Scholl (1974) observes that the Queen Charlotte trough has stratigraphic and structural features typical of North Pacific trenches such as the Washington-Oregon trench which is filled with 1-2 km of sedimentary deposits.

Uplift has been occurring along the west coast of the Queen Charlotte Islands for the last 10 Ma (Parrish, 1982) and is probably continuing presently (Riddihough, 1982b). Subsidence has been occurring in Hecate Strait, just 80 km to the east, for the last 6 Ma. Many subduction zones display this pattern of uplift and subsidence but several in particular are similar to the Queen Charlotte Islands. Scholz and Kato (1978) studied the South Kanto district in Japan where highly oblique subduction of the Pacific plate occurs at 3 cm/yr along the Sangami trough. Elevation profiles indicate that uplift of about 20 mm/yr occurs near the trench; the "uplift" falls to negative values 30 km landward of the trench axis. Seno (1977) has documented the

same pattern in the Nankai trough region. The Alpine Fault in New Zealand is a zone of oblique convergence at 4 cm/yr between the Pacific and Indian plates (Walcott, 1978). Although there is oblique convergence at 10°-15° there is no subduction occurring along the fault. Vertical movements near the fault reach +10 mm/yr but fall to negative values within 120 km of the trench (Lensen, 1975). The present uplift along the western edge of the Queen Charlotte Islands of +2 mm/yr drops to -1 mm/yr within 80 km (Riddihough, 1982b, and Parrish, 1982) which is compatible with highly oblique subduction and transform boundaries. Riddihough (1982b) indicates that subsidence at highly oblique convergent margins occurs closer to the margin than in areas where the tectonic regime is dominantly subduction. Subsidence in both the Andes and Alaska appears to occur further from the trench than in the Queen Charlotte Islands (see Plafker, 1972).

The seismicity recorded in the Queen Charlotte Islands region (Berube, 1985 and Rogers, 1983) indicates that compressional stress is being released in earthquakes along the boundary. Berube (1985) identified some shallow thrust events inland on Graham Island. The microseismicity is shallow (5-15 km) and it could not be associated with a Benioff zone. This may be a result of the short study length (3 months). This lack of seismicity associated with a subducting slab may be caused by:

     (1) aseismic slip,

     (2) a presently locked subduction process, or

     (3) the lack of subduction.

Since we are considering the subduction model at present only the first two possibilities are relevant.

Except for the seismicity, the Queen Charlotte Islands exhibit characteristics of subduction zones with shallowly dipping slabs where large coupling forces between the upper and lower plates cause large thrust type earthquakes (eg. N.E. Japan, the Aleutians, and South America). There are examples of shallowly subducting plates that do exhibit low seismicity. Scholz and Kato (1978) report that aseismic subduction is occurring below 15 km during the inter-seismic periods of the Sangami subduction zone. Rogers (1983) notes that the subduction of the Juan de Fuca plate beneath southern Vancouver Island is proceeding aseismically at present, indicating that north of Puget Sound there is little coupling between Vancouver Island and the shallowly dipping slab. Heaton and Kanamori (1984) suggest that the slow convergence rate across this boundary (3-4 cm/yr) may not result in strong coupling between the slab and the overriding plate. Back tilting of the coastal area of Vancouver Island may indicate low resistance to subduction (Riddihough, 1984). The shallow subduction zone along Columbia has several seismic gaps (Pennington, 1984). Pennington suggests that these areas of aseismic subduction may be due to topography on the subducting plate. Kelleher and McCann (1976) indicate that in areas where bathymetric highs interact with the overlying plate large earthquakes occur less frequently. All of this suggests that it is possible that aseismic subduction is occurring beneath the Queen Charlotte

Islands. The convergence rate is very low (2 cm/yr at maximum), and the oceanic crust is very young and ductile; therefore a large coupling between the Pacific slab and the overriding continent would not be expected. Also the Pacific plate north of Vancouver Island, the site of the initiation of subduction beneath the Queen Charlotte Islands, has very large topography. This topography has probably existed since the presence of the Juan de Fuca-Pacific-North America triple junction at that position (see figure 1, page 2). It may be possible that aseismic subduction is presently occurring along the Queen Charlotte transform fault zone.

Of course it is possible that the subduction zone is locked at present and no seismic activity related to underthrusting is observed. Since transcurrent motion is occurring along the boundary at present, this would indicate that the underthrust slab must be separate from the Pacific **plate** to the west for this condition to exist. Finally it is possible that no subduction is occurring along the Queen Charlotte transform fault zone. This possibility will be considered in some detail.

Relative plate motions, current uplift patterns along the west coast of the Queen Charlotte Islands, subdsidence inland, and sesimicity indicate that compression across the Pacific North America plate boundaries exists presently. If underthrusting of the Pacific plate is not occurring then this compression must be taken up by deformation of the Queen Charlotte Islands or the Pacific plate. This model is very similar to the plate boundary between the Pacific and Indian

plates at the Alpine Fault in New Zealand. The Alpine Fault connects the Tonga-Kermadec subduction zone in the north with the Macquarie Ridge complex in the south. Although the Alpine Fault is technically a transform fault the pattern of seismicity indicates that it is a wide zone of deformation (Walcott, 1978). The relative plate motions in this area are characterized by highly oblique convergence of the Pacific plate toward the Indian plate. The present component of convergence is about 2 cm/yr (Walcott, 1978). Seismicity in this area is shallow (4-15 km) (Caldwell and Frohlich, 1975) as in the Queen Charlotte Islands region. Uplift across the Alpine Fault has been discussed previously and is similar in pattern to that in the Queen Charlotte Islands. The Pacific plate is not, however, subducting beneath New Zealand along the Alpine Fault. Walcott (1978) suggests that the compressive stress is being taken up by deformation of a broad corridor paralleling the Alpine Fault. Twenty-five kilometres of crustal shortening will explain the uplift (Walcott, 1978). Crustal thickening on the order of 20 per cent of the shortening is thought to occur, and one fifth of this thickening is manifested as uplift. Walcott also suggests that some material may have been squeezed northwards to the Hikurangi subduction zone along the North Island.

It is possible that the Queen Charlotte Islands is a similar type of transform boundary. The seismicity is shallow and although most of it occurs along the inner scarp of the terrace, some seismicity was found to occur along the outer terrace scarp (Berube, 1985). There is a zone of activity

between the two plates. The deformation model can explain the seismicity along the Queen Charlotte transform fault but it cannot explain the thin crust beneath the Queen Charlotte Islands and western Hecate Strait. The final velocity model and the gravity model of Carbotte (personal communication, 1985) both indicate that the crust is 12 km thick at the west coast of the Queen Charlotte Islands and about 18 km thick at the east coast. Given that the Pacific plate has been convergent with North America at over 1 cm/yr for the past 6 Ma (as is also indicated by a study based on absolute Pacific plate motion by Cox and Engebretson, 1985) 60 km of movement must have been taken up by deformation in the Queen Charlotte Islands region. This infers that about 12 km of crustal thickening must have occurred. (Walcott (1978) uses a figure of 20 per cent of the crustal shortening for the amount of crustal thickening). This is incompatible with the thin crust beneath the Queen Charlotte Islands and western Hecate Strait. On the basis of evidence for a thin crust of the continent along the Queen Charlotte transform fault an oblique subduction model is preferred over a non-subduction model.

In summary the geologic, physiographic, and geophysical data collected thus far indicate that underthrusting of the Pacific plate beneath North America along the Queen Charlotte transform fault may have been occurring since 6 Ma. These data do not conclusively rule out other models as outlined above. The data analyzed in this study cannot delineate clearly the existence of an underthrust Pacific plate beneath the Queen

Charlotte Islands. Further work which would aid in resolving this question is necessary. A seismic refraction profile running north-south on the Queen Charlotte Islands would provide many additional constraints on the crustal structure in this region. Ultimately, a multi-channel deep seismic reflection survey in Hecate Strait would aid in mapping the deep crust and possibly answer some of the questions which still remain concerning this enigmatic plate boundary.

Bibliography

Atwater T., (1970). Implications of plate tectonics for the Cenozoic tectonic evolution of Western North America. Geological Society of America Bulletin, 81, 3513-3536.

Atwater T., P. Molnar, (1973). Relative motion of the Pacific and North America Plates deduced from sea-floor spreading in the Atlantic, India and South Pacific Oceans. In: Kovach R.L., A. Nur Eds. Proceedings of Conference on Tectonic Problems of the San Andreas Fault System: Stratford University Publications Geological Sciences, 13, 136-148.

Berg H.C., D.L. Jones, D.H Richter, (1972). Gravina-Nutzotin belt - tectonic significance of an upper Mesozoic sedimentary and volcanic sequence in southern and southeastern Alaska. United States Geological Survey, Professional Paper 800-D, D1-D24.

Berg H.C., D.L. Jones, P.J. Coney, (1978). Pre-Cenozoic tectonostratigraphic terranes of southeastern Alaska. U.S. Geological Survey Open File Report, 78-1085.

Berube J., (1985). A seismicity study of the Queen Charlotte Islands/Hecate Strait region. M. Sc. Thesis, University of British Columbia, Vancouver, 100 pp.

Bostwick T.K., (1984). A re-examination of the August 22, 1949 Queen Charlotte earthquake. M. Sc. Thesis, University of British Columbia, Vancouver, 115 pp.

Byrne T., (1979). Late Paleocene demise of the Kula-Pacific spreading center. Geology, 7, 341-344.

Caldwell J.G., C. Frolich, (1975). Microearthquake study of the Alpine fault zone near Haast, South Island, New Zealand. Bulletin of the Seismological Society of America, 65, 1097-1104.

Chase R.L., D.L. Tiffin, (1972). Queen Charlotte Fault-Zone British Columbia. 24th International Geological Congress, Montreal, Marine Geology and Geophysical Section, Section 8, 17-28.

Chase R.L., D.L. Tiffin, J.W. Murray, (1975). The western Canadian continental margin, In: Canada's continental margins and offshore petroleum exploration, Eds. C.J. Yorath, E.R. Parker, D.J. Glass. Canadian Society of Petroleum Geologist, Memoir 4, 701-721.

Clowes R.M., (1984). Acquisition of a crustal refraction
    profile across the Queen Charlotte Islands and Hecate
    Strait. Earth Physics Branch Open File Report, No. 84-22,
    Ottawa, 55 pp.

Cockerham R.S, (1984). Evidence for a 180-km long subducted
    slab beneath northern California. Bulletin of the
    Seismological Society of America, 74, 569-576.

Coney P.J., (1976). Plate tectonics and the Laramide Orogeny,
    In: Tectonics and Mineral Resources of Southwestern North
    America. New Mexico Geological Society Special Publication,
    6, 5-10.

Coney P.J., D.L. Jones, J.W.H. Monger, (1980). Cordilleran
    suspect terranes. Nature, 288, 329-333.

Coney P.J., (1970). The geotectonic cycle and the new global
    tectonics. Geological Society of America Bulletin, 81, 739-
    748.

Cooper A.K., D.W. Scholl, M.S. Marlow, (1976). Plate tectonic
    model for the evolution of the eastern Bering Sea Basin.
    Geological Society of America Bulletin, 87, 1119-1126.

Couch R.W., (1969). Gravity and structures of the crust and
    subcrust in the southeast Pacific Ocean west of Washington
    and British Columbia. Ph.D thesis, University of Oregon
    State, Corvallis.

Cox A., D. Engebretson, (1985). Change in motion of Pacific
    plate 5 Myr BP. Nature, 313, 472-474.

Currie R.G., L.E. Stephens, D.L. Tiffin, R.P. Riddihough,
    (1980). Marine geophysical survey off the west coast of the
    Queen Charlotte Islands (Abstract). Transactions of the
    American Geophysical Union (EOS), 61, 71.

Davis E.E., Seemann D.A., (1981). Compilation of seismic
    reflection profiles across the continental margin of western
    Canada. Geological Survey of Canada Open File Report, 75-
    1.

Dickinson W.R., W.S. Snyder, (1979). Geometry of subducted
    slabs related to San Andreas transform. Journal of Geology,
    87, 609-627.

Forsyth D.A. M.J. Berry, R.M. Ellis, (1974). A refraction survey across the Canadian Cordillera at 54 N. Canadian Journal of Earth Sciences, 11, 533-548.

Gebrande H., (1976). A seismic ray-tracing method for two-dimensional inhomogeneous media, In: Explosion Seismology in Central Europe: Data and Results. Eds. P. Giese, C. Prodehl, A. Stein, Springer-Verlag, Berlin.

Grow J., T. Atwater, (1970). Mid-Tertiary tectonic transition in the Aleutian arc. Geological Society of America Bulletin, 81, 3715-3722.

Harper J.F., A.M. Hurley, A.G. Smith, (1981). Plate driving forces at anomaly 23 time. Tectonophysics, 74, 169-187.

Heaton T.H., H. Kanamori, (1984). Seismic potential associated with subduction in the Northwestern United States. Bulletin of the Seismological Society of America, 74, 933-941.

Heffler D.E., D.L Barret, (1979). OBS development at Bedford Institute of Oceanography. Marine Geophysical Researches, 4, 227-245.

Hilde T.W.C., S. Uyeda, L. Kroenke, (1977). Evolution of the Western Pacific and its margin. Tectonophysics, 38, 145-165.

Hillhouse J.W., (1977). Paleomagnetism of the Triassic Nikolai greenstone, McCarthy quadrangle, Alaska. Canadian Journal of Earth Sciences, 14, 2578-2592.

Hillhouse J.W., C.S. Gromme, (1980). Paleomagnetism of the Triassic Hound Island Volcanics, Alexander Terrane, southeastern Alaska. Journal of Geophysical Research, 85, 2594-2602.

Horn J.R., (1982). A snap shot of the Queen Charlotte fault zone obtained from P wave refraction data. M.Sc. Thesis, University of British Columbia, Vancouver, 79 pp.

Horn J.R., R.M. Clowes, R.M. Ellis, D.N. Bird, (1984). The seismic structure across an active oceanic/continental transform fault zone. Journal of Geophysical Research, 89, 3107-3120.

Hyndman R.D., R.M. Ellis, (1981). Queen Charlotte fault zone:
    microearthquakes from a temporary array of land stations and
    ocean bottom seismographs. Canadian Journal of Earth
    Sciences, 18, 776-788.

Hyndman R.D., R.P. Riddihough, R. Herzer, (1979). The Nootka
    fault zone - a new plate boundary off western Canada.
    Geophysical Journal of the Royal Astronomical Society, 58,
    667-683.

Hyndman R.D., T.J. Lewis, J.A. Wright, M. Burgess, D.S.
    Chapman, M. Yamano, (1982). Queen Charlotte fault zone:
    heat flow measurements. Canadian Journal of Earth
    Sciences, 19, 1657-1669.

Irving E., G.J. Woodsworth, P.J. Wynne, A. Morrison, (1985).
    Paleomagnetic evidence for displacement from the south of
    the Coast Plutonic Complex, British Columbia. Canadian
    Journal of Earth Sciences, 22, 584-598.

Johnson S.H., R.W. Couch, M. Gemperle, E.R. Banks, (1972).
    Seismic refraction measurements in southeast Alaska and
    western British Columbia. Canadian Journal of Earth
    Sciences, 9, 1756-1765.

Jones D.L., N.J. Silberling, J. Hillhouse, (1977). Wrangellia
    - a displaced terrane in northwestern North America.
    Canadian Journal of Earth Sciences, 14, 2565-2577.

Karig D., (1977). Growth patterns on the upper trench slope.
    in: island arcs, deep sea trenches and back-arc basins,
    eds. M. Talwani and W.C. Pittman, American Geophysical
    Union, Washington D.C. , Maurice Ewing Series I, 163-174.

Kelleher J., W. McCann, (1977). Bathymetric highs and the
    development of convergent plate boundaries. in: island
    arcs, deep sea trenches and back-arc basins Eds. M.
    Talwani and W.C. Pitman, American Geophysical Union,
    Washington, D.C. , Maurice Ewing Series I, 115-122.

Lensen C.J., (1975). Earth deformation studies in New Zealand.
    Tectonophysics, 29, 901-925.

McKenzie D.P., W.J. Morgan, (1969). The evolution of the
    triple junction. Nature, 224, 125-133.

Minster J.B., T.H. Jordan, P. Molnar, E. Haines, (1974).
    Numerical modelling of instantaneous plate tectonics.
    Geophysical Journal of the Royal Astronomical Society, 36,
    541-576.

Minster J.B., T.H. Jordan, (1978). Present day plate motions. Journal of Geophysical Research, 83, 5331-5354.

Monger J.W.H. , (1984). Cordilleran tectonics: a Canadian perspective. Bulletin de la Societe geologique de France, (7), t. XXVI no.2, 255-278.

Monger J.W.H., J.G. Souther, H. Gabrielse, (1972). Evolution of the Canadian Cordillera: a plate tectonic model. American Journal of Science, 272, 577-602.

Monger J.W.H., R.A. Price, (1979). Geodynamics evolution of the Canadian cordillera - progress and problems. Canadian Journal of Earth Sciences, 16, 770-791.

Monger J.W.H, E. Irving, (1980). Northward displacement of north-central British Columbia. Nature, 285, 289-294.

O'Brien, P.W.S., (1960). Seismic energy from explosions. Geophysical Journal, 3, 29-44.

Packer D.R., D.B. Stone, (1974). Paleomagnetism of Jurrassic rocks from southern Alaska and tectonic implications. Canadian Journal of Earth Sciences, 11, 976-997.

Parrish R.R., (1982). Cenozoic thermal and tectonic history of the Coast Mountains of British Columbia as revealed by fission track and geological data and quantitative thermal models. Ph. D. Thesis, University of British Columbia, Vancouver, 166 pp.

Pennington W.D., (1984). Subduction of the eastern Panama Basin and Seismotectonics of Nortwestern South America. Journal of Geophysical Research, 86, 10753-10770.

Pitman W.C. III, D.E. Hayes, (1968). Sea-floor spreading in the Gulf of Alaska. Journal of Geophysical Research, 73, 6571-6580.

Plafker G., (1972). Alaskan earthquake of 1964 and Chilean earthquake of 1960: Implications for arc tectonics. Journal of Geophysical Research, 77, 901-925.

Riddihough R.P., (1977). A model for recent plate interactions off Canada's west coast. Canadian Journal of Earth Sciences, 14, 384-396.

Riddihough R.P., (1981). Gravity modelling across the Queen Charlotte fault zone (Abstract). Transactions of the American Geophysical Union (EOS), 62, 60.

Riddihough R.P., (1982a). One hundred million years of plate tectonics in Western Canada. Geoscience Canada, 9, 28-34.

Riddihough R.P., (1982b). Contemporary movements and tectonics on Canada's west coast. Tectonophysics, 86, 319-341.

Riddihough R.P., (1984). Recent movements of the Juan de Fuca plate system. Journal of Geophysical Research, 89, 6980-6994.

Roddick J.A., W.W. Hutchison, (1974). Setting of the Coast Plutonic Complex, British Columbia. Pacific Geology, 8, 91-108.

Rogers G.C., (1983). Seismotectonics of British Columbia. Ph. D. Thesis, University of British Columbia, Vancouver, 247 pp.

Ruff L., H. Kanamori, (1980). Seismicity and the subduction process. Physics of the Earth and Planetary Interiors, 23, 240-252.

Saleeby J.B.., (1983). Accretionary tectonics of the North American Cordillera. Annual Review of Earth and Planetary Science, 15, 45-73.

Sass J.H., L.A. Lawver, R.J. Munroe, (1985). A heat-flow reconnaissance of southeastern Alaska. Canadian Journal of Earth Sciences, 22, 416-421.

Scholl D.W., 1974. Ed. Sedimentary Sequences In The North Pacific Trenches, in: The Geology of Continental Margins Eds. C.A.Burke, C.L. Drake, Springer Verlag, New York, 93-504.

Scholz C.H., T. Kato, (1978). The behaviour of a convergent plate boundary: crustal deformation in the South Kanto District, Japan. Journal of Geophysical Research, 83, 783-797.

Schwartz E.J., J.E. Muller, K.R. Clark, (1980). Paleomagnetism of the Karmutsen basalt from southeastern Vancouver Island. Canadian Journal of Earth Sciences, 17, 389-399.

Seno T., (1977). The instantaneous rotation vector of the Philippine Sea plate relative to the Eurasian plate. Tectonophysics, 42, 209-226.

Spence G.D. , (1984). Seismic structure across the active subduction zone of western Canada. Ph. D. Thesis, University of British Columbia, Vancouver, 191 pp.

Spence G.D., K.P. Whittall, R.M. Clowes, (1984). Practical synthetic seismograms for laterally varying media calculated by asymptotic ray theory. Bulletin of the Seismological Society of America, 74, 1209-1223.

Srivastava S.P., (1973). Interpretation of gravity and magnetic measurements across the continental margin of British Columbia, Canada. Canadian Journal of Earth Sciences, 10, 1664-1677.

Srivastava S.P, D.L. Barrett, C.E. Keen, K.S. Manchester, K.G. Shin, D.L. Tiffin, R.L. Chase, A.G. Thomlinson, E.E. Davis, C.R.B. Lister, (1971). Preliminary analysis of geophysical measurements north of the Juan de Fuca Ridge. Canadian Journal of Earth Sciences, 8, 1265-1281.

Stauder W., (1975). Subduction of the Nacza plate under Peru as Evidenced by Focal Mechanism and by Seismicity. Journal of Geophysical Research, 80, 1033-1064.

Stone D.B., (1977). Plate tectonics, paleomagnetism and the tectonic history of the N.E. Pacific . Geophysical Surveys, 3, 3-37.

Strutt J.W., (1917). On the pressure developed in a liquid during the collapse of a spherical cavity. Philosophical Magazine, 34, 94-98.

Sutherland Brown A., (1968). Geology of the Queen Charlotte Islands. British Columbia Department of Mines and Petroleum Resources, Bulletin 54, 226.

Symons D.T.A., (1973). Unit correlations and tectonic rotation from paleomagnetism of the Triassic Copper Mountain intrusions, British Columbia. Geological Survey of Canada Paper, 73-19, 11-28.

Symons D.T.A., (1976). Paleomagnetism of the Triassic Guichon batholith and rotation in the interior plateau, British Columbia. Canadian Journal of Earth Sciences, 8, 1388-1396.

Tipper H.W, G.J. Woodsworth, H. Gabrielse, (1981). Tectonic assemblage map of the Canadian Cordillera and adjacent parts of the United States of America . Geological Survey of Canada, Map 1505A.

Uyeda S., H. Kanamori, (1979). Back-arc opening and the mode of subduction. Journal of Geophysical Research, 84, 1049-1061.

Van der Voo R., R. Jones, C.S. Gromme, G.D. Eberlein, M. Churkin, (1980). Paleomagnetism and the northward drift of the Alexander terrane, southeastern Alaska. Journal of Geophysical Research, 85, 5281-5296.

Vlaar N.J, M.J.R. Wortel, (1976). Lithospheric aging instability, and subduction. Tectonophysics, 32, 331-351.

von Huene R., L.D. Kuln, J. Miller, (1985). Structure of the Frontal Part of the Andean convergent margin. Journal of Geophysical Research, 90, 5429-5447.

Walcott R.I., (1978). Present tectonics and Late Cenozoic evolution of New Zealand. Geophysical Journal of the Royal Astronomical Society, 52, 137-164.

Watts A.B, M. Talwani, (1974). Gravity anomalies seaward of deep sea trenches and their tectonic implications . Geophysical Journal of the Royal Astronomical Society, 36, 57-90.

Whittall K.P., R.M. Clowes, (1979). A simple, efficient method for the calculation of traveltimes and ray paths in laterally inhomogeneous media. Journal of the Canadian Society of Exploration Geophysicists, 15, 21-29.

Willis H.F., (1941). Underwater explosions, time interval between successive explosions. British Report, WA-47-21.

Wortel M.J.R., (1980). Age-dependent subduction of oceanic lithosphere. Ph.D thesis, Vening Meinesz Laboratory, State University of Utrech, Utrech, The Netherlands, 147 pp.

Yole R.W., E. Irving, (1980). Displacement of Vancouver Island: paleomagnetic evidence from the Karmutsen formation. Canadian Journal of Earth Sciences, 17, 1210-1288.

Yorath C.J., B.E.B. Cameron, (1982). Oil on the West Coast?. GEOS, 11, 13-15.

Yorath C.J., R.D. Hyndman, (1983). Subsidence and thermal history of the Queen Charlotte basin. Canadian Journal of Earth Sciences, 20, 135-159.

Yorath C.J., R.L. Chase, (1981). Tectonic history of the Queen Charlotte Islands and adjacent areas - a model . Canadian Journal of Earth Sciences, 18, 1717-1739.

Yorath C.J, R.M. Clowes, A.G. Green, A. Sutherland Brown, C. Spencer, E.R. Kanasewich, R.D. Hyndman, (1985). Lithoprobe - Phase 1: Southern Vancouver Island: Preliminary analysis of reflection profiles and surface geological studies. in: Curent Research, Part A, Geological Survey Of Canada, Paper 85-1A, 543-544.

Young I.F., (1981). Geological development of the western margin of the Queen Charlotte basin. M. Sc. Thesis, University of British Columbia, Vancouver, 380 pp.

APPENDIX A - ESTIMATION OF EXPLOSION DETONATION TIMES

Two methods were used to estimate the detonation time of the time fused explosions. The first method relies on the geometry of the ship, shot, and ocean bottom; the second on measuring the period of the oscillating gas bubble produced by the explosion.

The geometrical method, first described in Horn (1982), can be used when the ocean floor beneath the shot is flat and horizontal (figure 36). The time lag between the time when the explosion is dropped and the direct water wave arrival (called the ditch time, t_{ℓ}); and the ship's average ground velocity (v_s) over the ditch time were measured allowing an estimate of the ship-shot distance x. The depth of the water, D, was estimated using echo sounding equipment assuming a water velocity of $v_w = 1.49$ km/s. By trailing a hydrophone immediately behind the ship and recording the output along with the WWVB time code, the arrival times of the direct water wave (t_d), and the bottom reflected water wave (t_r), were obtained. As Horn (1982) shows, the shot depth, d, can then be expressed to second order as:

$$d = \frac{-b \pm \sqrt{b^2 - 4ac}}{2A} \qquad (1)$$

where
$$a = 4D^2$$
$$b = 8xD^2 - x^3$$
$$c = 8x^2D^2 - 16D^3x + 8xD^2v_w\Delta t - 2x^3D$$
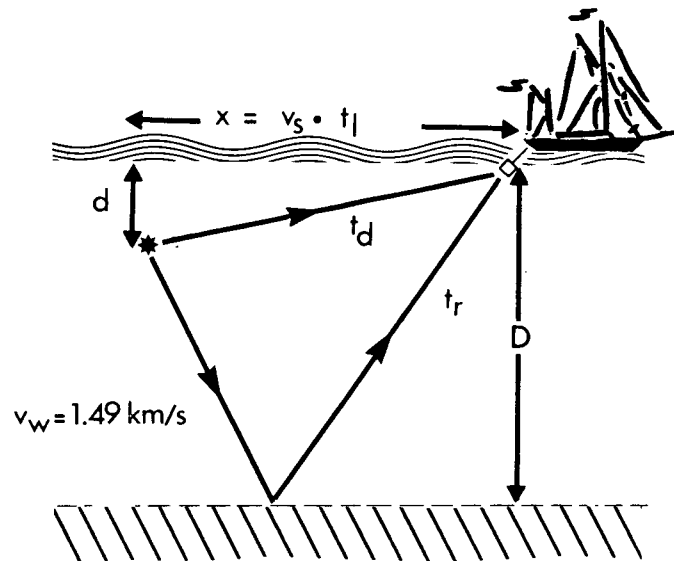$$\Delta t = t_r - t_d \quad \text{and}$$

Figure 36 - Geometrical method of determining shot origin time.

$$v_W = 1.49 \text{ km/s.}$$

Knowing d, the origin time, t_o, is then given by:

$$t_o = t_d - \frac{\sqrt{d^2 - x^2}}{v_W} \qquad (2)$$

The geometrical method was used for final origin time estimates when the ocean floor topography beneath the shot profile was flat (shots 6 to 33). Above the Queen Charlotte terrace the flat seafloor assumption is invalid and another approach was attempted.

The bubble pulse method, used over the Queen Charlotte terrace, relies on measuring the period, τ, of the first oscillation of the gas bubble produced by the explosion. τ is a function of the shot depth, d, since the hydrostatic pressure opposing the expansion of the gas bubble depends on depth. Work by Strutt (Lord Rayleigh) in 1917, and Willis (1941) resulted in the Rayleigh-Willis bubble formula:

$$\tau = \frac{2.13 \ W^{1/3}}{(d+10)^{5/6}} \qquad (3)$$

where   d = shot depth and

W = energy of explosion expressed as explosive weight (kilograms) in TNT equivalents.

Errors in this method arise because the Rayleigh-Willis formula assumes a spherically expanding bubble at a constant depth. In reality, because of the the non-spherical symmetry of

the explosion and the rise of the bubble as it oscillates, this method is not as accurate as equation (1). The bubble pulse method does not rely, however, on the ocean bottom topography. The shot depths for the experiment were estimated by both methods. Agreement between the methods was good except for the shots above the Queen Charlotte terrace where the bottom topography is variable. The depths are in agreement to within 30 m except for shots 3 to 5 which were located over the Queen Charlotte terrace. A geometrical solution was not possible for shot 1 and 2 as the roots of equation (1) were complex. The only other discrepancies were for shots 10 and 24 and to be consistent with the other shots the geometrical method results were used. The maximum probable error for shot depth is ± 30 m. This error, in addition to errors in t_r, v_w, v_s and t_d give a maximum estimated error in the origin time t_o of about ± 0.03 s.

APPENDIX B - COMMON RECEIVER RECORD SECTION PLOTS

A plot of the total explosion data set is included in the form of common receiver sections. The data are plotted with true relative amplitudes. A correction for varying shot size was attempted by multiplying the amplitudes by $W^{2/3}$, where W is the explosive weight in TNT equivalents. To correct for spherical spreading and other energy loss the data amplitude was also scaled by the factor r^2, where r is the shot-receiver distance. No corrections for receiver elevation or shot depth have been made to the data presented in this Appendix. The data were filtered, as noted on specific plots, using an 8-pole zero-phase Butterworth bandpass filter.

T-D/8.0 (SEC)

Shot-Receiver Distance (km)

RECEIVER 1

114

RECEIVER 2

115

SHOT-RECEIVER DISTANCE (km)

RECEIVER 3

116

RECEIVER 4

117

SHOT-RECEIVER DISTANCE (km)

RECEIVER 5

SHOT-RECEIVER DISTANCE (km)

RECEIVER 6

119

Shot-Receiver Distance (km)
RECEIVER 7
filter: 1.5-20Hz

Shot-Receiver Distance (km)

RECEIVER 8

filter: 1.5-20Hz

121

Shot-Receiver Distance (km)

RECEIVER 9
filter: 1.5-10Hz

Shot-Receiver Distance (km)

RECEIVER 10

filter:2-20Hz

Shot-Receiver Distance (km)

RECEIVER 11

filter: 1-5Hz

124

Shot-Receiver Distance (km)
RECEIVER 12
filter: 1-5Hz

SHOT-RECEIVER DISTANCE (km)

RECEIVER 13

filter: 1-5Hz

T-D/8.0 (SEC)

126

Shot-Receiver Distance (km)

RECEIVER 14
filter: 1-5Hz

SHOT-RECEIVER DISTANCE (km)

RECEIVER 15
filter : 2-10Hz

128

Shot-Receiver Distance (km)

RECEIVER 16

filter: 2-10Hz

RECEIVER 17
filter: 2-8Hz